University of Alberta

Mesophase Formation in Heavy Oil

by

Seyed Reza Bagheri

A thesis submitted to the Faculty of Graduate Studies and Research
in partial fulfillment of the requirements for the degree of

Doctor of Philosophy
in
Chemical Engineering

Department of Chemical and Materials Engineering

Fall 2012
Edmonton, Alberta

In Memory of my Father,

Hossein Bagheri

Abstract

Coke formation is a major problem in the petroleum industry because of its effect on liquid yield, catalyst deactivation, and fouling of reactor internals and downstream vessels. Carbonaceous mesophase is a liquid crystalline phase which forms during cracking of heavy oil, as a subset of coke. A novel hot-stage reactor was designed and built to allow the *in situ* observation of mesophase formation at operating conditions of industrial reactors. The reactor was equipped with a magnetic stirrer to allow the addition of catalyst particles. The effect of cooling and depressurization on the formation and growth of carbonaceous mesophase in petroleum vacuum residue was studied using this reactor. The results showed that cooling below the cracking temperature at constant pressure can stop the formation and growth of mesophase by stopping chemical reactions. On the other hand, depressurization to atmospheric pressure, while maintaining reaction temperature, can promote the formation and growth of mesophase.

The effect of stirring on mesophase formation was also investigated. Stirring can result in a bimodal distribution of size of mesophase domains in which very large mesophase regions coexist with a large number of small mesophase domains. Catalyst gives a delay in the onset of mesophase formation by its chemical activity, and a decrease in the amount of bulk mesophase regions by suppressing the coalescence of smaller mesophase domains as a physical effect. The results showed catalyst is less effective at higher catalyst concentrations due to the agglomeration of its particles.

Mesophase formation was studied by a depolarized light scattering technique. A mechanism for mesophase formation in pitches has been suggested based on the evaluation of the previous models for mesophase formation with the scattering results. The results suggest that mesophase formation is a not a phase separation or nucleation process, but the homogeneous self-assembly of planer aromatic molecules into clusters and finally spherical submicron domains that coalesce to form the final micron-scale mesophase spheres. The role of asphaltenes in mesophase formation suggests that asphaltenes are a more aggregated phase in comparison to maltenes at high temperatures.

Acknowledgement

I would like to thank my supervisors, Dr. Murray R. Gray, Dr. William C. McCaffrey, and Dr. John M. Shaw who supported me throughout my doctoral program with their patience and knowledge whilst allowing me the room to work in my own way. It would not have been possible to write this doctoral thesis without the help and support of these kind people. One simply could not wish for a better or friendlier supervisor.

Special thanks also to all my graduate friends, especially group members; Kasra Nikooyeh and Dr. Arash Karimi, for sharing the literature and invaluable assistance. I would also like to thank Dr. Suzanne Kresta and Dr. John Nychka for their comments, ideas and suggestions. I thank Walter Boddez, Richard Cooper, and Les Dean for their technical assistance throughout my experiments. I thank Tuyet Lee and Mildred Becerra for the technical assistance in the lab. I gratefully acknowledge the financial support by UOP.

Finally, I like to thank my mother (Soudabeh) and brother (Ramtin) for their support, encouragement, and endless love throughout the duration of my studies.

Table of Contents

List of Tables

List of Figures

List of Symbols

ABBREVIATIONS

LIDAR	Light Detection And Ranging
MCR	Micro–Carbon Residue
NMR	Nuclear Magnetic Resonance
SANS	Small Angle Neutron Scattering
SARA	Saturates-Aromatics-Resins-Asphaltenes
SEM	Scanning Electron Microscopy
TEM	Transmission Electron Microscopy
XRD	X-ray Diffraction

SYMBOLS

E	The electric field of the incident light beam
F	Scattering matrix
I	Light intensity
$I_{\perp}$	Intensity of the perpendicular component of scattered light
$I_{\parallel}$	Intensity of the parallel component of scattered light
n	Index of refraction
V	Scattering volume
λ	Wavelength
δ	Depolarization ratio
γ	Molecular optical anisotropy

1. Introduction

Petroleum is one of the most important substances used in modern society. It has been the world's most important source of energy since the mid-1950s because of its high energy density, easy transportability and relative abundance. Petroleum is also the raw material for many chemical products, including solvents, fertilizers, pesticides, and plastics. As the world's supply of light crude oil is declining, refiners are forced to depend increasingly on nonconventional feedstocks such as heavy oils and bitumen to supply the increasing demand for fuels. The bitumen reserves in Alberta, Canada, are estimated to be at least 1.7 billion barrels, which is a large supply of energy[1], and makes Canada to have the third-largest proven crude oil reserve in the world, next to Saudi Arabia and Venezuela[2]. The Canadian Association of Petroleum Producers (CAPP) continues to forecast significant growth in Canadian crude oil production over the next 15 years, driven largely by oil sands. Canadian oil sands production is expected to reach to 3.5 million barrels/day by 2025[3].

These heavy crudes often contain components which make the refining processing difficult, such as sulphur, nitrogen, and metals. Therefore, an upgrading process is required to remove these components before these heavy crudes can be used for conventional refinery processes. In addition, it is desirable to convert heavy feeds to lower boiling products which have higher hydrogen to carbon ratio and improved properties as a fuel. The chemistry of the upgrading process is very complex and involves reactions that not only result in desired lighter products, but also lead to the formation of an undesirable carbon-rich

material known as coke. Coke formation is a major problem in the petroleum industry because of its effect on liquid yield and catalyst deactivation. In addition, coke is insoluble in the flowing liquid streams, and in common solvents, therefore, it can foul reactor internals and downstream vessels and force shutdowns[4]. Any reduction in coke yield during heavy oil upgrading can have a significant impact on the economics of this process.

Carbonaceous mesophase appears during the heat treatment of heavy oil in the temperature range of 350 to 500°C as optically anisotropic spheres surrounded by an isotropic liquid matrix. Mesophase is believed to consist of a clusters of approximately planar aromatic molecules with significant orientational order but no long range positional order[5]. As a result mesophase is regarded as a liquid crystalline byproduct which forms during the upgrading of heavy oil and can also regarded as a subset of the insoluble coke phase which forms an anisotropic ordered phase. The onset of mesophase is of particular interest in hydroconversion processes, because this phase can give severe fouling of the reactor internals due to coalescence[6]. Once mesophase spheres begin to form, they can coalesce to form larger mesophase domains, which eventually deposit as coke on the interior surfaces of process equipment. If the coalescence process can be slowed down or prevented, the size of mesophase domains would be smaller and, consequently, be carried out of the process lines and vessels without fouling the equipment[7].

Since mesophase is defined based on its optical anisotropy, hot-stage microscopy is a powerful technique for the characterization of mesophase. Polarized-light hot-stage microscopy is used for the determination of both phase

transition temperatures and phase type, and can also be used to observe the mesophase growth at the temperature of formation[8]. On the other hand, optical microscopy has a limited resolution and cannot detect any particles much smaller than the wavelength of the light used for microscopy. So the main question is: can hot-stage microscopy detect the onset of mesophase formation properly? What if mesophase forms sooner but is in domains too small to be detected in this way?

In some studies of mesophase formation, *in situ* microscopy is not applied and the sample is observed after rapid cooling and depressurization from actual reactor conditions. These studies implicitly assume that the mesophase content does not change as the sample is cooled and depressurized. This brings up the question: is hot-stage microscopy really necessary for the study of mesophase formation or not? In addition, it is desirable to know how to stop the formation or growth of mesophase. Heterogeneous catalyst has been widely used to suppress coke formation[9]. The question in this case is how effective is catalyst for suppressing mesophase formation?

In order to answer all these questions, we need to understand the mechanisms and rate processes that govern the formation and growth of mesophase domains in a reacting liquid medium. Despite many advances, the current knowledge of mesophase formation is still incomplete. The study of mesophase formation is hindered by the ultra-complex nature of heavy oil and its chemical instability in the temperature range where mesophase forms. Under these conditions the liquid phase is progressively altered by complex cracking and polymerization reactions, to the point where the main components in mesophase are likely not present in the

initial vacuum residue, but are formed by reactions in the liquid phase. In order to distinguish the initial vacuum residue material from the thermally altered liquid that surrounds mesophase domains, we adopt the term "pitch" for the thermally altered liquid medium that is present when mesophase is observed. Because mesophase forms under reacting conditions, even the use of simple model compounds can result in a large number of products due to chemical addition reactions which can ultimately result in a mixture which rivals the complexity of a heavy oil.

There is not a consensus on how mesophase forms and a number of different mechanisms for mesophase formation have been proposed so far which are not in agreement with each other. As a result, a fundamental study on the formation and growth of mesophase is necessary to explain when and how mesophase forms. Important questions include: what factors can influence its formation and growth, and how can mesophase formation be suppressed during cracking of heavy oil?

1.1. Research objectives

The objective of this thesis is to study the mechanisms of mesophase formation during the cracking Athabasca vacuum residue and its fractions in both catalytic and non-catalytic systems. Hot-stage microscopy was our main tool to study such mechanisms. A new hot-stage reactor was designed for in-situ observation of mesophase formation. Following the identification of the above significant questions regarding the formation and behavior of mesophase during the cracking of heavy oil and bitumen fractions, this study has the following objectives:

1. Design of a hot-stage reactor to study mesophase formation at actual conditions of industrial reactors (in terms of pressure and temperature). This hot-stage reactor should be equipped with a stirrer to allow the addition of heterogeneous catalyst to study hydroconversion reactions.

2. Study the effect of cooling and depressurization on mesophase formation to find a correlation between the amount of mesophase in a sample at actual reactor conditions and ambient conditions.

3. Study the effects of pressure, temperature, stirring, and catalyst concentration on formation and growth of mesophase during cracking of vacuum residue.

4. Develop a conceptual model for formation and growth of mesophase during cracking of vacuum residue.

1.2. Thesis outline

Given our objective of studying the mechanisms of mesophase formation, chapter 2 reviews the relevant literature. A brief overview of the heavy oil, asphaltenes, cracking and hydroconversion, is presented, along with background on liquid crystals and the definition, properties, and detection limits carbonaceous mesophase. Chapter 3 addresses the approach to designing, testing and validating a novel hot-stage reactor. The rest chapters of this thesis are in format of independent papers. Chapter 4 shows how this hot-stage reactor can be used to study the onset and rate of growth of mesophase in both catalytic and non-catalytic mixtures. The effect of catalyst on formation and growth of mesophase is

investigated, to demonstrate that catalyst can suppress both the formation and growth of mesophase.

The intent of chapter 5 is to study the effect of depressurizing and cooling on mesophase formation. The main question is whether the amount of mesophase at actual reactor conditions correlates with the measurement of mesophase in the reactor product at ambient conditions or not?

Chapter 6 describes a new depolarized light scattering method to study the *in situ* formation of mesophase. This method is far more sensitive than optical microscopy in detecting the early stages of mesophase formation, before the domains are big enough to be detectable by an optical microscope. Based on the results of this light scattering method, a mechanism for mesophase formation is suggested. Finally Conclusions are presented in chapter 7.

1.3. References

1. Ancheyta, J.; Speight, J. G., Hydroprocessing of Heavy Oils and Residua. CRC Press: Boca Raton, 2007.
2. http://www.eia.gov/emeu/international/reserves.html.
3. Canadian Crude Oil Forecast and Market Outlook. CAPP Report, 2010.
4. Gray, M. R., Upgrading Petroleum Residues and Heavy Oils. Marcel Dekker Inc.: New York, 1994.
5. Hurt, R. H.; Hu, Y., Thermodynamics of Carbonaceous Mesophase. Carbon 1999, 37, (2), 281-292.

6. Lott, R.; Cyr, T. J., Study of mechanisms of coking in heavy oil processes. In Proc. - Int. Symp. Heavy Oil Residue Upgrading Util.: Beijing Peop. Rep. China., 1992; pp 309-315.
7. Rahimi, P.; Gentzis, T., The Chemistry of Bitumen and Heavy Oil Processing. In Practical Advances in Petroleum Processing Hsu, C. S.; Robinson, P. R., Eds. Springer: New York 2006.
8. Dierking, I., Textures of Liquid Crystals. Wiley-VCH: Weinheim, 2003.
9. Delbianco, A.; Panariti, N.; Dicarlo, S.; Beltrame, P. L.; Carniti, P., New Developments in Deep Hydroconversion of Heavy Oil Residues with Dispersed Catalysts .2. Kinetics Aspects of Reaction. Energy Fuels 1994, 8, (3), 593-597.

2. Literature Review

2.1. Heavy oil

As the world's supply of light crude oil is declining, refiners are forced to depend increasingly on nonconventional feedstocks such as heavy oils and bitumen to supply the increasing demand of fuels. As a result, the study of heavy oil upgrading is of great importance. The definition of heavy oil is usually based on the API gravity and the viscosity. Heavy oil and bitumen are usually considered to be those crude oils with an API gravity less than 10, while conventional oils have a API gravities higher than 20[1]. A residuum is a black, viscous or solid material which is obtained by distillation of a crude oil under atmospheric pressure (atmospheric residuum) or under reduced pressure (vacuum residuum). The distillation is performed at a temperature below 350°C (660°F) to avoid the thermal decomposition of the crude oil. When a residuum is obtained from a crude oil and thermal decomposition has commenced, it is more usual to refer to this reacted fraction as pitch[1]. Vacuum residue is a fraction of conventional or heavy oil that does not distill under vacuum, and boils above 525°C[2]. It is the heaviest and the most complex fraction of petroleum and contains the majority of the heteroatoms originally in the petroleum. Vacuum residue is expected to have API gravity on the order of 5 to 10° API. It also contains up to 50 wt% of the asphaltene fraction which is the most problematic fraction of petroleum for upgrading processes (asphaltenes will be discussed later

in details). Another important feature of vacuum residue is the presence metals like vanadium and nickel in that as organometallic compounds[1].

2.2. Characteristics of heavy oil

Knowing the chemical composition of heavy oil can be useful for the design and operation of any upgrading process. Heavy oil is an ultra-complex mixture comprises tens of thousands of components[3] with broad ranges of molar mass, elemental composition and structure, so it is not possible to characterize by doing a chemical analysis on a molecular basis. Solvent fractionation is on the other hand, a widely used method to characterize heavy oil. In this way heavy oil or bitumen is first separated into maltenes and asphaltenes using n-pentane or n-heptane. Maltenes are by definition the class which is soluble in both toluene and n-pentane or n-heptane, and Asphaltenes are the class which is soluble in toluene but insoluble in n-pentane or n-heptane. Maltenes can be further separated using chromatography, based on the adsorption interactions with high-surface area chromatographic materials. In this way the fraction of Maltenes which is adsorbed by silica gel or Attapulgus clay from a solution in n-pentane is called Resins, and the non-adsorbed fraction is called Oils. The fraction of Oils adsorbed from a solution of n-pentane by a silica/alumina column is called aromatics, and the non-adsorbed fraction is called Saturates (Figure 2-1). The fractionation of heavy oil into these products (Saturates, Aromatics, Resins, Asphaltenes) is commonly known as SARA analysis. These fractions give no information about detailed chemistry, and combine solubility and chromatographic separations without distinction. The distinctions between aromatics, resins and asphaltenes are not

clearly based on chemical or physical properties, giving considerable ambiguity. Partly for this reason, different SARA methodologies do not generate similar results, and comparing results from different methodologies can be very risky and result in erroneous conclusions[4].

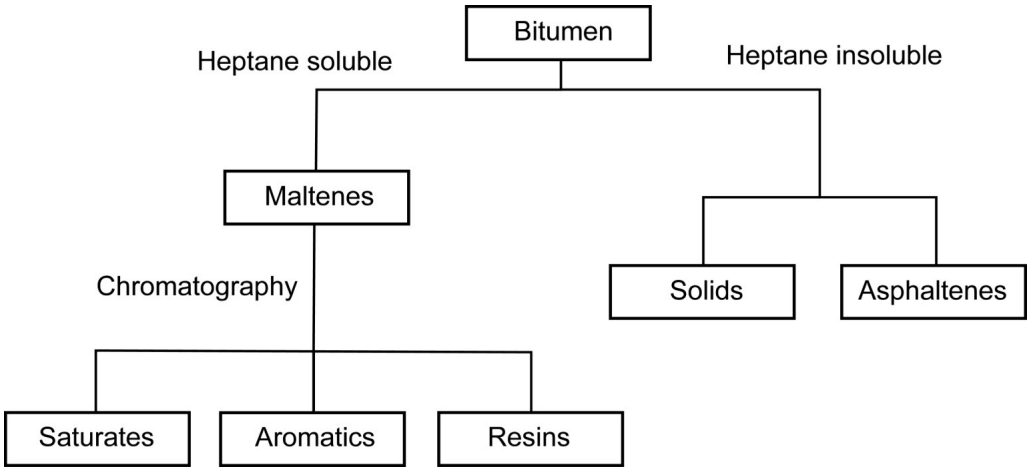

Figure 2-1. Schematics of SARA analysis of bitumen

2.2.1. Asphaltenes

Asphaltenes is the most important class of heavy oil, however its importance lies in its negative impact on the various operations in petroleum industry such as transportation and upgrading. Asphaltenes are the densest fraction of crude oil, and have the highest range of molecular weight, although molecular weight overlaps dramatically with the maltenes. Asphaltenes constitute the most aromatic fraction in heavy oil and have a high content of heavy metals and heteroatoms like sulphur[5]. Asphaltenes are the most reactive part of heavy oil and the main precursor for coke formation[6]. In addition, the asphaltene molecules can aggregate in the crude oil medium, and the size of aggregates is temperature sensitive. Because asphaltenes are a solubility class composed of thousands of compounds,

it is not possible to give an exact molecular formula. However, it is possible to find hypothetical or representative structures for asphaltene molecules using the analytical data.

Qian et al.[7] suggested a mean molecular weight of 1238 amu for a typical asphaltene using field-desorption mass spectrometry. There is no consensus regarding the maximum value of the molecular weight of asphaltenes, but the mean value should be in the range of 1000 to 2000 amu[7-9].

Two different views of the molecular structure of asphaltenes can be found in the literature: pericondensed and the archipelago structures. A pericondensed structure with five to seven rings was suggested by Groenzin and Mullins[10] , consisting of a condensed aromatic core group with several alkyl chains attached. In contrast, the archipelago structure is characterized by smaller aromatic groups linked by aliphatic bridges. This structure was supported by the work of Strausz et al.[11], Pelet et al.[12], Sheremata et al.[13]. and Karimi et al.[14]This molecular structure is shown in Figure 2-2. The polynuclear aromatic groups in asphaltenes with more than 10 rings are unlikely to exist[15], and the average number of rings per cluster is estimated to around 7[16]. Pyrolysis studies have shown that monoaromatics can exist in asphaltene structure[17-18]. As a result, the size of ring groups in asphaltenes can range from 1 to 7 based on the current results. The existence of bridges between ring groups in petroleum asphaltenes has been proved by the results of the thermal cracking of the asphaltenes[19]. Thermal cracking of pericondensed structures, as suggested by Groenzin and Mullins[10] should result in light naphtha-range alkanes and alkenes and heavy vacuum residue as liquid products, which is

contrary to the results of the cracking of asphaltenes. Any process studies can only be reconciled with representations of asphaltenes as a variety of aromatic groups joined by bridges and substituted by aliphatic groups experimental observations[19].

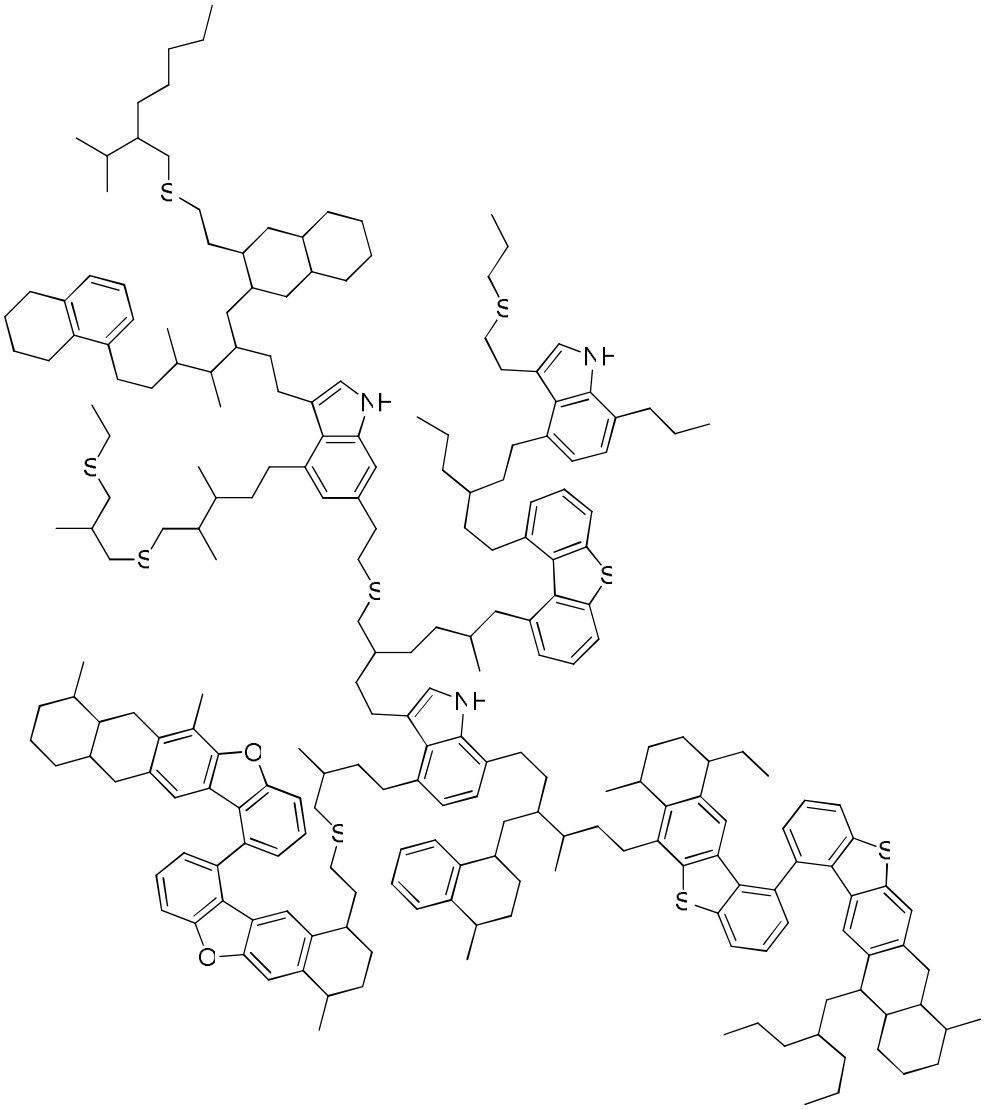

Figure 2-2. Archipelago structure suggested for asphaltenes. (After Sheramata et al.13)

While a mixture of types cannot be ruled out, the performance of thermal cracking experiments[14] and refinery processes such as coking and hydroconversion[13] suggest that most crude oils contain a larger mass fraction of the archipelago type than large condensed alky-aromatics. The only possible conclusion from this review is that bridges between clusters of ring groups (aromatic, naphthenoaromatic, or saturated) are abundant in the petroleum asphaltene samples used in this study.

2.3. Thermal cracking

Thermal cracking is one of the earliest conversion processes used in the petroleum industry[20] which results in the thermal decomposition of larger molecules of heavy oil into smaller molecules by bond breakage. The cleavage of carbon-carbon bonds is the result of free radical chain reactions. It does not require catalyst addition, and its severity determines the rate of conversion and the characteristics of products. Thermal cracking in heavy oil occurs spontaneously at temperatures above 400°C[2], and the majority of the thermal cracking processes use temperatures in the range of 455°C to 540°C and pressures in the range of 100 to 1000 psi[1]. Mild cracking conditions which results in a low conversion rate, gives a high yield of gasoline components with low gas and coke production. However, the gasoline quality is not high. On the other hand, severe cracking conditions result in an increased gas and coke production and reduced gasoline yield which has a better quality[1]. The detailed mechanisms of coke formation are discussed later. Severe cracking conditions without coke formation can only be achieved by using high pressure hydrogen and a catalyst.

2.3.1. Hydroconversion

The use of thermal cracking reactions in the presence of high-pressure hydrogen and catalyst is most properly called hydroconversion, because the role of the catalyst is not to directly promote breakage of carbon-carbon bonds[21]. This process uses the fact that the presence of hydrogen during a thermal reaction of petroleum feedstocks prevents many of coke-forming reactions and improves the yields of the lower boiling components such as gasoline, kerosene, and jet fuel[1]. Hydroconversion is a refining technology that falls under the general umbrella of hydroprocessing. In hydroconversion processes, the reactor is under high pressure (7-25 MPa) and high temperature (400-500°C) operating conditions in the presence of hydrogen. The cracking and hydrogenation of heavy hydrocarbon molecules and the removal of heteroatoms result in a product with lighter oil fractions and a lower level of contaminants with an increased commercial value [22].

2.3.2. Hydroprocessing reactors

Different types of reactors can be used in hydroprocessing, depending on the nature of the feed that should be treated. Figure 2-3 shows the schematics of the reactors that can be used for hydroprocessing of heavy oils. In fixed-bed reactors, the liquid feed trickles downward through the fixed catalyst bed in the reactor while hydrogen passes concurrently[5]. These reactors are simple and easy to use. however, deposition of coke and metals in the catalyst pores and between the pellets is the main limitation of this reactor[20].

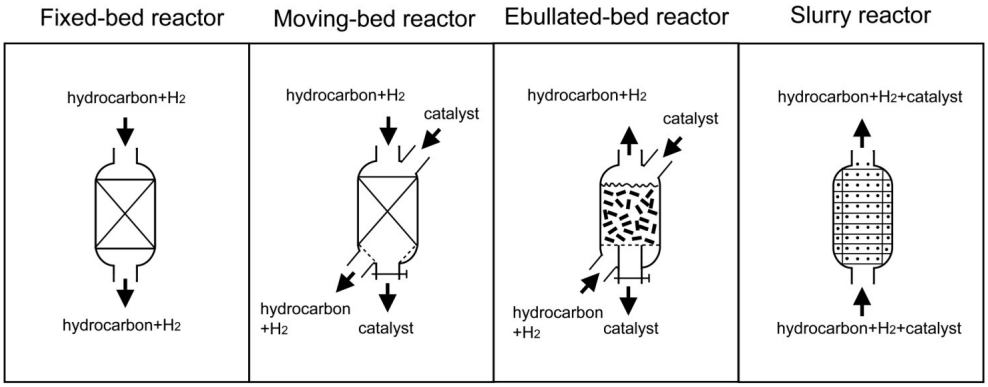

Figure 2-3. Reactors used in hydroprocessing. (After Ancheyta et al.[5])

In moving-bed reactors, the catalyst moves downward through the reactor by gravitational force. The fresh catalyst is added at the top of the reactor, and the deactivated catalyst come out of the reactor at the bottom. In this design, the tolerance of the reactor operation to metals can be increased and more catalyst can be used, however, the mechanical shape and strength of the catalyst is important[5].

In ebullated bed reactors the mixtures of feed and hydrogen is circulating upward through a bed of catalyst in the reactor which results in the expanding and back-mixing of the catalyst bed. Because of the liquid recycle in the reactor it can behave like a continuous stirred-tank reactor and the reactor is almost isothermal. This process is very flexible, and catalyst can be added to it without interrupting the operation. This reactor can be used for more problematic feeds.

Slurry hydroconversion processes utilize finely dispersed catalysts which can be introduced into the feed as finely divided powders, water-soluble or oil-soluble precursors[23]. The reactor can use disposable catalysts at low costs. This reactor is simple, and is intended to process problematic feeds with high levels of metals

and asphaltenes. Several slurry hydroconversion demonstration plants have been built so far, including the CANMET process at the Petro-Canada Montreal Refinery in the mid 1980's[24], but slurry hydroconversion technologies are still at the demonstration scale. These technologies have not yet been commercialized at a larger scale; therefore, refiners do not yet consider this a commercially competitive alternative.

2.3.3. Coke formation

Coke is the solid carbonaceous material which is produced during thermal conversion of vacuum residue or other petroleum fractions. It is has a high carbon content, and is insoluble in organic solvents[1]. It has a low value in comparison with other petroleum products. Coke formation is a major problem in petroleum industry because of its effect on liquid yield and catalyst deactivation[25-26]. In addition, it can contribute to the fouling of reactor internals and downstream vessels[27]. Like other petroleum materials, coke is not a well-defined substance, and in the petroleum industry, it is usually defined as a carbonaceous material which is not soluble in aromatic solvents like toluene[2].

2.3.3.1 Mechanisms of coke formation

It is widely accepted that coke formation is the result of a liquid-liquid phase separation. Magaril[28] was the first one who suggested that coke formed via condensation and polymerization reactions in a new solid phase that formed by precipitation of the asphaltenes.

Liquid-liquid phase separation was observed by Shaw et al.[29] in pyrene-tetralin-hydrogen mixtures in the temperature range of 347-427 °C and pressures up to 19 MPa, who suggested that coke formation can be the result of such phase separation. Abedi et. al[30] developed a phase diagram for a model heavy oil mixture containing Athabasca vacuum bottom, dodecane and hydrogen in the temperature range 152 to 452 °C and the pressure range 2 MPa to 7 MPa. They reported an irreversible asphaltene precipitation for the heavy liquid phase (L2) above 377 °C. But this asphaltene precipitation did not happen for the light liquid phase L1 even at temperatures up to 427 °C. They suggested that there is a strong link between asphaltene precipitation and multiphase behaviour.

A kinetic model involving liquid-liquid phase separation of asphaltenes has been suggested by Wiehe[31] which can successfully explain some phenomena occurring in the coking of heavy oil. The schematic of this theory has been shown in Figure 2-4. In this theory asphaltenes are the major contributor to mesophase formation in thermal cracking of heavy oil. According to his theory asphaltenes are composed of thermally stable, polynuclear aromatic cores with pendant groups connected to the cores by thermally unstable bonds. When the cracking reactions start, these bonds break to form free radicals, and asphaltenes crack off their pendent groups to form asphaltene cores which are initially dissolved in maltenes. When asphaltenes are dispersed in the rest of the oil (maltenes), radicals on the asphaltene cores can abstract hydrogen from hydroaromatics in the resid and terminate the free radicals. As the thermal cracking reactions proceed, more asphaltene cores form, while the amount of maltenes decreases. A liquid-liquid

phase separation occurs when the concentration of these asphaltene cores exceed their solubility limit in the remaining maltenes. As a result, a new phase containing the excess asphaltene cores separates from the oil phase[31].

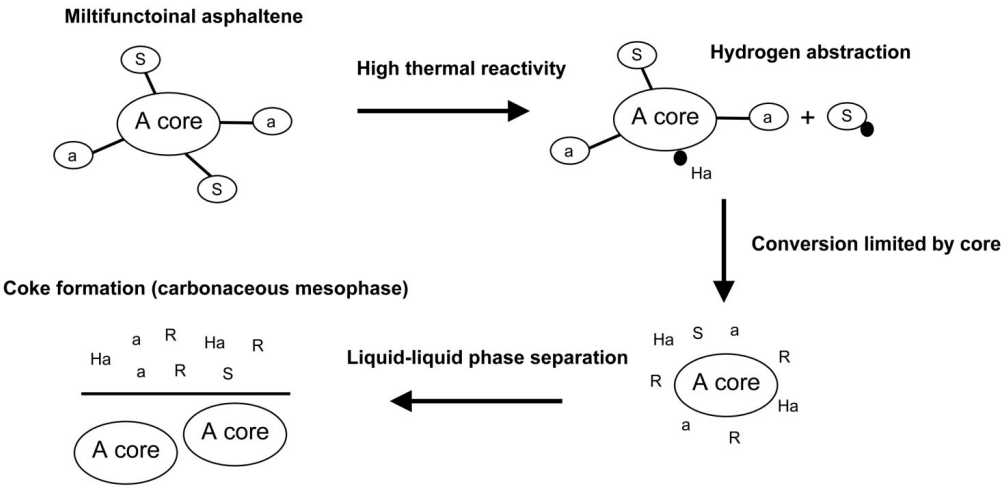

Figure 2-4. Phase-separation mechanism for coke formation (After Wiehe[31])

The free radicals in this asphaltene-rich phase now have little or no donor hydrogen to abstract, so the asphaltene free radicals combine to form high-molecular-weight and this asphaltene rich phase rapidly turns into insoluble coke. Wiehe used the concept of solubility limit to explain the induction observed during the cracking of pitches. The induction time is assumed to be a period in which the thermal cracking reactions occur but no mesophase or coke is formed. In this theory, the induction time is the time needed to reach the solubility limit of asphaltene cores in maltenes. Wiehe developed a kinetic model based on the liquid-liquid phase separation of asphaltenes. Wiehe's model[31] was extended by Rahmani et al.[32] to incorporate hydrogen transfer to the asphaltenes from solvents,

which was in a good agreement with the experimental results over a range of asphaltene concentrations and solvent conditions.

2.3.3.2 Mesophase a component of coke

As mentioned above coke is defined by its solubility, usually defined as a carbonaceous material which is not soluble in toluene. This definition encompasses a diverse range of materials; however, it is possible to divide coke to sub-phases based on the physical properties of each phase. Carbonaceous mesophase is a subset of coke phases which is distinguished by its anisotropy. The term mesophase is a general term used to describe to various intermediate phases which can be formed by the liquid crystalline materials[33]. The formation of liquid crystals is not a unique process to heavy oil and pitches. Many studies have been done during the last century describing the formation and properties of liquid crystals[34]. Brooks and Taylor[35], who first discovered the formation of liquid crystalline materials in pitches, used the term "carbonaceous mesophase" to distinguish it from conventional liquid crystals[36]. In fact, carbonaceous mesophase can be regarded as a liquid crystalline material which shares many common properties of conventional liquid crystals, however, it there are a few features which distinguish between carbonaceous mesophase and conventional liquid crystals. As a result, familiarity with conventional liquid crystals and their properties is a requirement for studying carbonaceous mesophase. The next section will summarize the basic concepts of liquid crystals, their properties, and related experimental techniques.

2.4. Liquid crystals

Liquid crystals are a state of matter with molecular order between that of a crystalline solid and an isotropic liquid. Liquid crystalline substances have physical properties similar to both solids and liquids. The materials flow like a liquid but possess the optical properties of some solids. These behaviours are due to the orientational, but not positional, long-ranged ordering of their molecules[37]. The atoms and molecules within a crystalline solid are rigidly held in their position by strong intermolecular or ionic forces and chemical bonding. Only small amounts of motion are present due to thermal vibrations. However, the molecules within a liquid are constant moving within the volume exhibiting a large degree of disorder and rapid fluctuations of position and orientation with time so there is no intrinsic order. Liquid crystal state is something between solid and liquid phases in which the translational order is lost, but the orientational order is partially retained as shown in Figure 2-5.

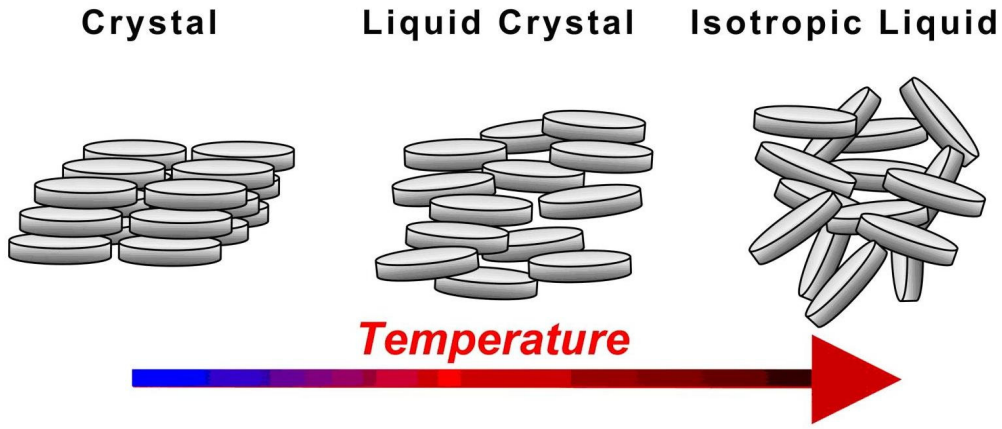

Figure 2-5. Liquid crystal versus crystal and isotropic phase.

2.4.1. History

In 1888, the Austrian chemist Friedrich Reinitzer, discovered a strange phenomenon. He was working on a cholesterol based substance, known as cholesteryl benzoate, trying to measure its melting point which is an important indicator of the purity of a substance. He discovered that this substance seemed to have two melting points. At 145.5°C the solid crystal melted into a cloudy liquid which existed until 178.5°C. After that the cloudiness suddenly disappeared, giving way to a clear transparent liquid. At first Reinitzer attributed this behaviour to the impurities in the material, but further purification did not change this behaviour. Reinitzer turned for help to an expert in optics named Otto Lehmann. Lehmann found out that a unique kind of order existed in the cloudy liquid, but the transparent liquid at higher temperatures showed the characteristic disordered state of all common liquids. He concluded that the cloudy liquid was a new state of matter and called them "liquid crystal" for it, to emphasize that it was a state of matter between a liquid and a solid, showing important properties of both.

2.4.2. Director vector in liquid crystals

The molecules in a liquid crystal tend to align themselves pointing along one particular direction, which is called the director vector and is shown here with *n*. The angle between individual liquid crystal molecules and the director gives an indication of the orientational order of the system[33] (Figure 2-6). There are many types of liquid crystal states, depending upon the amount of order in the material. What they all share is that they are anisotropic. The tendency of the liquid crystal molecules to point along the director leads to a condition known as anisotropy.

This term means that the properties of the material depend on the direction in which they are measured[33].

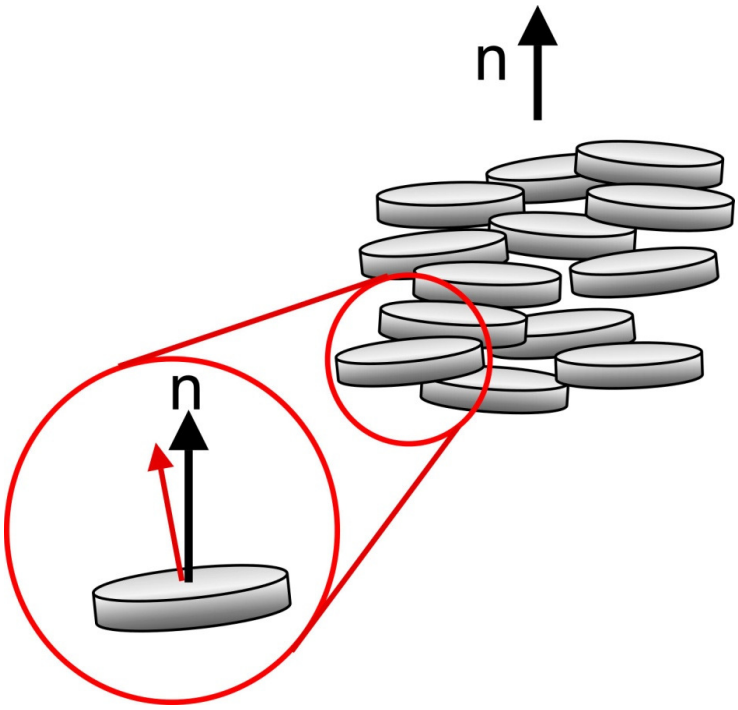

Figure 2-6. Molecular order in liquid crystals and the director vector of the liquid crystal.

2.4.3. Types of liquid crystals

One can classify the liquid crystals in terms of the shape of their molecules, the physical parameters controlling the existence of the liquid crystalline phases, and the amount of order in each phase. If the liquid crystal is formed by heating a crystalline solid compounds or cooling its isotropic liquid, the liquid crystal is called *thermotropic,* and if it is formed upon addition of a solvent at a given temperature it is called *lyotropic*[38]. Most liquid crystals are thermotropic. If the liquid crystal shows both the thermotropic and lyotropic properties then it is

called *amphotropic*[39]. Molecules which are components of liquid crystalline materials are called mesogen, because they contribute to the formation of a *mesophase*, a term which is applied to some liquid crystals and which is defined below. For thermotropic liquid crystals, they can be rod-like (calamitic) or disk-like (discotic) as shown in Fig 2-7. Rod-like molecules are the most common type of molecule that can form the liquid crystal; however, disk-like molecules can also form liquid crystals[33].

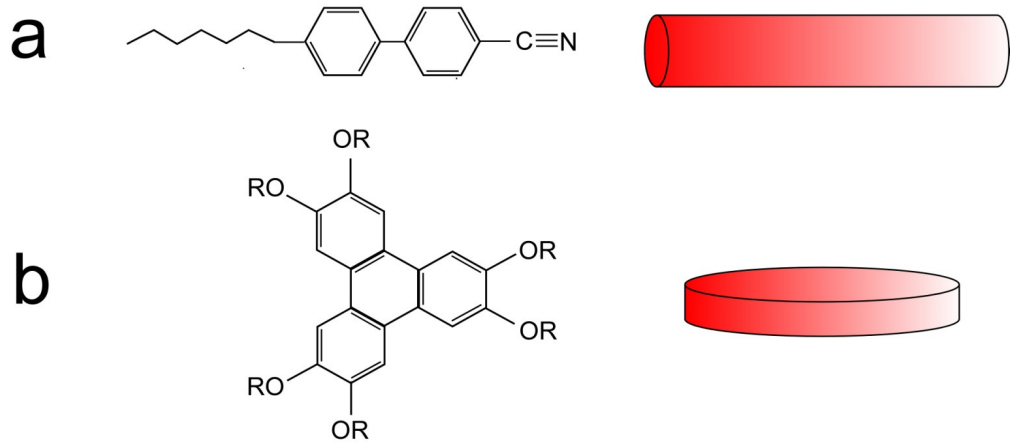

Figure 2-7. Different types of liquid crystal molecules (mesogens): (a) Rod-like (calamitic), (b) disk-like (discotic).

2.4.4. Phases of liquid crystals

The nematic liquid crystal phase is characterized by molecules that have no positional order but tend to point in the same direction. The name nematic is derived from the Greek word *nematos* which means thread, since this phase shows many dark lines visible in thick film samples with a polarizing microscope[33] as shown in Figure 2-8. Smectic is another common phase in calamitic liquid crystals. The word "smectic" is derived from the Greek word for

soap, because soaps exhibit this structure at normal temperature conditions. The molecules in the smectic phase show a degree of translational order which is not present in the nematic phase. In this phase, the molecules tend to align themselves in layers or planes. In contrast, a columnar phase is usually formed in discotic liquid crystals. In this phase the molecules tend to align themselves in two-dimensional lattice which can be rectangular or hexagonal. Lyotropic liquid crystals also form some different phases which are not discussed here.

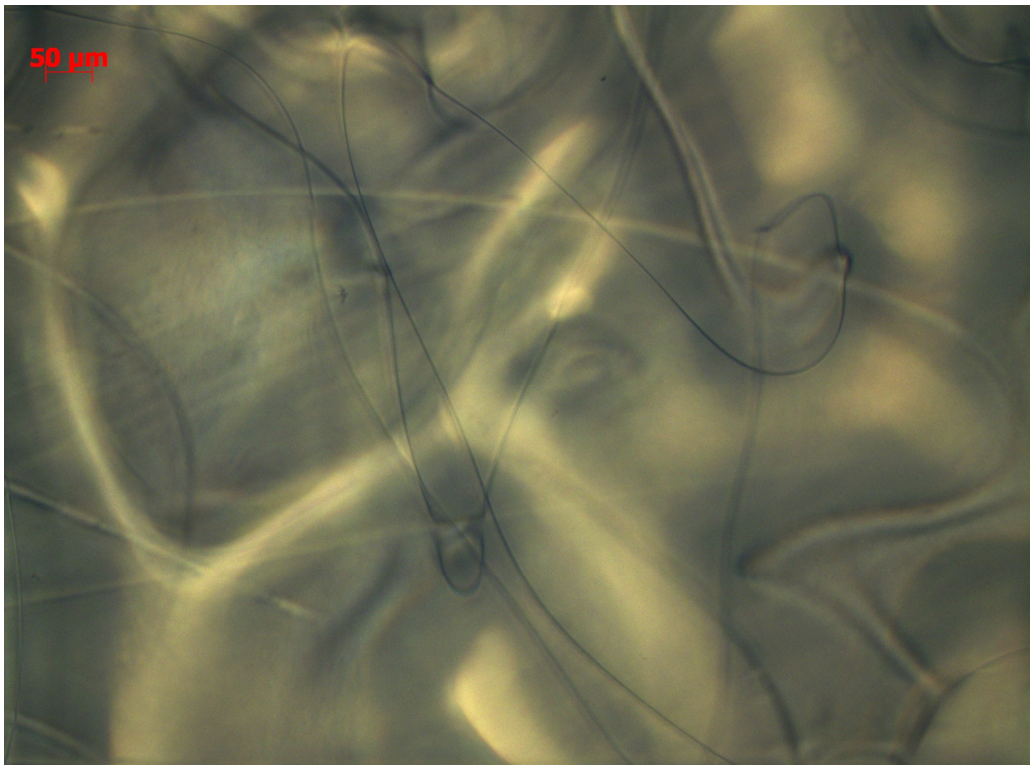

Figure 2-8. dark lines visible in thick film of a typical nematic liquid crystal.

2.5. Polarized light microscopy

The formation of liquid crystals can be studied by various methods such as polarized microscopy, X-ray diffraction (XRD), and differential scanning calorimetry (DSC). Polarizing optical microscopy is capable of the determination of both phase transition temperatures and phase type, and with a hot-stage reactor can be used to observe the mesophase growth at the temperature of formation[38]. DSC is a fast and easy technique, but it merely provides information on phase transition temperatures and the order of the transitions. X-ray diffraction can be used to map the relative position of the molecules, i.e. the nature of the ordering, in each phase revealing the phase type and structure of the liquid crystal[33].

2.5.1. Principles of polarized light microscopy

Light can be thought of as an electromagnetic wave made up of mutually perpendicular electric and magnetic fields that vibrate back and forth as it moves. Traditionally, we only deal with the electric field vector since the magnetic field component is perpendicular to it at all times[40]. The light is called plane-polarized or linearly polarized, if the vector of the electric field oscillates in one specific plane as shown in Figure 2-9. The vibration direction of natural light points to all the directions, so the natural light is not polarized. As a result, a polarizer is used as the device to change natural light into linearly polarized light. The polarizer only allows the light with a specific angle of vibration to pass through as shown in Figure 2-10. Because of their anisotropy, all liquid crystals have a physical property known as *birefringence* which means they have two indices of refraction.

The index of refraction of a material is defined as the ratio of the speed of light in the vacuum

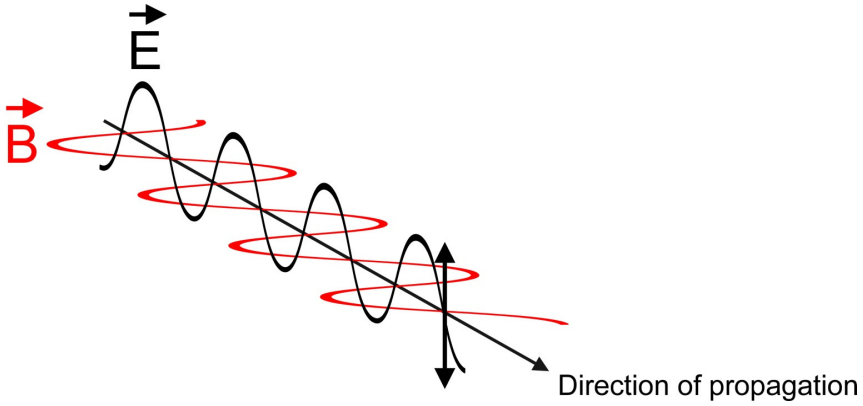

Figure 2-9. Plane polarized light as an electromagnetic wave with mutually perpendicular electric and magnetic fields.

to that in the material. In birefringent materials like liquid crystals, light polarized parallel to the director will have a different index of refraction than light polarized perpendicular to the director. When light enters a liquid crystal, it is broken up

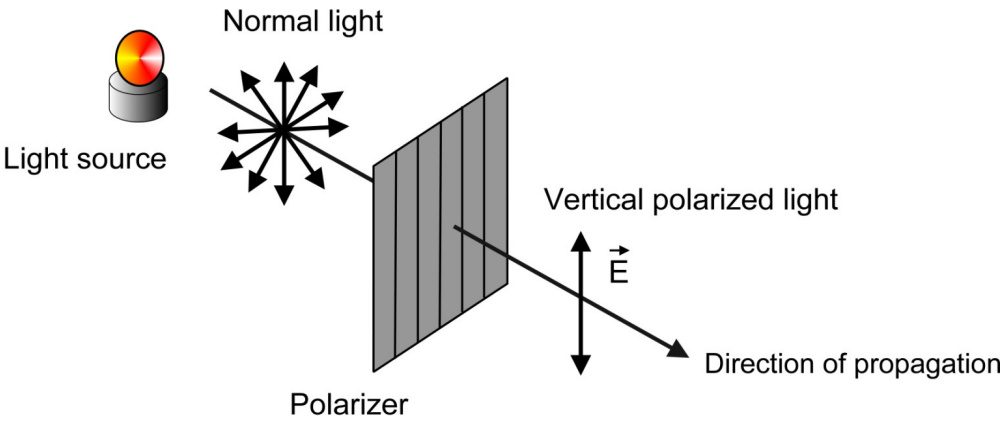

Figure 2-10. Dark Polarizer can be used to turn the normal light into plane polarized light.

into two rays. One of these rays follows the Snell's law of refraction, and the polarization plane of it is perpendicular to the director. This ray is called an ordinary ray. The polarization plane of the other ray is parallel to the director and it is called an extraordinary ray[40]. When these rays enter the liquid crystal, they are in phase, but they travel at different velocities in the liquid crystal, so they get out of phase. As a result, when the rays are recombined as they exit the liquid crystal, the polarization state will change because of this phase difference. The polarization change depends on the birefringence nature of the liquid crystal and the length of the sample.

If two polarizers are set up in series so that their optical axes are parallel, light will pass through both. However, if the axes are set up 90 degrees apart, the polarized light from the first is extinguished by the second polarizer as shown (Figure 2-11). This setup is called crossed polarizers. Placing an isotropic sample between these polarizers does not change anything and this sample looks dark between them. Now if a birefringent sample like a liquid crystal is placed between these crossed polarizers, it will change the polarization state the of the light coming from out of the first polarizer. When this light reaches the second polarizer, there is now a component that can pass through, and the sample looks bright**.** In a typical liquid crystal, the birefringence and length are not constant over the entire sample. The light which is polarized parallel or perpendicular to the director of the liquid crystal sample is transmitted unchanged. As a result, the regions at which the director is parallel or perpendicular to one of the crossed polarizers look dark and the other regions look bright. In this way crossed

polarized microscopy can distinguish between isotropic and anisotropic materials like liquid crystals and the dark bands define the texture of the liquid crystal. Figure 2-12 shows the typical texture of nematic liquid crystals. The regions at which the director is parallel or perpendicular to one of the crossed polarizers, looks dark under the microscope.

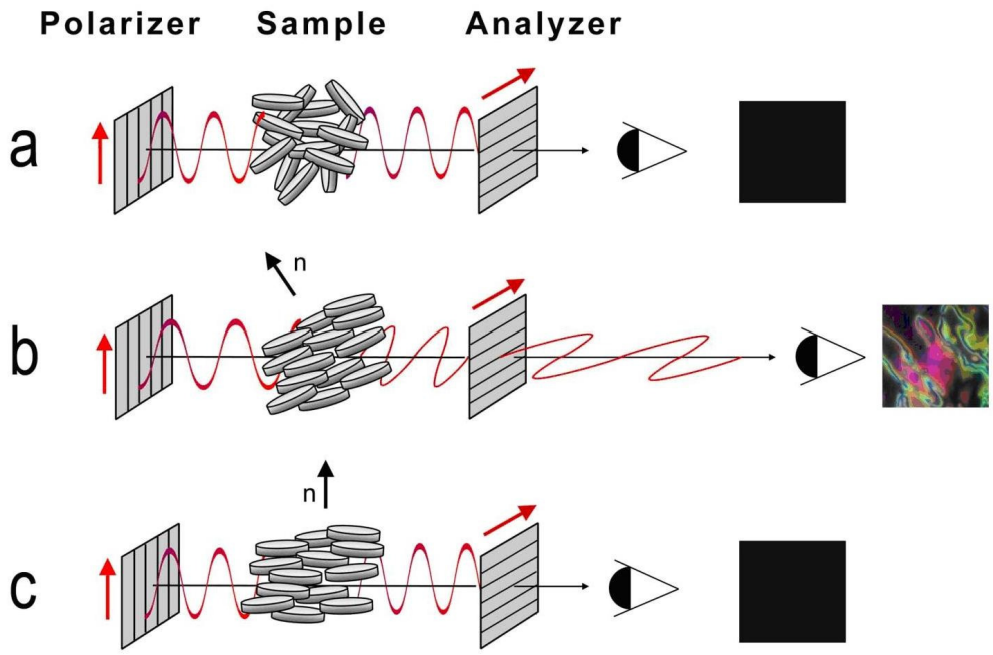

Figure 2-11. Crossed polarizers can be used to distinguish between the liquid crystals and isotropic phases.

between these polarizers does not change anything and this sample looks dark between them. Now if a birefringent sample like a liquid crystal is placed between theses crossed polarizers, it will change the polarization state the of the light oming from out of the first polarizer. When this light reaches the second polarizer,

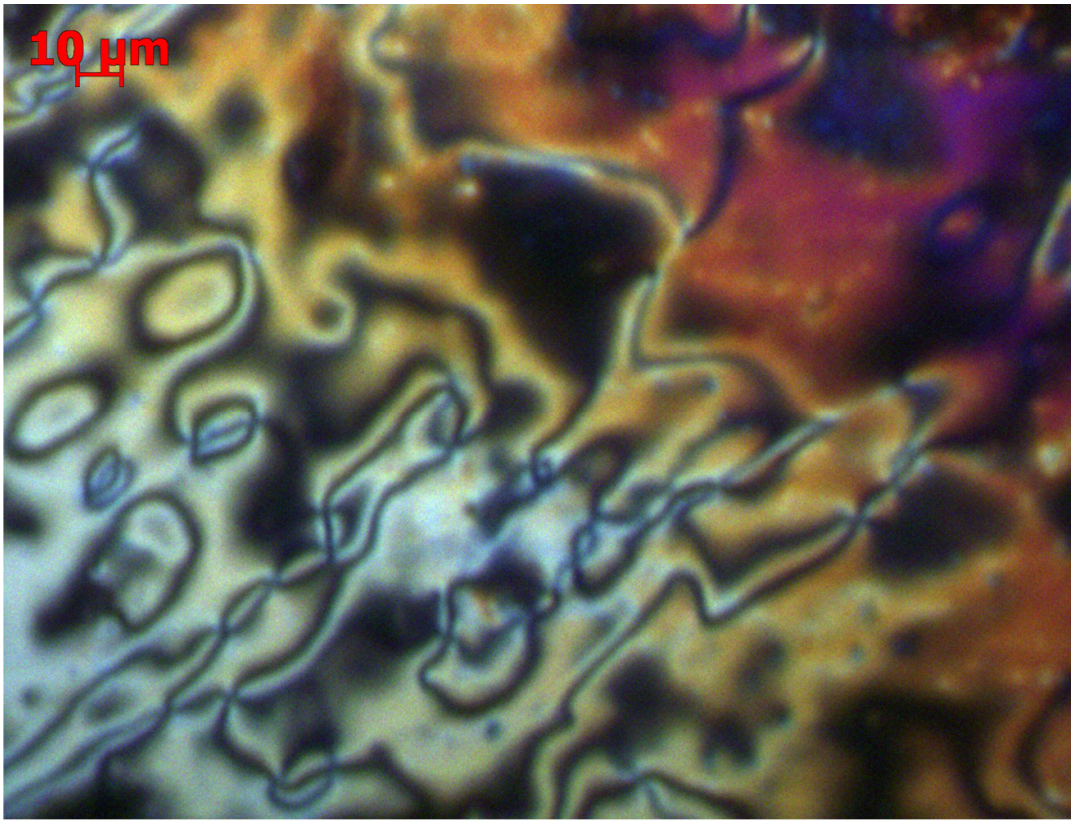

Figure 2-12. The typical texture of a nematic liquid crystal under microscope with crossed polarized light.

there is now a component that can pass through, and the sample looks bright**.** In a typical liquid crystal, the birefringence and length are not constant over the entire sample. The light which is polarized parallel or perpendicular to the director of the liquid crystal sample transmitted unchanged. As a result, the regions at which the director is parallel or perpendicular to one of the crossed polarizers look dark and the other regions look bright. In this way crossed polarized microscopy can distinguish between isotropic and anisotropic materials like liquid crystals and the dark bands define the texture of the liquid crystal. Figure 2-12 shows the typical

texture of nematic liquid crystals. The regions at which the director is parallel or perpendicular to one of the crossed polarizers, looks dark under the microscope.

2.6. Carbonaceous mesophase

2.6.1. History

The term *carbonaceous mesophase* was first used by Brooks and Taylor in 1965[35]. The initial work was started by Taylor who made some observations in the Wogawillie coal seam in New South Wales, Australia. An igneous dyke passed vertically through a coal seam which resulted in the slow carbonization of the coal over long distances. Taylor[41] examined the coal samples approaching the dyke using polarized-light microscopy and discovered small anisotropic spheres. The spheres were larger, apparently due to coalescence to form anisotropic coke, on approaching the dyke. Brooks and Taylor concluded that these spheres are discotic nematic liquid crystals which can form in the early stages of carbonization. Mesophase means "intermediate phase" , and was suggested by Georges Friedel in 1922 to discriminate these materials from conventional "liquid crystals"[34]. Brooks and Taylor suggested the name carbonaceous mesophase to emphasize on the liquid crystal nature of these carbon-rich materials.

2.6.2. Mesophase formation

Carbonaceous mesophase appears during the heat treatment of pitch in the temperature range of 350 and 500°C, as optically anisotropic spheres surrounded by an isotropic liquid matrix. During the cracking of pitches, polycondensed aromatic hydrocarbons are formed by thermal decomposition and polymerization

reactions, and the mesophase spherule is formed as a result of the accumulation of these oriented polycondensed aromatic hydrocarbons in layers[42].

Mesophase is believed to consist of aromatic disk-like molecules with significant orientational order but no long range positional order like liquid crystals. Large planar aromatic molecules are produced as a result of thermal cracking and condensation reactions, and tend to align themselves toward a common director to form a discotic nematic liquid crystal[43]. When pitch is heated above the cracking temperature, either at constant temperature or with gradually increasing temperature, small mesophase spheres which are detectable by an optical microscope appear and gradually increase in size with time. The mesophase spheres are liquid droplets at the temperature of formation, and immiscible with the surrounding isotropic phase. They are slightly denser than the isotropic phase, and can sediment slowly in the preparation, if left undisturbed[44].

Carbonaceous mesophase is an important precursor for advanced carbon materials like pitch-based carbon fibers[45], carbon microbeads[46], and battery anodes[47], however, in petroleum upgrading mesophase is an unwanted by-product of cracking reactions, which is a subset of insoluble coke material[48]. Coke formation, as mentioned before, is a major problem in petroleum industry since it can foul reactor internals and downstream vessels and force shutdowns[2]. Hydroconversion of bitumen can also result in the formation of mesophase[49]. Nandi et al.[50] studied the texture of mesophase and coke formed during the hydroconversion of Athabasca bitumen. Munoz et al.[51] observed the formation of

mesophase in the coke deposits within spent catalysts that had been exposed to a range of feeds, from naphtha through to residue, during hydroprocessing.

2.6.3. Mesophase texture

Brooks and Taylor[52] studied mesophase spherules using electron and optical microscopy and suggested a micro-structure of lamellae composed of molecules with condensed aromatic planes as shown in Figure 2-13a[53]. Figure 2-14a shows the optical micrographs of Brooks/Taylor mesophase spheres in the coke, and Figure 2-14b shows how the extinction contour changes of one sphere in this sample by rotating the stage of polarized light microscope clockwise.

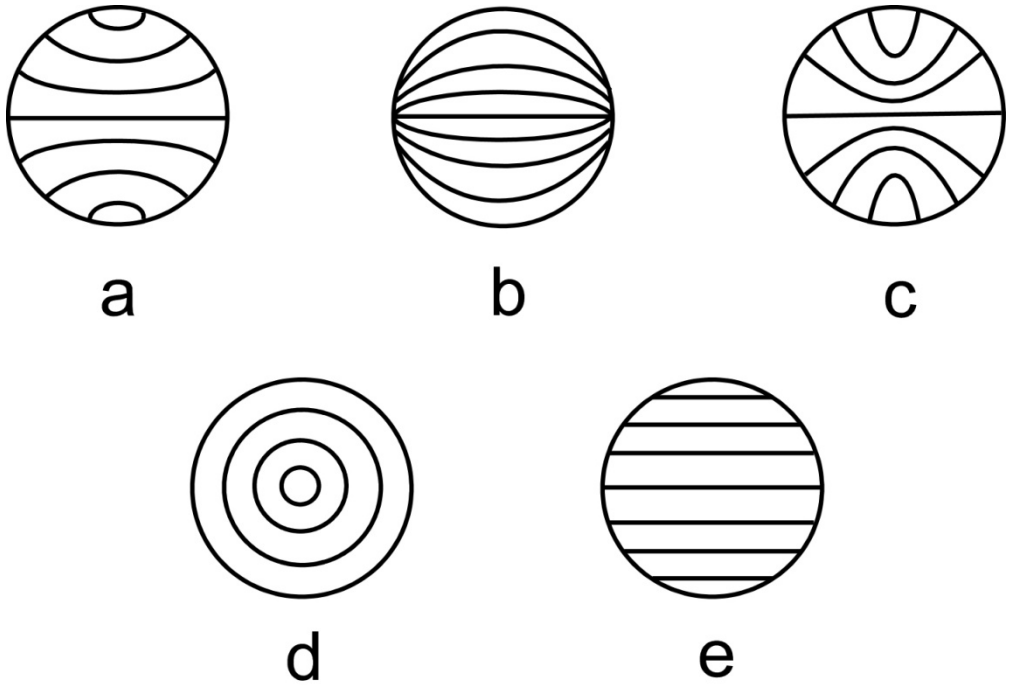

Figure 2-13. Different mesophase micro-structures: (a) Brook/Taylor, (b) anti-Brooks/Taylor, (c) Imamura type, (d) concentric, (e) unichromic.

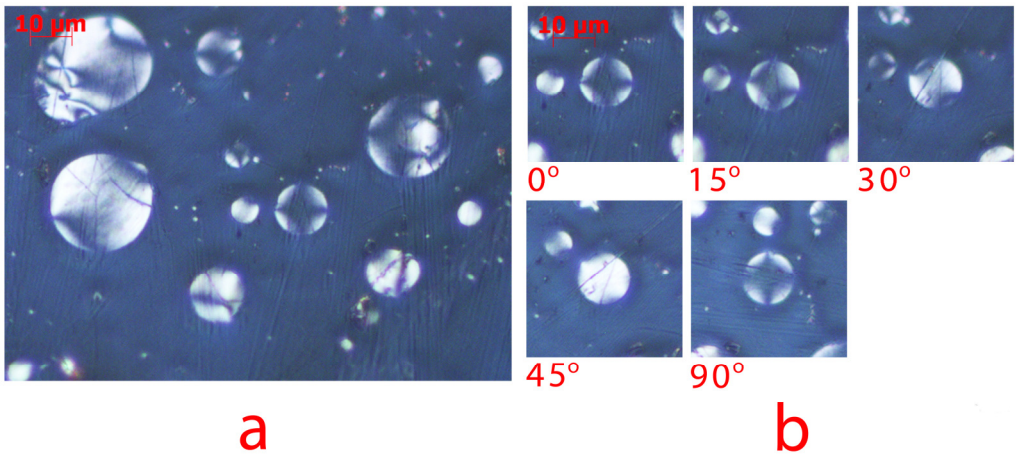

Figure 2-14. Polarized optical microphotograph of mesophase spheres with Brooks/Taylor texture. (a) a typical micrograph, (b) regular extinction contour changes of one sphere when rotating the stage clockwise.

The regular extinction contour changes can determine the molecular alignment in the mesophase sphere, since the regions at which the director is parallel or perpendicular to one of the crossed polarizers looks dark and the other regions look bright. The patterns of dark and light in these micrographs are commonly referred to as "texture", and these patterns provide clues to the underlying molecular orientation. For example, studying the texture of the Brooks/Taylor mesophase spheres shows that the molecular layers become oriented towards the poles of the sphere and that they tend to have a perpendicular alignment at the surface of the sphere as shown in Figure 2-15. Since the work of Brooks and Taylor, more mesophase micro-structures with different orientations of aromatic planes have been reported based on examination of samples under cross-polarized light. Honda reported an anti-Brooks/Taylor mesophase texture during the heat reatment of the quinoline soluble fraction of coal tar pitch containing carbon

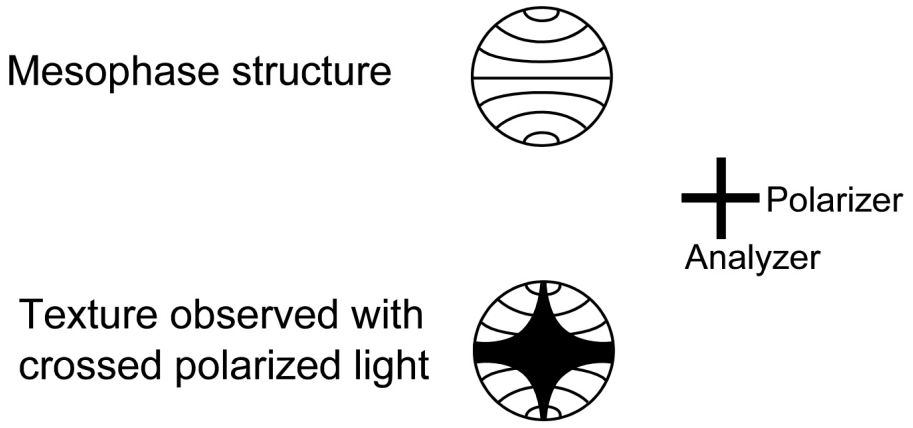

Figure 2-15. Mesophase sphere with Brooks/Taylor texture and the associated molecular structure.

black[54] consistent with a microstructure in which the outer layers are parallel to the spherule surface as illustrated in Figure 2-13b. Kovac and Lewis found the same texture[55]. Imamura et al.[56] obtained another structure similar to Brooks/Taylor texture from both the quinoline soluble fraction of coal tar pitch and Khafji asphalt heat treated below 370°C which is shown in Figure 2-13c. Huttinger reported another mesophase texture, consistent with a microstructure in which all the layers lay in concentric circles around the centre of the spherule[54] as shown in Figure 2-13d, and Chang et al.[47] reported a unichromic texture consistent with parallel arrangements of aromatic molecular planes in mesophase from cracking of synthetic naphthalene pitch (Figure 2-13e). Despite the observation of these different textures, the mechanisms responsible for the formation of the underlying microstructures are not well understood. Hurt et al. attributes the origin of the Brooks/Taylor structure to the strong preference for

edge-on molecular orientation at the phase boundary[57]. They suggested that the large disc-like polyaromatics inside the mesophase sphere prefer to preserve internal π- π bonds at the expense of the weaker potential π bonds with isotropic disordered liquid surrounding the sphere; however, this cannot explain the other mesophase miscrostructures in Fig 13. Inagaki[58] suggested that the interface between mesophase and its surrounding during heat treatment can determine its texture. The mesophase spheres formed during the cracking of heavy oil fractions have a liquid/liquid interface with the surrounding isotropic pitch, which results in a radial alignment of aromatic layers at the surface of the sphere.

2.6.4. Molecular structure of mesophase

Mochida et al.[59] performed the chemical analysis of mesophase spheres by extracting the quinoline-insoluble fraction of a coal-derived carbonized pitch. The fraction was hydrogenated or alkylated to be soluble in organic solvents for the structural analyses. They suggested a model for the mesophase sphere in which the aromatic units of 0.6 to 1.5 nm in diameter are linked by aryl-aryl or methylene bridges to give molecular weights in the range of 400 to 4000 amu. These aromatic and planar molecules carry attached alkyl and naphthenic groups. In this structure, a wide molecular weight distribution is necessary to reveal the liquid crystalline nature of mesophase, and the smaller molecules should be stacked by π–π interactions between large planar molecules. Smaller molecules are important to keep the viscosity low enough that the species in the pitch and the mesophase are mobile [59].

Zimmer and White[60] suggested another model fro the molecular structure of mesophase in which the molecular weight distribution of mesophase was ranging between 400 and 10000 amu. The molecules are oligomeric with aromatic nuclei connected by aryl-aryl and methylene linkages. This molecular structure echoes the archipelago structure suggested for petroleum asphaltenes.

2.6.5. Mesophase versus traditional liquid crystals

Carbonaceous mesophase has some difference with traditional liquid crystals:

1-Traditional liquid crystals are stable products, however, mesophase is an intermediate product which never reaches to equilibrium with the isotropic phase, and continues to develop and grow as long as there remains a liquid phase[61].

2-Carbonaceous mesophase has never been observed in a pure compound[62].

3-Carbonaceous mesophase forms upon heating the pitch; however, traditional liquid crystals can also form upon cooling the isotropic phase[62].

4-Traditional liquid crystals have a strong kinetic signature. The cross linking reactions which happen during the pyrolysis of pitch make the formation of carbonaceous mesophase an irreversible process. As a result, unlike traditional liquid crystals, mesophase does not disappear upon heating to higher temperatures[62].

2.6.6. Suggested mechanisms of mesophase formation

Different theories have been suggested to describe the phenomenon of mesophase formation. In a phase equilibrium model, pitches are considered solutions of mesogenic disc-like molecules in a solvent made of non-mesogenic

smaller molecules, and these disc-like molecules can contribute to mesophase formation[63]. Based on this hypothesis, a pseudo binary phase diagram for mesophase formation analogous to a diagram of a nematic liquid crystal was suggested by Riggs and Diefendorf[63]. In this phase diagram these are 3 regions for isotropic, nematic, and nematic-isotropic phase. The evaporation or solvent extraction of non-mesogenic molecules can shift the composition toward the nematic region, and result in a phase transition of the isotropic phase into nematic phase (mesophase). Mochida et al.[64] mixed the benzene soluble and benzene insoluble fractions of coal tar pitch in various weight ratios, and observed these mixtures using hot-stage microscopy at different temperatures to obtain such a partial phase diagram for mesophase formation.

As mentioned above, a phase separation model for coke formation from petroleum residua was given by Wiehe[31]. In this theory, Wiehe assumed that a phase separation occurs when the concentration of these asphaltene cores exceed their solubility limit in the remaining maltenes, and a new phase containing the excess asphaltene cores separates from the oil phase. Wiehe also assumed that the polynuclear aromatics in the converted asphaltenes cores tend to orient parallel to each other to form carbonaceous mesophase. He assumed that the presence of spherical, ordered particles of carbonaceous mesophase is a direct proof for the formation of coke by a liquid-liquid-phase separation[65]. In other words, he attributed the phenomenon of mesophase formation to a phase separation process.

In colloidal models, pitch is assumed to consist of asphaltene aggregates, as colloidal particles, dispersed in maltenes. The precipitation or flocculation of

these dispersed asphaltene aggregates then results in mesophase formation For example, the model suggested by Storm[66] assumes that asphaltenes are initially dispersed in oil by adsorbing a layer of non-asphaltene molecules. However this protective layer can be dissipated, at higher temperatures, resulting in the flocculation of asphaltenes which can act as the coke precursors.

Marsh et al.[61] suggested that mesophase formation is not a process of crystallization or precipitation, but a process of molecular self-assembly. This theory emphasizes the fact that the mesophase generated during pyrolysis of pitches never reaches to an equilibrium state with the isotropic phase, and mesophase will continue to develop and grow as long as there remained a liquid phase, so processes such as precipitation and crystallization which are normally precisely defined thermodynamically can not be used to describe mesophase formation[67]. In this view, the generation of mesophase is a process of homogeneous self-assembly of aromatic molecules. In conventional liquid crystals the transition from isotropic phase to liquid crystal phase is the result of lowering the temperature which reduces the kinetic energy of the molecules. The average molecular weight of pitch at 200°C is around 200 amu. At this temperature, the translational energy of molecules exceeds the cohesion energy and the pitch remains isotropic. But at temperature above 400°C, the molecular weight increases as a result of cracking and condensation reaction and reaches to 600-900 amu, and a point is reached where the kinetic energy of the molecules is not enough to prevent the association of the molecules by van der Waals forces. These molecules remain attached after a collision. These molecular units grow by

attachment of further liquid crystal molecules (mesogen). These molecular clusters are eventually large enough to be seen by an optical microscope[61, 67]. The thermotropic behavior of conventional liquid crystal cannot be observed in carbonaceous mesophase since polymerization and cross-linking reactions occur between constituent liquid crystal molecules (mesogens), such that the cohesion energies always exceed the translational energies. As a result, with increasing the temperature, mesophase will not transform into the isotropic phase unlike the conventional liquid crystals[61]. A similar theory was suggested by Mochida et al.[68] in which is a self-assembly mechanism is responsible for mesophase formation. Here the planar molecules in the pitch can be stacked by van der Waals forces to form clusters, and the clusters gather to form microdomains. These microdomains ultimately form the textural units macroscopic of mesophase.

2.6.7. Effect of additives and catalyst on mesophase formation

Many authors have examined the influence of solid additives on the nucleation and growth of the mesophase spherules. There are different opinions on the effect of solid additives on mesophase formation. Tillmans et al.[69] has reported that the QI particles in pitch accelerate the mesophase formation as a result of the presence of abundant nuclei. However, Romovacek et al.[70] has found that the QI particles retard the formation of mesophase. On the other hand Stadelhofer[71] reported that the presence of up to 10 wt% QI had no accelerating effect on the rate of mesophase formation during the early stages of pitch carbonization. Brooks and Taylor[52] reported that quinoline insoluble materials particles attach on

the outer surface of mesophase and that pitches with high quinoline insoluble content develop more mesophase spheres, but of small size.

The same phenomenon happens for inorganic catalyst particles, where the catalyst particles usually attach to the outer surface of mesophase spheres[72]. Braun et al.[73] found that the addition of an organic iron compound to coal tar pitch led to products with a high content of mesophase spherules. Iron had an important effect on the nucleation and growth of the mesophase spherules, which was also observed by Marsh et al.[74]. Bernhauer et al.[75] reported that ferric chloride, ferrocene, and iron benzoate and naphthoate promote the formation of mesophase. Alain et al.[76] studied the pyrolysis of coal tar pitch by addition of $FeCl_3$-graphite and reported that it can enhance the formation of mesophase.

2.6.8. Solubility of mesophase

Brooks and Taylor[77] first showed that mesophase spheres could be separated from pitch by dissolving the surrounding isotropic pitch. This observation was probably the origin of the hypothesis of equating mesophase content with the insoluble fraction of pitch in strong solvents like quinoline[78]. An ideal solvent should extract all the isotropic phase without dissolving any of the mesophase material. Chwastiak et al.[79] showed that the amount of mesophase measured by optical microscopy is not necessarily equal to the amount of quinoline, pyridine or toluene insolubles in pitch . They attributed this result to the fact that mesophase can include low-molecular weight components which are still soluble in solvents like toluene or quinoline. Torregrosa-Rodriguez et al.[80] also reported different values for the estimated area of mesophase particles on the polished surface of the

sample, and toluene and 1-methyl-2-pyrrolidinone insolubles in the pyrolysis of petroleum residues. They mentioned that the number of submicron mesophase domains, the mesogen molecules not incorporated into mesophase, and the large amount as side-chains in molecules are the factors that can cause such a difference. In summary, solubility methods are not an attractive way to measure the amount of mesophase, and one must rely on optical microscopy.

2.6.9. Coke versus mesophase

Mesophase is traditionally defined by its optical properties rather than its solubility[35]. Wang et al.[81] showed that in some cases the toluene-insoluble coke from thermal cracking can be completely soluble in quinoline, which does not conform to the commonly held view that carbonaceous mesophase is not completely soluble in any solvents[82]. As discussed above, one cannot rely on solubility results to measure the amount of mesophase. Even if you want to use the solubility results, then mesophase can be regarded as a subset of coke as a toluene insoluble material, which is also quinoline insoluble, and mesophase and coke are not identical phases.

2.6.10. Limits of mesophase detection

As mentioned before, mesophase was first discovered by Brooks and Taylor[35] using polarized microscopy and defined based on its optical anisotropy. With this definition the optical birefringence has been used as a main characteristic of carbonaceous mesophase, and hot-stage microscopy is usually regarded as the most powerful technique for the characterization of mesophase. However, there is

a limit of detection for using an optical microscope in terms of its resolution. It Mesophase is a liquid crystalline phase that can exist even if it is not visible in the optical microscope. Domains of mesophase smaller that 0.5 μm can exist in the pitch and such a sample may appear to be isotropic when viewed under the optical microscope[36].

Domains of mesophase smaller than 0.1 μm in size have been detected using scanning electron microscopy (SEM)[83]. In addition transmission electron microscopy (TEM)[84-85] has been used to detect units of mesophase of size of less than 0.1 micron. However, TEM techniques cannot be used to study the *in situ* mesophase formation inside a reactor. A technique which can show the *in situ* interaction of molecules during the early stages of pyrolysis is needed to reveal the mechanisms of mesophase formation. The current knowledge of the carbonization process is incomplete, and the exact behavior of pitches during pyrolysis which leads to mesophase formation is not still well understood. That is because there is not an appropriate method to reveal the details of this phenomenon *in situ*. In addition there is no practical way to define the true onset of mesophase formation, and say when it starts to exist in the pitch.

2.7. References

1. Speight, J. G., The Chemistry and Technology of Petroleum. 4th ed.; CRC Press, Taylor and Francis Group: Boca Raton, 2006.
2. Gray, M. R., Upgrading Petroleum Residues and Heavy Oils. Marcel Dekker Inc.: New York, 1994.

3. Hughey, C. A.; Rodgers, R. P.; Marshall, A. G., Resolution of 11,000 Compositionally Distinct Components in a Single Electrospray Ionization Fourier Transform Ion Cyclotron Resonance Mass Spectrum of Crude Oil. Anal. Chem. 2002, 74, 4145-4149.
4. Kharrat, A. M.; Zacharia, J.; Cherian, V. J.; Anyatonwu, A., Issues with Comparing SARA Methodologies. Energy Fuels 2007, 21, (6), 3618-3621.
5. Ancheyta, J.; Speight, J. G., Hydroprocessing of Heavy Oils and Residua. CRC Press: Boca Raton, 2007.
6. Wiehe, I. R., Process Chemistry of Petroleum Macromolecules 1st ed.; CRC Press: Boca Raton, 2008.
7. Qian, K. N.; Edwards, K. E.; Siskin, M.; Olmstead, W. N.; Mennito, A. S.; Dechert, G. J.; Hoosain, N. E., Desorption and ionization of heavy petroleum molecules and measurement of molecular weight distributions. Energy Fuels 2007, 21, (2), 1042-1047.
8. Akbarzadeh, K.; Dhillon, A.; Svrcek, W. Y.; Yarranton, H. W., Methodology for the characterization and modeling of asphaltene precipitation from heavy oils diluted with n-alkanes. Energy Fuels 2004, 18, (5), 1434-1441.
9. Agrawala, M.; Yarranton, H. W., An asphaltene association model analogous to linear polymerization. Ind. Eng. Chem. Res. 2001, 40, (21), 4664-4672.
10. Groenzin, H.; Mullins, O. C., Molecular Size and Structure of Asphaltenes from Various Sources. Energy Fuels 2000, 14, (3), 677-684.

11. Strausz, O. P.; Mojelsky, T. W.; Lown, E. M., The Molecular-Structure of Asphaltene - an Unfolding Story. Fuel 1992, 71, (12), 1355-1363.

12. Pelet, R.; Behar, F.; Monin, J. C., Resins and Asphaltenes in the Generation and Migration of Petroleum. Org. Geochem. 1986, 10, (1-3), 481-498.

13. Sheremata, J. M.; Gray, M. R.; Dettman, H. D.; McCaffrey, W. C., Quantitative Molecular Representation and Sequential Optimization of Athabasca Asphaltenes. Energy Fuels 2004, 18, (5), 1377-1384.

14. Karimi, A.; Qian, K. N.; Olmstead, W. N.; Freund, H.; Yung, C.; Gray, M. R., Quantitative Evidence for Bridged Structures in Asphaltenes by Thin Film Pyrolysis. Energy Fuels 25, (8), 3581-3589.

15. Speight, J. G., Petroleum Asphaltenes - Part 1 - Asphaltenes, Resins and the Structure of Petroleum. Oil Gas Sci. Technol. - Rev. IFP 2004, 59, (5), 467-477.

16. Calemma, V.; Iwanski, P.; Nali, M.; Scotti, R.; Montanari, L., Structural Characterization of Asphaltenes of Different Origins. Energy Fuels 1995, 9, (2), 225-230.

17. Payzant, J. D.; Lown, E. M.; Strausz, O. P., Structural Units of Athabasca Asphaltene - the Aromatics with a Linear Carbon Framework. Energy Fuels 1991, 5, (3), 445-453.

18. Liao, Z. W.; Zhao, J.; Creux, P.; Yang, C. P., Discussion on the Structural Features of Asphaltene Molecules. Energy Fuels 2009, 23, 6272-6274.

19. Gray, M. R., Consistency of Asphaltene Chemical Structures with Pyrolysis and Coking Behavior. Energy Fuels 2003, 17, (6), 1566-1569.

20. Speight, J. G., The Chemistry and Physics of Coking. Korean J. Chem. Eng. 1998, 15, (1), 1-8.

21. Miki, Y.; Yamadaya, S.; Oba, M.; Sugimoto, Y., Role of Catalyst in Hydrocracking of Heavy Oil. J. Catal. 1983, 83, (2), 371-383.

22. Carbonell, M. M.; Guirardello, R., Modelling of a Slurry Bubble Column Reactor Applied to the Hydroconversion of Heavy Oils. Chem. Eng. Sci. 1997, 52, 4179-4185.

23. Del Bianco, A.; Panariti, N.; Dicarlo, S.; Beltrame, P., New Developments in Deep Hydroconversion of Heavy Oil Residues with Dispersed Catalysts. 2. Kinetic Aspects of Reaction. Energy Fuels 1994, 8, 593-597

24. Pruden, B.; Denis, J. M.; Muir, G., Upgrading of Cold Lake Heavy Oil in the CANMET Hydrocracking Demonstration Plantprocess. In 4th ITAR/UNDP Conf. Heavy Crude Tar Sands, Edmonton, 1989.

25. Furimsky, E.; Massoth, F. E., Deactivation of Hydroprocessing Catalysts. Catal. Today 1999, 52, (4), 381-495.

26. Bartholomew, C. H., Catalyst Deactivation in Hydrotreating of Residua: A Review. In Catalytic Hydroprocessing of Petroleum and Distillates, Oballa, M. C.; Shih, S. S., Eds. Marcel Dekker: New York, 1994.

27. Watkinson, A. P.; Wilson, D. I., Chemical Reaction Fouling: A Review. Exp. Therm Fluid Sci. 1997, 14, (4), 361-374.

28. Magaril, R. Z.; Aksenova, E. I., Study of Mechanism of Coke Formation in Cracking of Petroleum Resins. Int. Chem. Eng. 1968, 8, (4), 727-729.

29. Shaw, J. M.; Gaikwad, R. P.; Stowe, D. A., Phase Splitting of Pyrene-Tetralin Mixtures under Coal-Liquefaction Conditions. Fuel 1988, 67, (11), 1554-1559.

30. Abedi, S. J.; Seyfaie, S.; Shaw, J. M., Unusual Retrograde Condensation and Asphaltene Precipitation in a Model Heavy Oil System. Pet. Sci. Technol. 1998, 16, (3-4), 209-226.

31. Wiehe, I. A., A Phase-Separation Kinetic-Model for Coke Formation. Ind. Eng. Chem. Res. 1993, 32, (11), 2447-2454.

32. Rahmani, S.; McCaffrey, W.; Gray, M. R., Kinetics of Solvent Interactions with Asphaltenes during Coke Formation. Energy Fuels 2002, 16, (1), 148-154.

33. Collings, P. J.; Hird, M., Introduction to Liquid Crystals: Chemistry and Physics. . Taylor and Francis: London, 1997.

34. Oswald, P.; Pieranski, P., Nematic and Cholesteric Liquid Crystals. CRC Press: Boca Raton, 2005.

35. Brooks, J. D.; Taylor, G. H., Formation of Graphitizing Carbons from Liquid Phase. Nature 1965, 206, (4985), 697-699.

36. Marsh, H.; Latham, C. S., The Chemistry of Mesophase Formation. Am. Chem. Soc., Symp. Ser. 1986, 303, 1-28.

37. Khoo, I.-C., Liquid Crystals. 2nd ed.; Wiley-Interscience: New Jersey, 2007.

38. Dierking, I., Textures of Liquid Crystals. Wiley-VCH: Weinheim, 2003.

39. Corcoran, J.; Fuller, S.; Rahman, A.; Shinde, N.; Tiddy, G. J. T.; Attard, G. S., Amphitropi Liquid Crystals 1. Effect of a Thermotropic Mesogen on Lyotropic Mesomorphism, and of a Surfactant on Thermotropic Mesomorphism. The C16EO8-5-CB-Water System. J. Mater. Chem. 1992, 2, (7), 695-702.

40. Hecht, E., Optics. 4th ed.; Addison Wesley: Reading, MA, 2001.

41. Taylor, G. H., Development of Optical Properties of Coke during Carbonization. Fuel 1961, 40, (6), 465-472.

42. Honda, H., Carbonaceous Mesophase-History and Prospects. Carbon 1988, 26, (2), 139-156.

43. Hurt, R. H.; Hu, Y., Thermodynamics of Carbonaceous Mesophase. Carbon 1999, 37, (2), 281-292.

44. Singer, L. S., The Mesophase in Carbonaceous Pitches. Faraday Discuss. 1985, 79, 265-272.

45. Yoon, S. H.; Korai, Y.; Mochida, I., Spinning Characteristics of Mesophase Pitches Derived from Naphthalene and Methylnaphthalene with HF/BF3. Carbon 1993, 31, (6), 849-856.

46. Yamada, Y.; Imamura, T.; Kakiyama, H.; Honda, H.; Oi, S.; Fukuda, K., Characteristics of Meso-Carbon Microbeads Separated from Pitch. Carbon 1974, 12, (3), 307-319.

47. Chang, Y. C.; Sohn, H. J.; Ku, C. H.; Wang, Y. G.; Korai, Y.; Mochida, I., Anodic Performances of Mesocarbon Microbeads (MCMB) Prepared from Synthetic Naphthalene Isotropic Pitch. Carbon 1999, 37, (8), 1285-1297.

48. Rahimi, P.; Gentzis, T.; Dawson, W. H.; Fairbridge, C.; Khulbe, C.; Chung, K.; Nowlan, V.; DelBianco, A., Investigation of Coking Propensity of Narrow Cut Fractions from Athabasca Bitumen Using Hot-Stage Microscopy. Energy Fuels 1998, 12, (5), 1020-1030.

49. Nowlan, V. J.; Srinivasan, N. S., Control of Coke Formation from Hydrocracked Athabasca Bitumen. Fuel Sci. Technol. Int. 1996, 14, (1-2), 41-54.

50. Nandi, B. N.; Belinko, K.; Pruden, B. P.; J.M., D., Microscopic Studies for Structure of Coke Formed during Thermal Hydrocracking of Athabasca Bitumen. Prepr. Pap.s Am. Chem. Soc., Div. Pet. Chem. 1977, 22, (2), 733-738.

51. Munoz, V. A.; Ghorpadkar, S. V.; Gray, M. R., Characterization of Coke on Spent Hydroprocessing Catalysts by Optical Microscopy. Energy Fuels 1994, 8, (2), 426-434.

52. Brooks, J. D.; Taylor, G. H., The Formation of Graphitizing Carbons from the Liquid Phase. Carbon 1965, 3, (2), 185-193.

53. Auguie, D.; Oberlin, M.; Oberlin, A.; Hyvernat, P., Microtexture of Mesophase Spheres as Studied by High-Resolution Conventional Transmission Electron-Microscopy (CTEM). Carbon 1980, 18, (5), 337-346.

54. Imamura, T.; Yamada, Y.; Oi, S.; Honda, H., Orientation Behavior of Carbonaceous Mesophase Spherules Having a New Molecular Arrangement in a Magnetic-Field. Carbon 1978, 16, (6), 481-486.

55. Kovac, C. A.; Lewis, I. C., Magnetic Orientation Studies of Synthetic Mesophase Pitches. Carbon 1978, 16, (6), 433-437.

56. Imamura, T.; Nakamizo, M.; Honda, H., Formation of Crbonaceous Mesophase at Lower Temperature. Carbon 1978, 16, (6), 487-490.

57. Hurt, R.; Krammer, G.; Crawford, G.; Jian, K. Q.; Rulison, C., Polyaromatic assembly mechanisms and structure selection in carbon materials. Chem. Mater. 2002, 14, (11), 4558-4565.

58. Inagaki, M., Discussion of the formation of nanometric texture in spherical carbon bodies. Carbon 1997, 35, (5), 711-713.

59. Mochida, I.; Maeda, K.; Takeshita, K., Comparative-Study of the Chemical-Structure of the Disk-Like Components in the Quinoline Insolubles. Carbon 1978, 16, (6), 459-467.

60. Zimmer, J. E.; White, J. L., Disclination Structures in the Carbonaceous Mesophase. Adv. Liq. Cryst. 1982, 5, 157-213.

61. Marsh, H.; Menendez, R., Mechanisms of Formation of Isotropic and Anisotropic Carbons. In Introductio to Carbon Science, Marsh, H., Ed. Butterworths: London, 1989; pp 37-73.

62. Hurt, R. H.; Chen, Z. Y., Liquid Crystals and Carbon Materials. Phys. Today 2000, 53, (3), 39-44.

63. Riggs, D. M.; Diefendorf, R. J., A Phase Diagram for Pitches. In Carbon '80., Baden-Baden 1980; pp 326-329.

64. Mochida, I.; Korai, Y., Chemistry for Preparation of Mesophase Pitches and Design of their Properties Nenryo Kyokaishi 1985, 64, (10), 796-808.

65. Gould, K. A.; Wiehe, I. A., Natural Hydrogen Donors in Petroleum Resids. Energy Fuels 2007, 21, (3), 1199-1204.

66. Storm, D. A.; Barresi, R. J.; Sheu, E. Y., Flocculation of Asphaltenes in Heavy Oil at Elevated Temperatures. Fuel Sci. Technol. Int. 1996, 14, (1-2), 243-260.

67. Marsh, H.; M.A., D., Mesophase of Graphitizable Carbons. In Liquid Crystalline and Mesomorphous Polynzers, Shibaev, V. P.; Lam, L., Eds. Springe: New York, 1993; pp 231-257

68. Mochida, I.; Korai, Y.; Ku, C. H.; Watanabe, F.; Sakai, Y., Chemistry of Synthesis, Structure, Preparation and Application of Aromatic-Derived Mesophase Pitch. Carbon 2000, 38, (2), 305-328.

69. Tillmanns, H.; Pietzka, G.; Pauls, H., Influence of Quinoline-Insoluble Matter in Pitch on Carbonization Behavior and Structure of Pitch Coke. Fuel 1978, 57, (3), 171-173.

70. Romovacek, G. R.; McCullough, J. P.; Perrotta, A. J., Formation of Measophase in Coal-Tar Pitches - Influence of Pyrolytic Carbon Particles. Fuel 1983, 62, (10), 1236-1238.

71. Stadelhofer, J. W., Examination of the Influence of Natural Quinoline-Insoluble Material on the Kinetics of Mesophase Formation. Fuel 1980, 59, (5), 360-361.

72. Marsh, H.; Martinez-Escandell, M.; Rodriguez-Reinoso, F., Semicokes from Pitch Pyrolysis: Mechanisms and Kinetics. Carbon 1999, 37, (3), 363-390.

73. Braun, M.; Kramer, J.; Huttinger, K. J., Kinetics of Mesophase Formation in a Stirred-Tank Reactor and Properties of the Products .6. Catalysis by Iron Benzoate and Naphthoate. Carbon 1995, 33, (10), 1359-1367.

74. Marsh, H.; Foster, J. M.; Hermon, G.; Iley, M., Carbonization and Liquid-Crystal (Mesophase) Development .2. Co-Carbonization of Aromatic and Organic-Dye Compounds, and Influence of Inerts. Fuel 1973, 52, (4), 234-242.

75. Bernhauer, M.; Braun, M.; Huttinger, K. J., Kinetics of Mesophase Formation in a Stirred-Tank Reactor and Properties of the Products .5. Catalysis by Ferrocene. Carbon 1994, 32, (6), 1073-1085.

76. Alain, E.; Begin, D.; Furdin, G.; Mareche, J. F., Effect of Graphite or FeCl3-Graphite Intercalation Compounds on the Mesophase Development in Coal Tar Pitch. Carbon 1996, 34, (5), 619-626.

77. Brooks, J. D.; G.H., T., The Formation of some Graphitizing Carbons Chem. Phys. Carbon 1968, 4, 243.

78. Mochida, I.; Oyama, T.; Korai, Y.; Fei, Y. Q., Study of Carbonization using a Tube Bomb - Evaluation of Lump Needle Coke, Carbonization Mechanism and Optimization. Fuel 1988, 67, (9), 1171-1181.

79. Chwastiak, S.; Lewis, I. C., Solubility of Mesophase Pitch. Carbon 1978, 16, (2), 156-157.

80. Torregrosa-Rodriguez, P.; Martinez-Escandell, M.; Rodriguez-Reinoso, F.; Marsh, H.; de Salazar, C. G.; Palazon, E. R., Pyrolysis of Petroleum Residues II. Chemistry of Pyrolysis. Carbon 2000, 38, (4), 535-546.

81. Wang, S.; Chung, K.; Masliyah, J. H.; Gray, M. R., Toluene-Insoluble Fraction from Thermal Cracking of Athabasca Gas Oil: Formation of a Liquid-in-Oil Emulsion that Wets Hydrophobic Dispersed Solids. Fuel 1998, 77, (14), 1647-1653.

82. Oberlin, A.; Bonnamy, S.; Rouxhet, P. G., Colloidal and Supramolecular Aspects of Carbon. In Chemistry and Physics of Carbon, Vol 26, Marcel Dekker: New York, 1999; Vol. 26, pp 1-148.

83. Qian, Z.; Clarke, D. E.; Marsh, H., Structure in Cokes from Coals of Different Rank. Fuel 1983, 62, (9), 1084-1089.

84. Lafdi, K.; Bonnamy, S.; Oberlin, A., TEM Studies of Coal Tars Influence of Distillation Process at Increasing Temperature. Carbon 1990, 28, (5), 631-640.

85. Oberlin, A., High Resolution TEM Studies of Carbonization and Graphitization. In Chemistry and Physics of Carbon, Marcel Dekker: New York, 1989; Vol. 22, pp 1-143.

3. Hot-stage reactor design

3.1. Introduction

The formation of mesophase can be studied by various methods such as nuclear magnetic resonance (NMR) spectroscopy[1], Raman spectroscopy[2], solvent fractionation, gel permeation chromatography[3], high-resolution transmission electron microscopy[4], hot-stage X-ray diffraction[5], and optical microscopy[6]. Hot-stage microscopy is a powerful technique for the characterization of liquid crystals, together with differential scanning calorimetry (DSC) and x-ray investigations. DSC is a fast and easy technique, but it merely provides information on phase transition temperatures and the order of the transitions. X-ray diffraction investigations can be used for structural evaluation, but the results only allow limited characterization of the structural features. Polarizing optical microscopy is capable of the determination of both phase transition temperatures and phase type, and can be used to observe the mesophase growth at the temperature of formation[7]. Hot-stage microscopy is a combination of a furnace, a temperature controller and a polarizing optical microscope between crossed polarizers[8]. It allows the visual observation of samples subjected to a temperature program. Hot-stage microscopy has been used since the early 1970s to study the mesophase formation and hydrocracking reactivity of heavy oil and bitumen feedstocks.

3.2. Preceding work

Hot-stage microscopy has been used to study the crystallization of polymers[9]. Onsager[10] predicted that rigid rod-like macromolecules should form liquid crystalline phase. However, it was not until 1975 that the first observation of a thermotropic liquid crystalline polymer was reported[11].

Lewis[12] did the first *in situ* observations of mesophase formation In 1975 using a modified hot-stage with a glass cover. In this design a metal probe was inserted into the hot-stage chamber to agitate the sample. Perrotta et al.[13] built a custom-made hot-stage reactor to observe the *in situ* mesophase formation in petroleum and coal tar pitch at elevated temperatures and pressures. Rodriguez et al.[14] used another high pressure high temperature hot-stage to observe the *in situ* mesophase formation in petroleum fractions. Rahimi et al.[15] at NCUT investigated the incipient mesophase formation of 10 narrow cut fractions from Athabasca bitumen vacuum bottoms using a modified version of Perrotta's design. Figure 3-1 shows a schematic setup of Rahimi et al.[15] design. They put the sample in aluminum cups which carefully placed into the hot-stage cell and covered by a set of soft copper O-rings and a YAG (yttrium-aluminum-garnet) crystal as the viewport. They used a stream of hydrogen and a reflective microscope with crossed polarizers to observe the mesophase formation. It is important to notice that in all of these designs the samples were not subjected to stirring. The only exception was the Lewis's design[12] which used a probe as simple agitator.

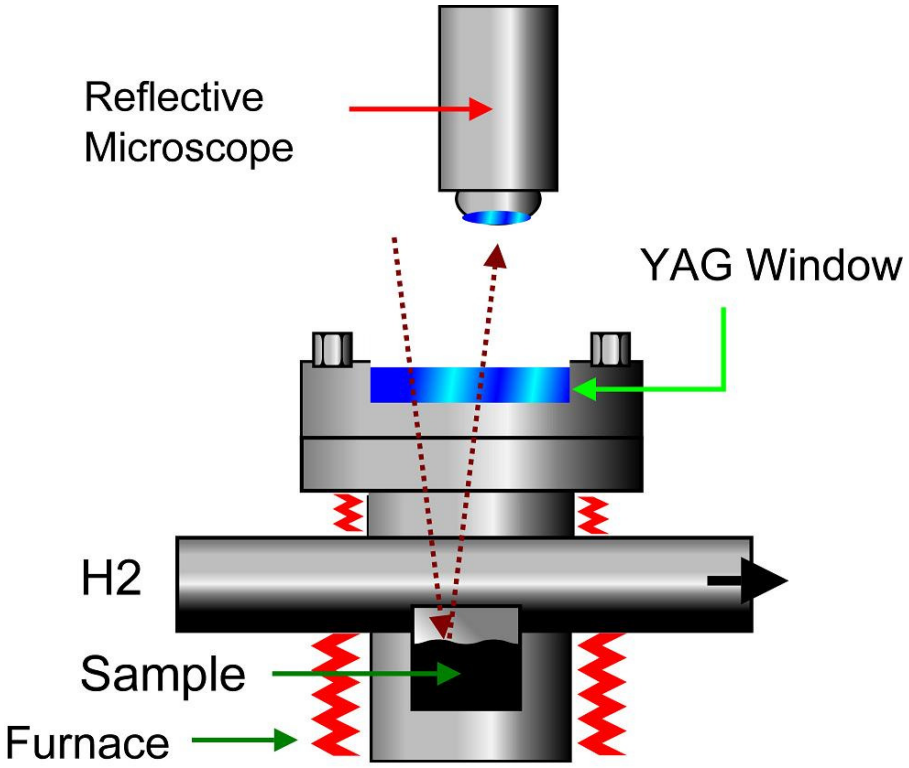

Figure 3-1. The hot-stage design used by Rahimi et al.15.

3.2.1. Experimental limitations

The hot-stage reactor used by Rahimi et al.[15] had some experimental limitations which can be summarized here:

1. Due to the forced convection with hydrogen and the natural convection with YAG window the temperature was not uniform through the sample. The thermal contact resistance between the aluminum cup and the cell walls made the heat transfer even worse. A new design with better heat transfer can overcome this problem.

2. Gas condensation on the cold YAG window made the observations difficult. Using a better design with improved heat transfer can solve this problem.

3. Due to the surface tension, the samples dispersed toward the edge of the cup, and formed a thicker layer near the edges and a thinner layer in the center. As a result, the coke texture near the center of the cup holder was different than at the margins. This problem can be solved if the sample could be agitated during the experiment, or if more liquid is present in the sample.

4. For most of the fractions, reproducing the times of incipient mesophase formation was not possible. Rahimi et al.[15] attributed this problem to differential volatilization, which resulted in different amounts of refractory material left behind at different time intervals. However, the poor heat transfer between the cup and the heater seems to be a better explanation for this problem. Agitation or a better design with improved heat transfer of the sample during heat treatment can improve the reproducibility considerably.

3.3. Transmission versus reflective microscopy

Before designing the hot-stage reactor, the type of microscope which will be used for mesophase observations must be determined. That's because each microscope needs a different optical set-up for the hot-stage reactor. When using a reflective microscope, you only see the surface of the sample, so the thickness of sample does not limit the observation. However, the transmission microscope is confined by the thickness of the sample. That is because vacuum residue is an opaque material which allows the light to pass through only in very thin samples. In order to find the maximum thickness of sample for a transmission microscope, a few samples of vacuum residue with deferent thicknesses were made, and theses

samples were observed under a transmission microscope as shown in Figure 3-2. From these observations, it was obvious that the maximum thickness of sample is approximately 50 microns. The practical problems of preparing such a thin sample led us to abandon the idea of using a transmission microscope, and select the reflective microscope as the best option for the hot-stage microscopy.

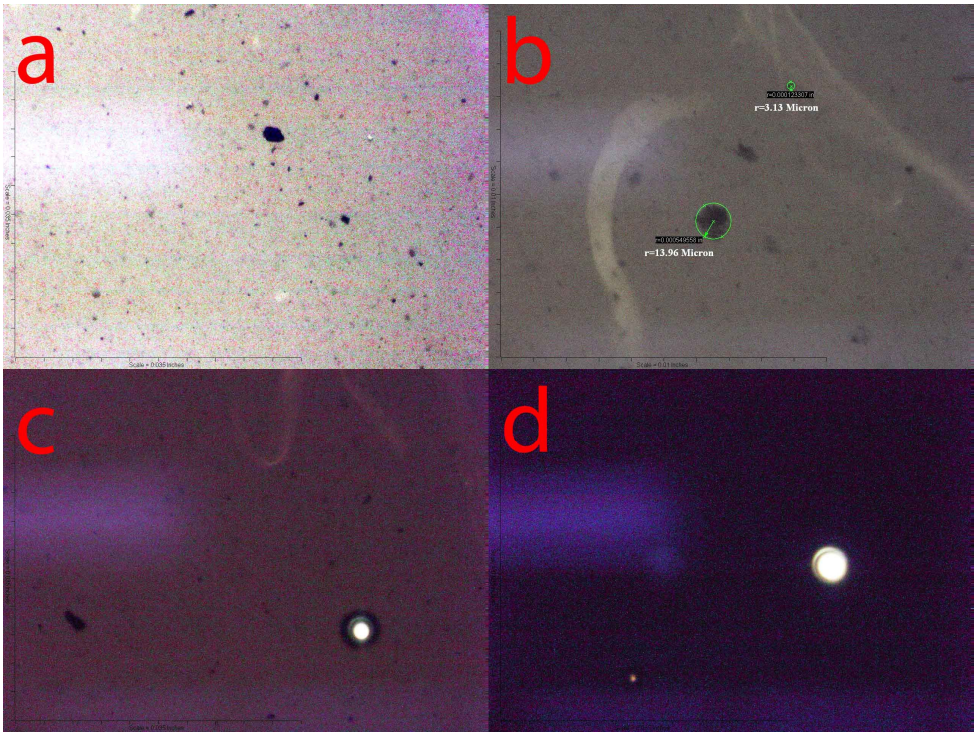

Figure 3-2. Athabasca bitumen vacuum bottom under transmission microscope: (a) Sample thickness- 20 Micron, magnification -200 (b) Sample thickness- 40 Micron, magnification -400 (c) Sample thickness- 50 Micron, magnification -200 (d) Sample thickness- 60 Micron, magnification -100.

3.4. Designing the hot-stage reactor

To overcome the limitations of the previous design of Rahimi et al.[15], a new hot-stage reactor was designed which can improve heat transfer in the sample significantly. Figure 3-3 shows a schematic setup of our new design. In the new design the hot-stage works with an inverted reflective microscope. In inverted microscopes the objective lens is placed under the cell. As a result, there will be no gap between the sample and the view port. The new design uses sapphire instead YAG as the window, which is a better heat conductor and can withstand higher pressures and temperatures. No aluminum cup is used to hold the sample which leads to better heat transfer. In addition the window is heated to improve the heat transfer.

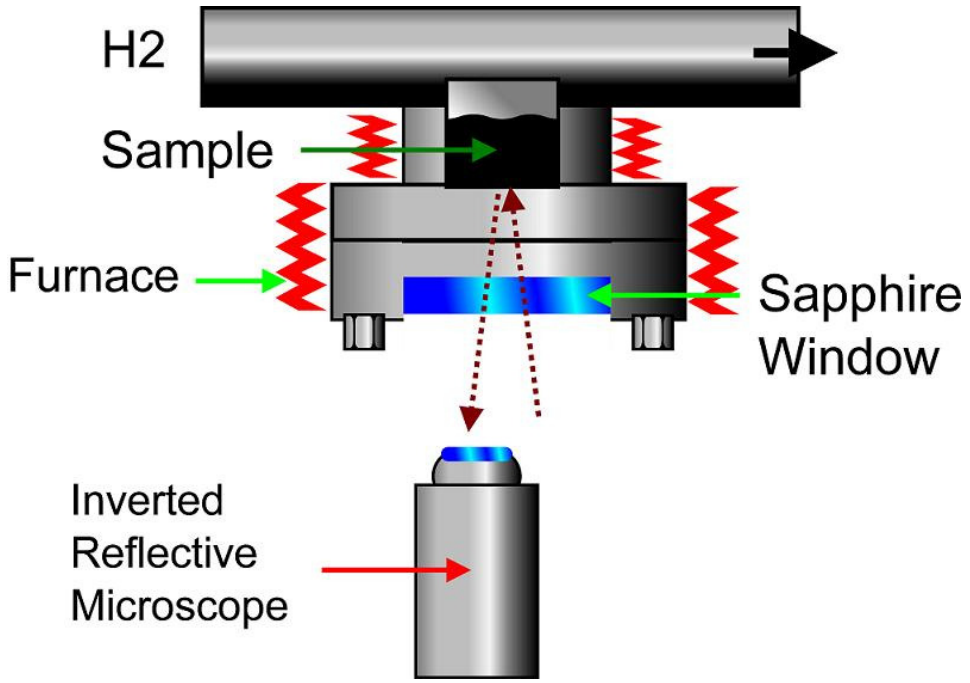

Figure 3-3. Schematic setup the new hot-stage design for inverted microscope.

3.4.1. Simulation results

Computer simulations were done to compare the performance of a traditional hot-stage compatible with an upright microscope (like Rahimi et al.[15] design) with our new design in terms of heat transfer. COMSOL Multiphysics was used to do the simulations. For hydrogen flow 2D, steady-state incompressible Navier-Stokes equations coupled with the heat equation for convection were used, and for hot-stage cell and bitumen film inside only conduction effects were considered. The heat of reaction and mass transfer effects were neglected. Figure 3-4 shows the geometry, materials, and boundary conditions used in the traditional design compatible with an upright microscope, and Figures 3-5 and 3-6 show the simulation results in terms of the temperature distribution inside the view cell.

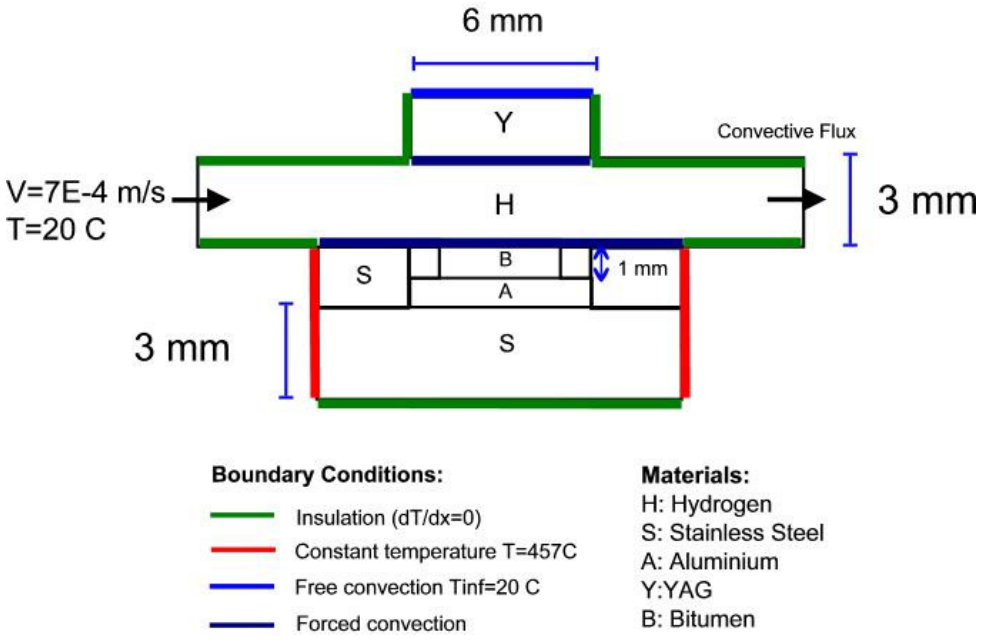

Figure 3-4. Geometry, materials, and boundary conditions used in simulations for a traditional hot-stage compatible with an upright microscope.

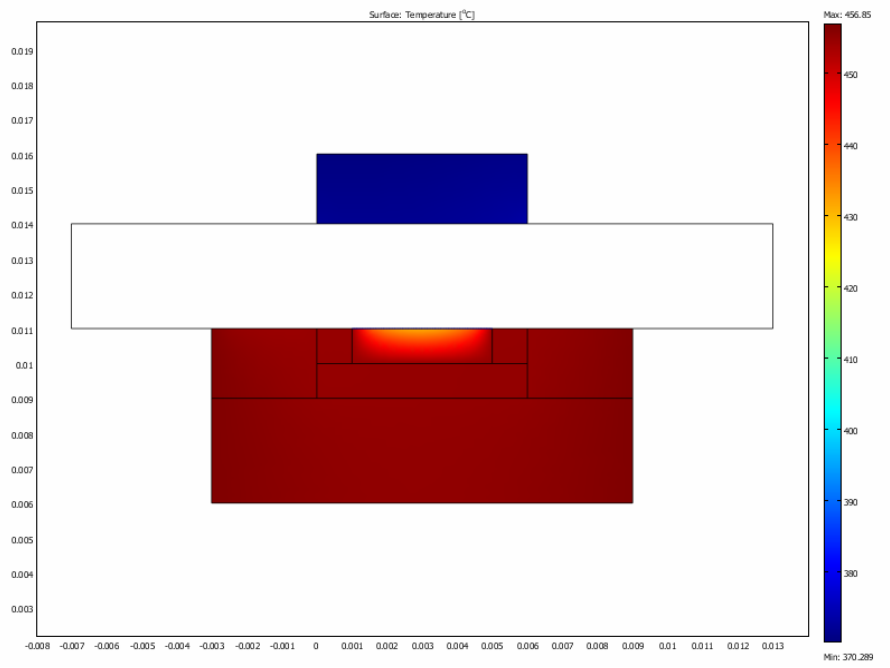

Figure 3-5. Simulation results for the traditional hot-stage compatible with an upright microscope: temperature distribution in the view cell.

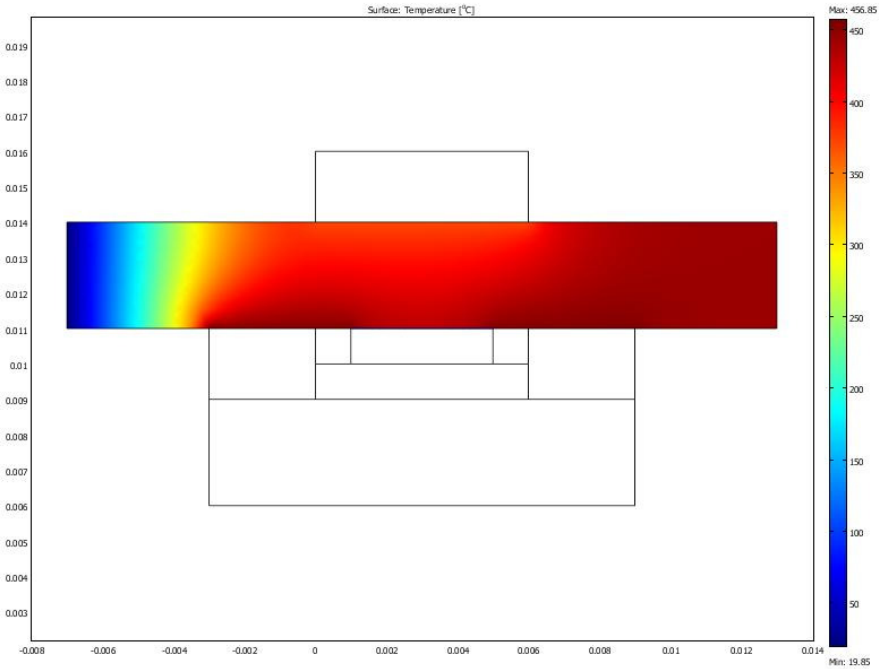

Figure 3-6. Simulation results for the traditional hot-stage compatible with an upright microscope: temperature distribution of hydrogen inside the view cell.

Figure 3-7 shows the results of simulations which include the horizontal and vertical thermal distribution inside the sample. Similarly Figure 3-8 shows the geometry, materials, and boundary conditions used in the new design. To have a better comparison, the window was assumed to be made of YAG in both designs. Figures 3-9 and 3-10 show the simulation results in terms of the temperature distribution inside the new view cell. Figure 3-11 shows the results of simulations which include the horizontal and vertical thermal distribution inside the sample. In the traditional design the temperature difference is nearly 25°C while in the new design it is less than 0.1°C which is significantly better. The difference is mainly attributed to the heat convection by YAG window which causes a huge heat loss in the traditional design. However, in our new design the hot surface (window) is above the air which can suppress the natural convection significantly.

3.5. Hot-stage reactor

In previous hot-stage designs, samples were first placed in metal cups made of stainless steel or aluminium, and the cups were placed into the hot-stage cell which was covered by a glass[12], spinel[14] or YAG[15] (yttrium-aluminium-garnet) crystal as the viewport. In such a configuration, there was a gap between the top surface of the sample and the viewport. The top surface of the sample is then observed with an upright reflective microscope during the heat treatment. As mentioned before, this design has several drawbacks. First, the viewport which is in direct contact with the outside air will be colder that the sampler during reaction and condensation on the cold window makes the observations difficult.

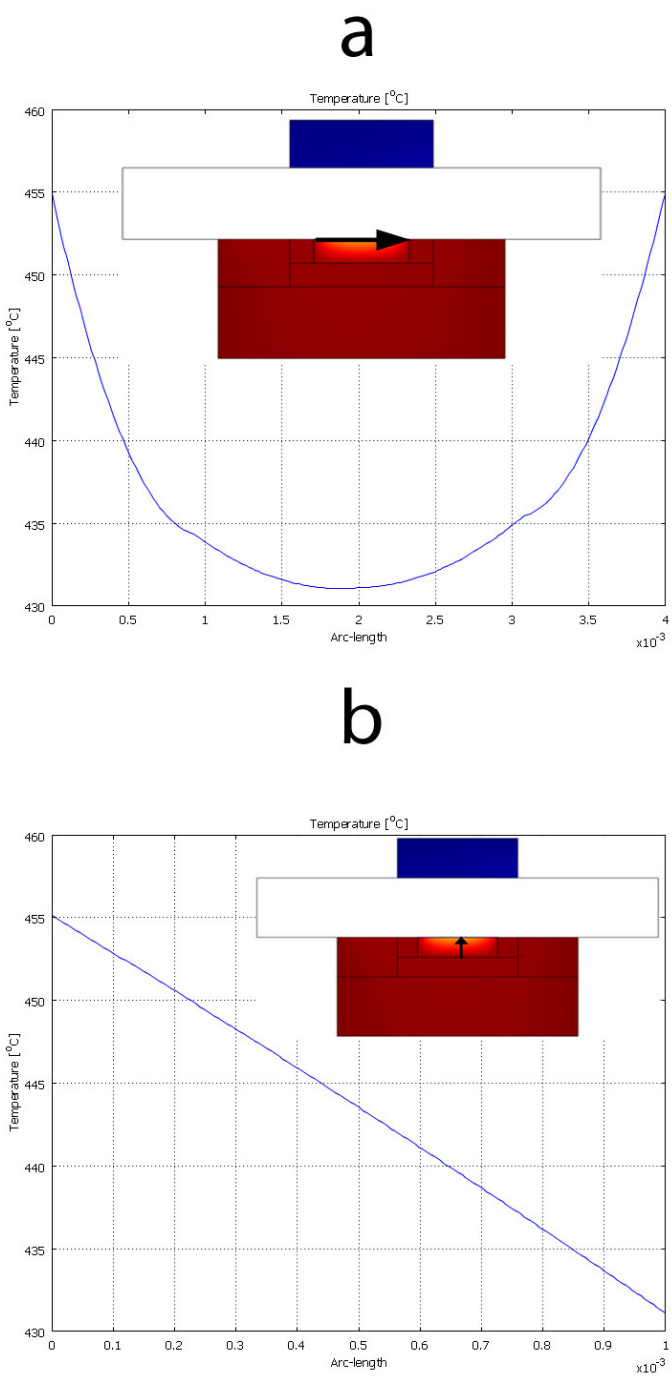

Figure 3-7. Simulation results for the horizontal (a) and vertical (b) temperature distribution inside the sample in the traditional hot-stage compatible with an upright microscope. The horizontal axis of the graph shows the distance along the arrow shown in the small panel inside the graph.

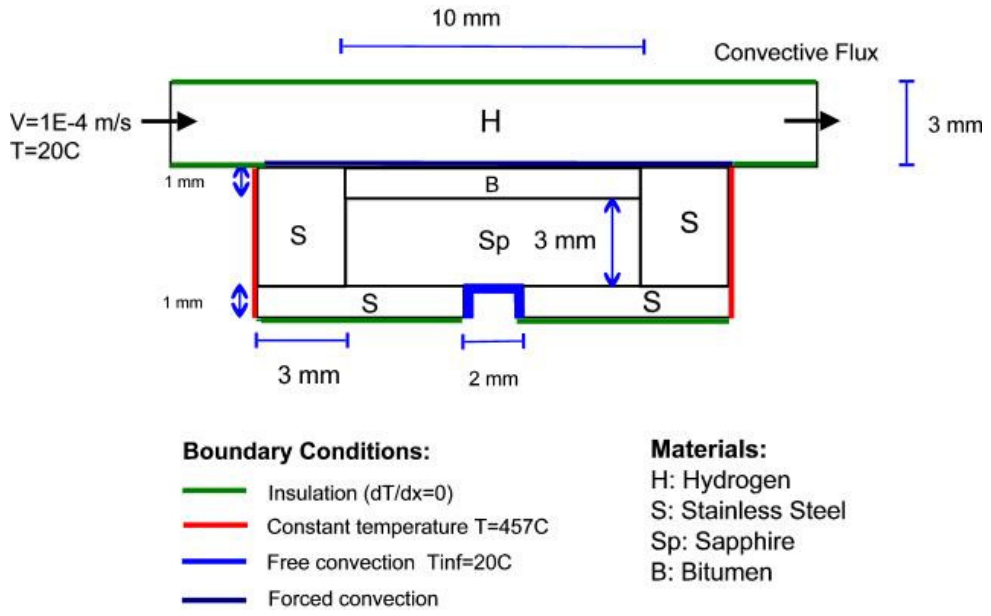

Figure 3-8. Geometry, materials, and boundary conditions used in simulations for the new design.

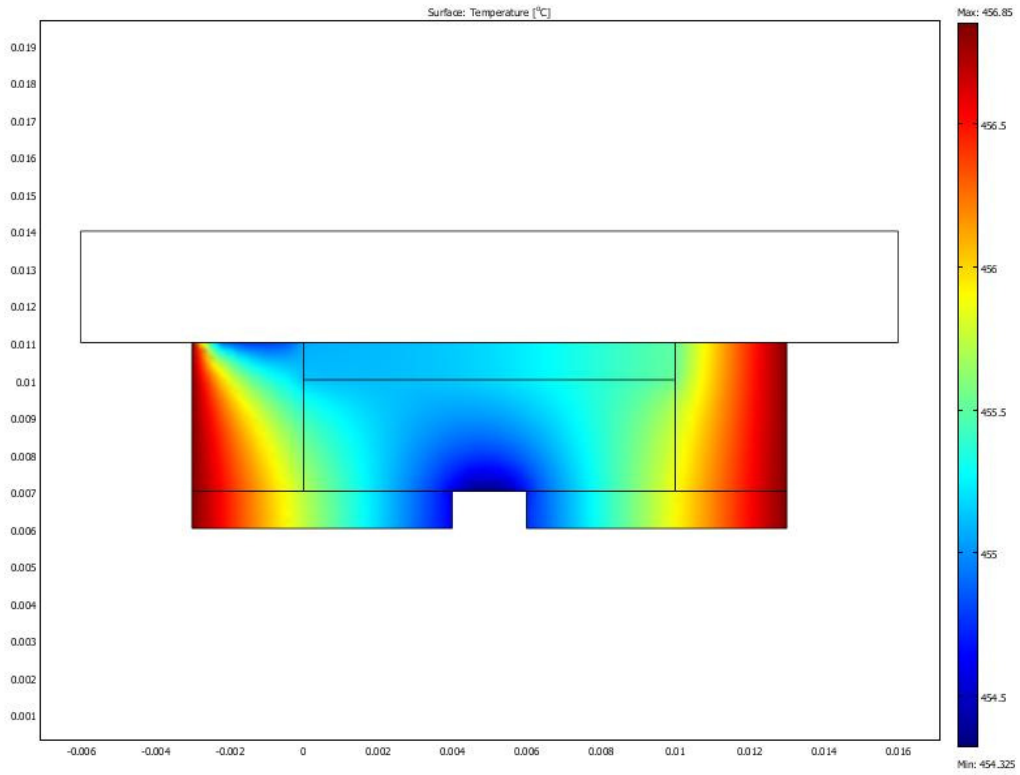

Figure 3-9. Simulation results for the new design: temperature distribution in the view cell.

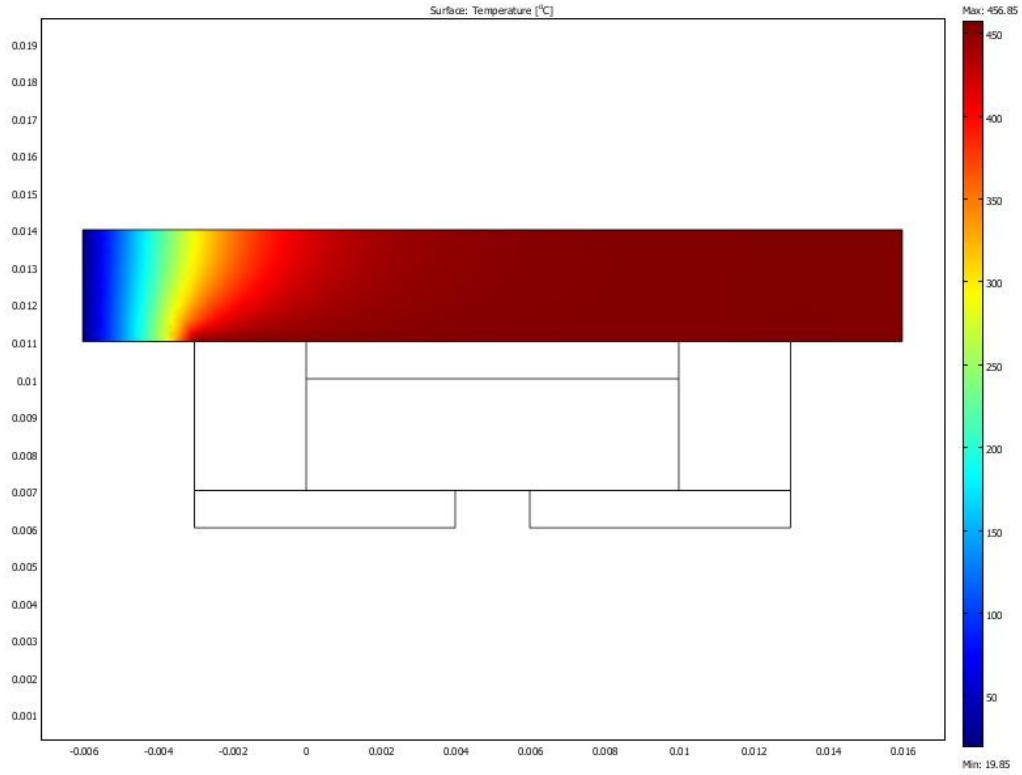

Figure 3-10. Simulation results for the new design: temperature distribution of hydrogen inside the view cell.

a

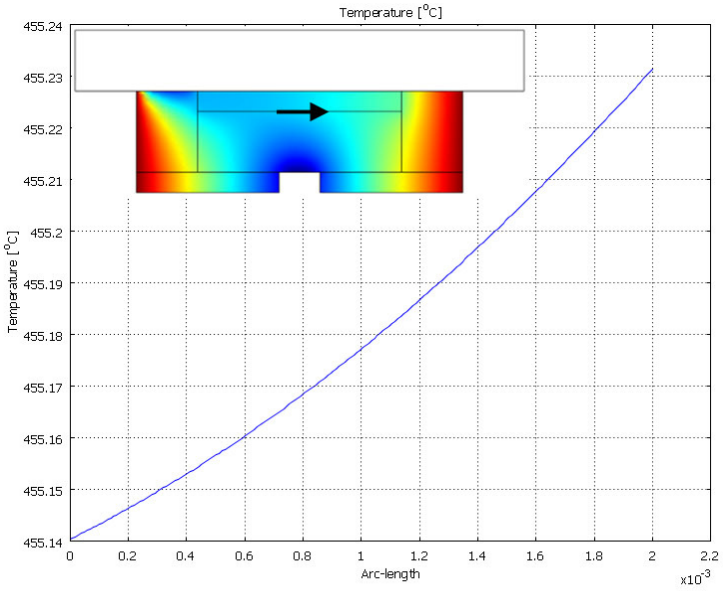

b

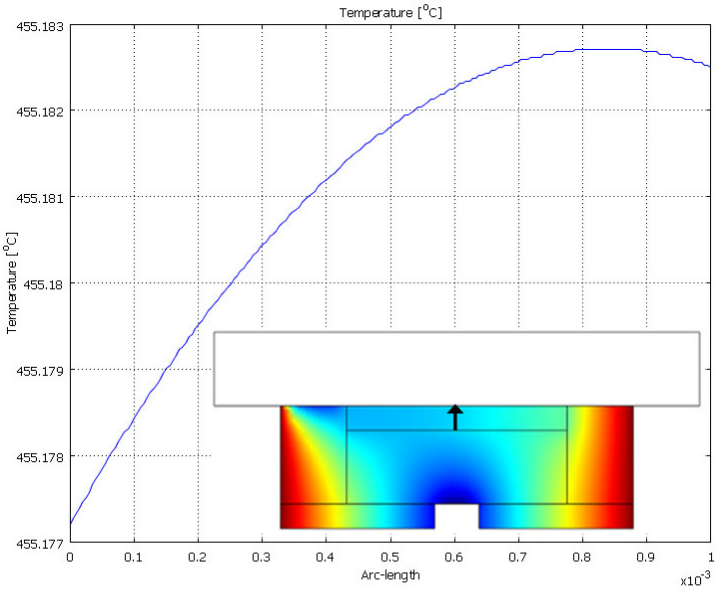

Figure 3-11. Simulation results for the horizontal (a) and vertical (b) temperature distribution inside the sample in the new design. The horizontal axis of the graph shows the distance along the arrow shown in the small panel inside the graph.

Secondly, forced convection with sweep gas (hydrogen or nitrogen) should be used throughout the experiments, to prevent gas condensation on the viewport. As a result, a batch experiment is not possible to be done with this configuration. However, the forced convection coupled with natural convection causes more heat losses to the outer surface of the viewport and leads in temperature gradients in the sample. In addition, the gap between the cup and the cell walls causes thermal contact resistance at that point which makes the heat transfer even worse. Finally, heavy oil is an opaque substance and a reflective microscope is usually used in such experiments, but an upright reflective microscope only covers the top surface of the sample. The mesophase particles are denser than the isotropic medium[16] which surrounds them and tend to sediment after formation. As a result, the top view is not a good representation of the whole sample.

A new hot-stage reactor was designed to overcome these limitation which was different form the previous designs in some aspects. This new hot-stage was compatible with an inverted microscope to observe the liquid from underneath. A schematic design of the high-pressure optical hot-stage apparatus is shown in Figure 3-12. The chamber was made of stainless steel tubing of 0.5 inch in diameter and 0.1 inch in thickness, and the end was fitted with a sapphire window supplied by MellerOptics with diameter of 0.782 inch, at the bottom of the hot-stage. Swagelok fittings were used to construct the reactor. The window was set in the hot-stage via a silver-plated stainless steel O-ring and a 0.001 inch thick brass ring, and it was fixed by a threaded steel nut. In this design sapphire windows were used instead of YAG because of its higher strength for high

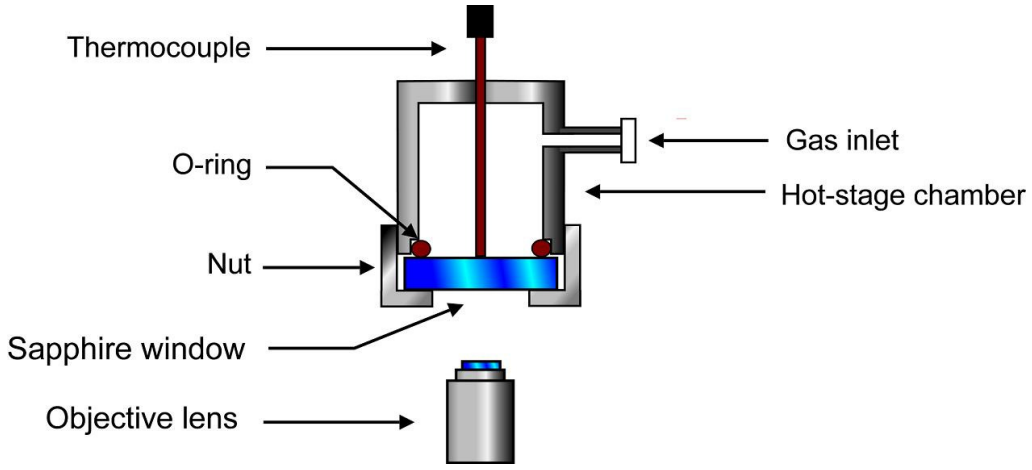

Figure 3-12. Schematic setup for the new hot-stage design for inverted microscope.

pressure and high temperature applications. Sapphire is also a better thermal conductor than YAG which gives a more uniform temperature distribution across the window. The sample was placed directly on the sapphire window during the experiments, and no cup was used for holding the sample. Sapphire is a birefringent crystal material, and when used with polarized reflective light looks bright and doesn't allow the sample to be observed. A C-Axis sapphire window can be used to minimize the birefringence. This approach works best for transmission microscopes in which the incident light is perpendicular to the window. However, in a reflective microscope, the incident light beam is not exactly perpendicular to the window in order to give reflection back to the objective lens. As a result, the light beam is not exactly parallel to the C-axis, and the sapphire window looks birefringent when observed under cross polarized light. However, in this hot-stage, the opaque vacuum residue was placed on the sapphire window at the start of the experiment. The sample melts upon heating

and the resulting liquid sample covers the whole window during the experiment. This can significantly reduce the brightness of the sapphire window and allows the observation of the sample despite the birefringence of the sapphire window.

A heating tape from Cole Parmer was used to heat the hot-stage which was thermally insulated by ceramic covers. The temperature was monitored by an Omegaclad XL type K 1/16" thermocouple inserted into the top of the hot-stage, which was in direct contact with the inside surface of the sapphire window. The precision in temperature measurement was approximately 0.1°C. The operational temperature range was from room temperature to about 500°C, and pressures up to 20 MPa. The hot-stage reactor was connected to a hydrogen or nitrogen cylinder to purge and pressurize head space.

3.5.1. Stirrer

As mentioned above, the poor heat transfer inside the hot-stage and the temperature gradient inside the sample was one of the biggest limitations of the previous designs. The use of a stirrer can significantly improve the heat transfer, and allows the addition of heterogamous catalyst to the system. An Alnico magnet stirrer was used inside the reactor. Alnico is not a very strong magnet, but that is the only magnet which can survive the high temperature inside the reactor (more than 400°C) without demagnetization. The magnet stirrer was coupled with an external rotating magnet to give stirring rates up to 150 rpm (Figure 3-13). At first very small magnet bars covered with glass was used to stir the hot-stage content (Figure 3-14). The thermocouple was bent to leave enough space for the magnet

Figure 3-13. Setup for the new hot-stage. A large magnet connected to an electromotor was used to rotate the magnet stirrer inside the hot-stage reactor.

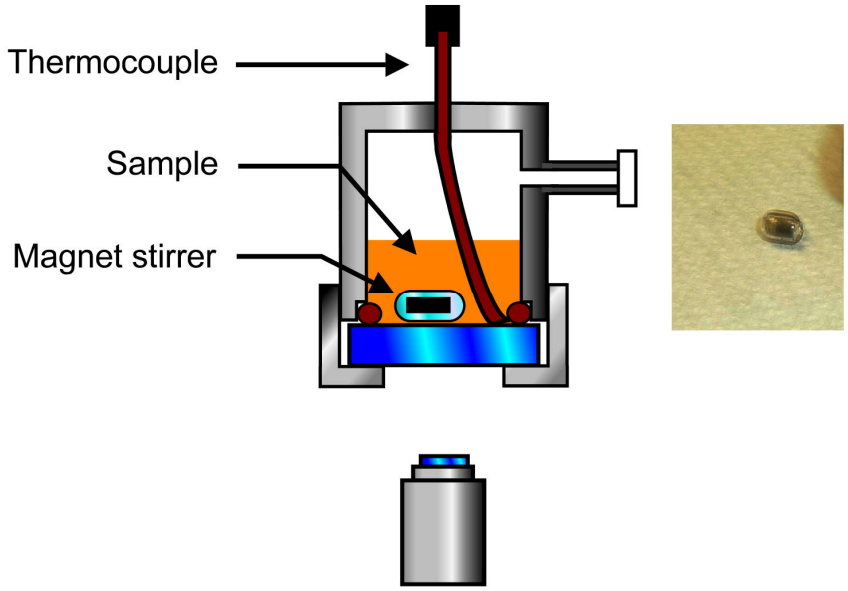

Figure 3-14. Setup for the new hot-stage with the addition of a glass covered magnet. The thermocouple was bent to leave some space for the magnet. The right picture shows the magnet stirrer.

(Figure 3-14). However, the experimental results showed that it could not give good mixing, and only a small part of the reactor was subjected to stirring as shown in Figure 3-15. The mesophase particles outside that area were not subjected to stirring and precipitated on the window while the stirrer was on. As a result a new design for the magnet was used, and this time the tip of the thermocouple passed through the magnet and acted as shaft for the magnet stirrer (Figure 3-16). At first two small magnet bar were connected to a small glass tube using high temperature ceramic glue to serve as the stirrer as shown in Figure 3-17a. The design was finally substituted by a custom made block magnet (Figure 3-17b). An Alnico block magnet (9.5*4*3 mm) was machined with a 2 mm hole inside to serve as the magnet.

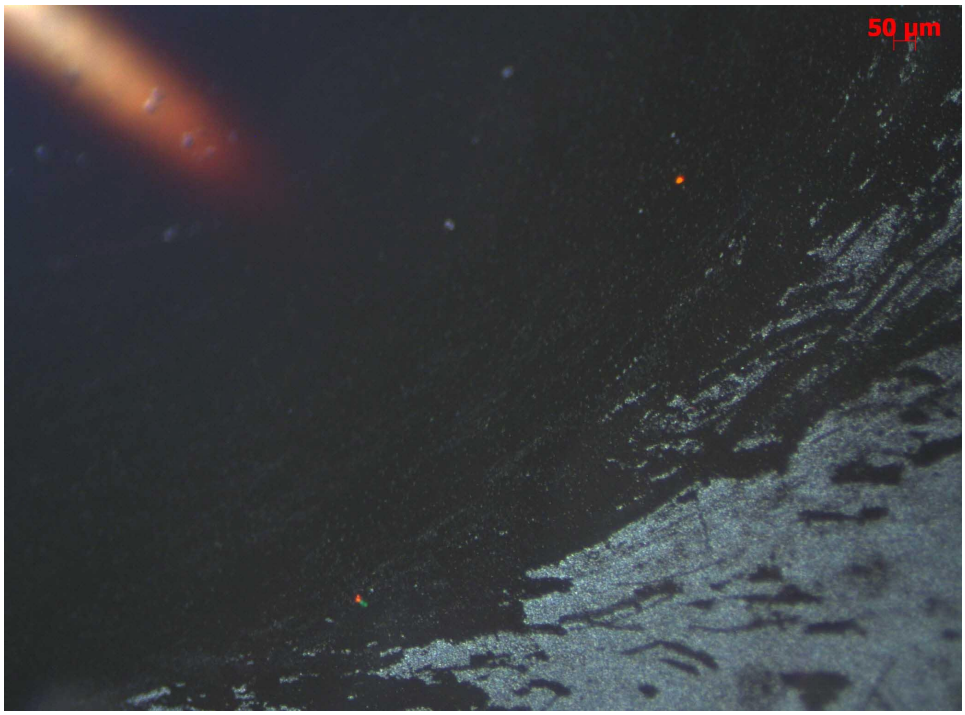

Figure 3-15. Mesophase formation in the stirred hot-stage reactor. The glass covered magnet only covers a small potion of the hot-stage.

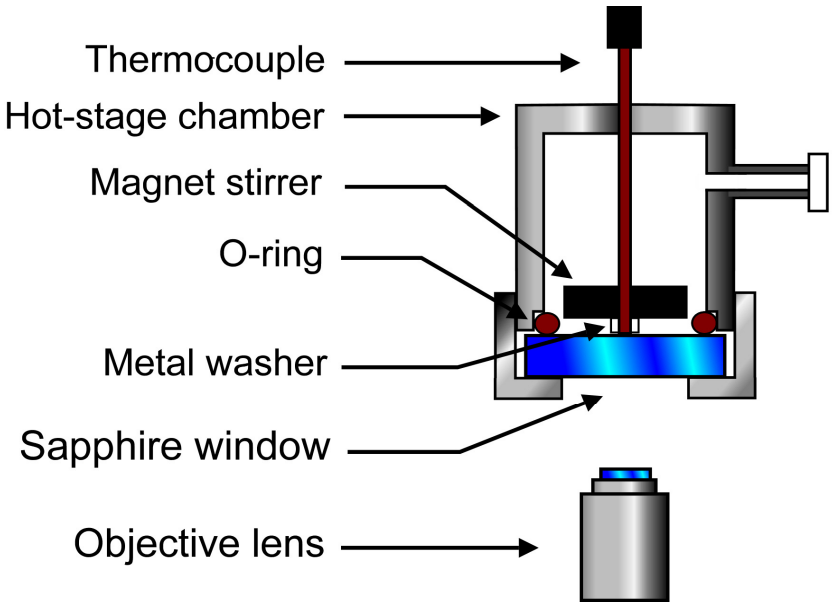

Figure 3-16. Setup for the new hot-stage with the addition of a magnet. The thermocouple acts as a shaft for the magnet and passes through it.

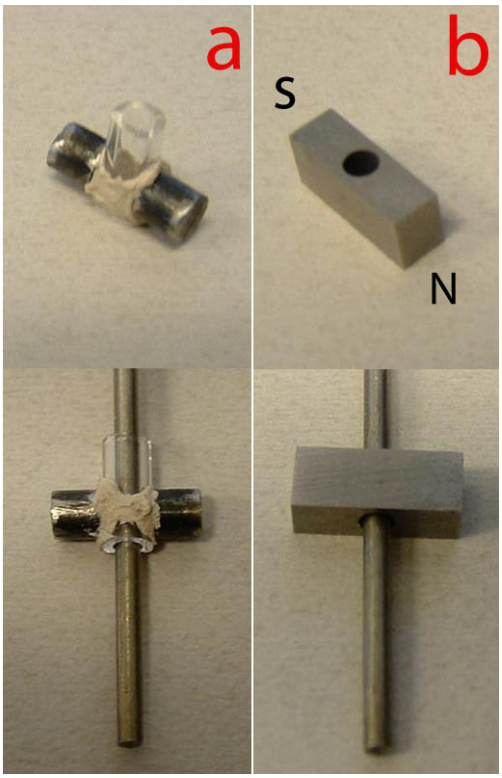

Figure 3-17. New magnet stirrer. (a) two small magnets glued to a glass tube. (b) a custom made black magnet with a hole inside.

Dye injection experiments were done to compare the performance of these different designs as shown in Figure 3-18. In these experiments the hot-stage was filled with water and a droplet of dye was injected into it while the stirrer was rotating at 140 rpm. The amount of time needed for the magnet stirrer to give a uniform mixture of dye in water after the injection of a dye droplet was measured for all the 3 magnets. For the glass covered magnet it took 25 sec. For the magnet bars connected to the glass tube the time was 6 sec, and for the block magnet only 2 sec. These experiments showed that the custom made block magnet had the best performance and could mix the due uniformly in the shortest time in comparison with other designs.

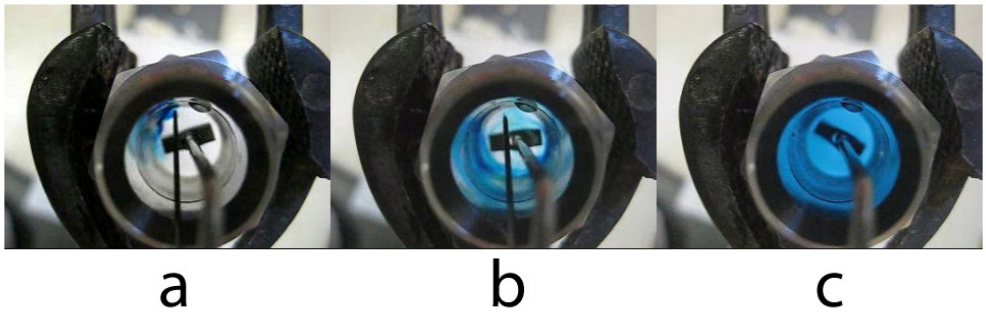

Figure 3-18. Dye injection experiment for the block magnet. (a) immediately after injection, (b) 1 second after injection, (c) 2 seconds after injection. After 2 second the dye is mixed uniformly in the water.

The block magnet was also tested with vacuum reside at high temperature and the results showed that it can uniformly spread the mesophase particles in the reactor as shown in Figure 3-19.

Figure 3-19. Mesophase formation in the stirred hot-stage reactor with the block magnet. Mesophase particles are uniformly distributed over the window after turning off the stirrer.

3.5.2. Set-up for the continuous system

To be able to have a continuous flow of gas in the hot-stage, the reactor fitting was changed to have an outlet for the reactor as shown in Figure 3-20. Figure 3-21 shows the schematic diagram of the set-up and Figure 3-22 shows the actual components added to the system. The gas comes from the cylinder through a mass flow controller (Brooks instrument Model 5850S) into the hot-stage which can set the volumetric flow of the gas. The gas goes through the hot-stage reactor and then goes into a trap to separate the entrained liquid from the gas. Then it goes

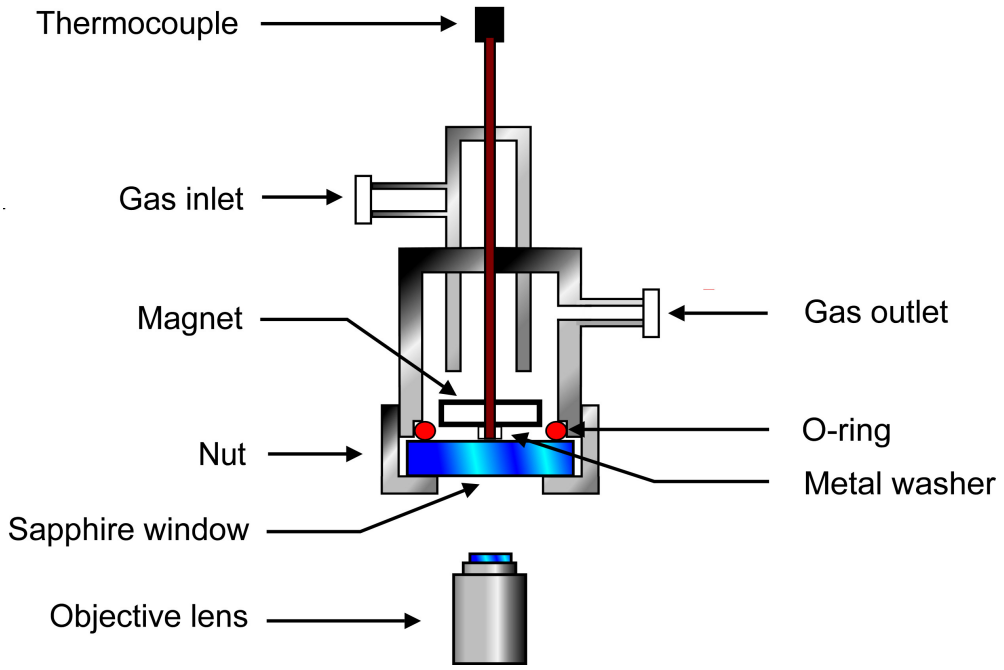

Figure 3-20. Set-up for the new hot-stage to have continuous flow of gas.

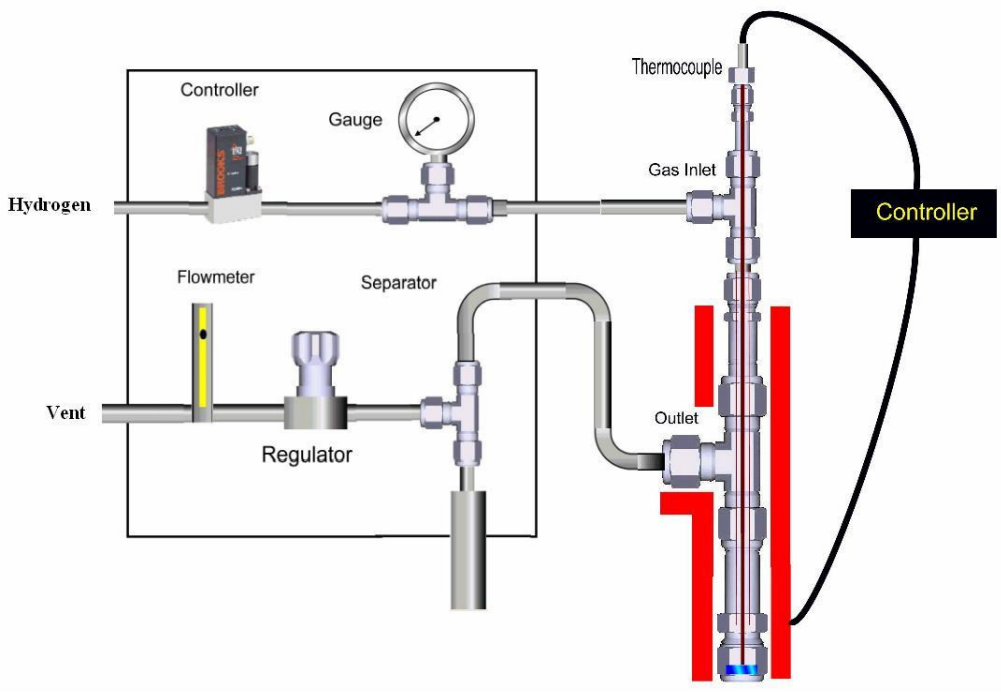

Figure 3-21. Set-up for the continuous flow of gas inside the hot-stage.

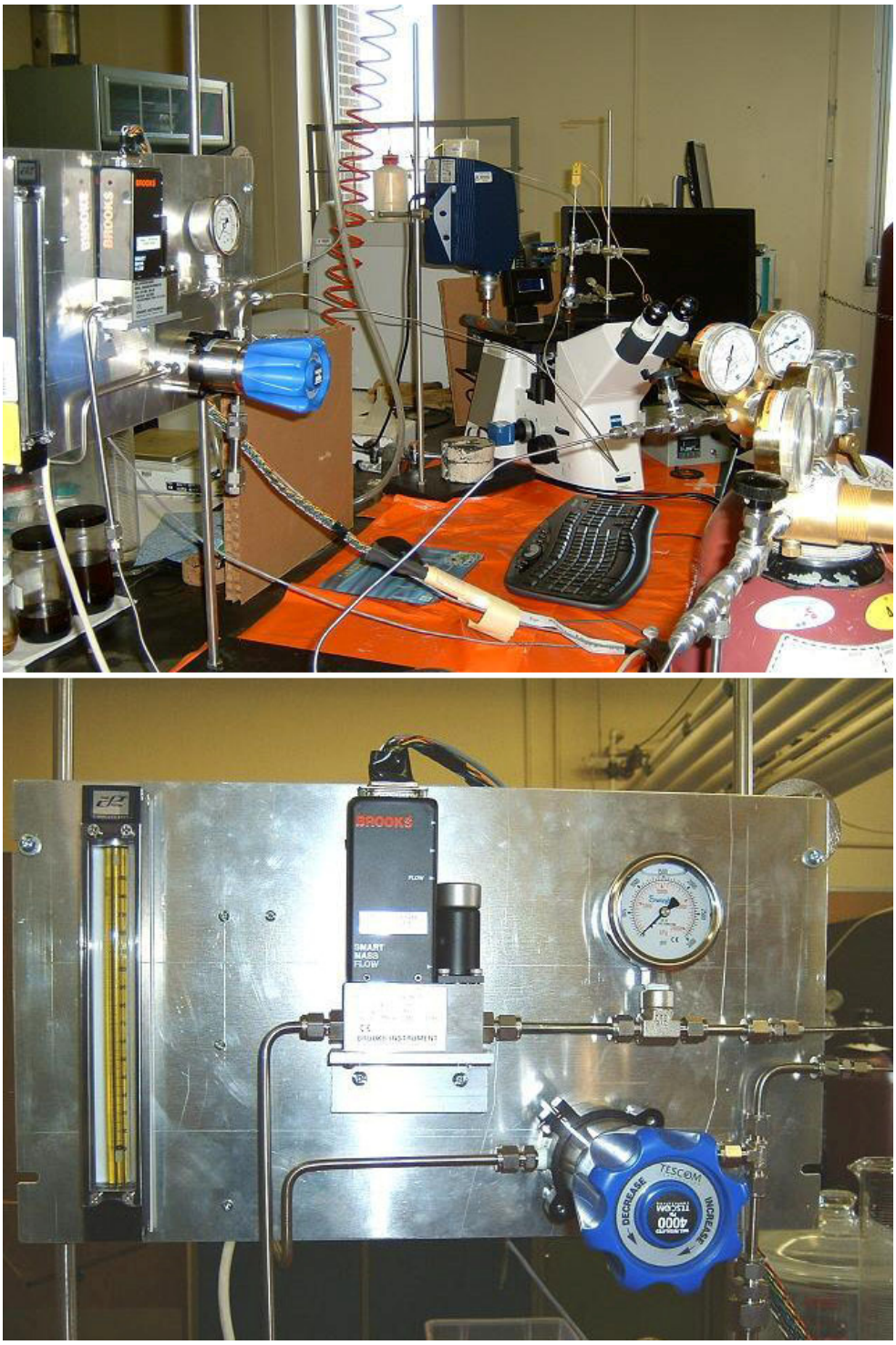

Figure 3-22. Set-up for the continuous flow of gas inside the hot-stage.

into a back pressure regulator (Tescom) which sets the pressure of the gas inside the hot-stage. A manometer was used to check the flow-rate of the gas before going into the vent. In this way a continuous flow of hydrogen or nitrogen at a constant flow rate and pressure can be passed through the hot-stage reactor during the experiment.

3.6. References

1. Azami, K.; Yamamoto, S.; Sanada, Y., Kinetics of Mesophase Formation of Petroleum Pitch. Carbon 1994, 32, (5), 947-951.
2. Cottinet, D.; Couderc, P.; Saintromain, J. L.; Dhamelincourt, P., Raman Microscope Study of Heat-Treated Pitches. Carbon 1988, 26, (3), 339-344.
3. Mochida, I.; Tamaru, K.; Korai, Y.; Fujitsu, H.; Takeshita, K., Carbonization Properties of Partially Hydrogenated Aromatic-Compounds .2. Factors Influencing the Coke Yield in the Carbonization of Hydrogenated Pyrene. Carbon 1982, 20, (3), 231-236.
4. Oberlin, A., High Resolution TEM Studies of Carbonization and Graphitization. In Chemistry and Physics of Carbon, Vol 26, Marcel Dekker: New York, 1989; Vol. 22, pp 1-143.
5. Korai, Y.; Mochida, I., Molecular Assembly of Mesophase and Isotropic Pitches at their Fused States. Carbon 1992, 30, (7), 1019-1024.
6. Gentzis, T.; Rahimi, P. M., A Microscopic Approach to Determine the Origin and Mechanism of Coke Formation in Fractionation Towers. Fuel 2003, 82, (12), 1531-1540.
7. Dierking, I., Textures of Liquid Crystals. Wiley-VCH: Weinheim, 2003.

8. Scharf, T., Polarized Light in Liquid Crystals and Polymers. Wiely: New Jersey, 2007.
9. Keller, A., The Spherulitic Structure of Crystalline Polymers .1. Investigations with the Polarizing Microscope. J. Polym. Sci. 1955, 17, (84), 291-308.
10. Onsager, L., The Effects of Shape on the Interaction of Colloidal Particles. Ann. N.Y. Acad. Sci. 1949, 51, (4), 627-659.
11. Roviello, A.; Sirigu, A., Mesophasic Structures in Polymers - Preliminary Account on Mesophases of some Poly-Alkanoates of P,P'-Di-Hydroxy-Alpha,Alpha-'-Di-Methyl Benzalazine. J. Polym. Sci., Polym. Lett. 1975, 13, (8), 455-463.
12. Lewis, R. T., Hot-Stage Microscopy of Mesophase Pitches. Ext. Abstr. 12th Bienn. Am. Conf. Carbon, Am. Carbon Soc. 1975, 215-216.
13. Perrotta, A. J.; McCullough, J. P.; Beuther, H., Pressure-Temperature Microscopy of Petroleum-Derived Hydrocarbons. Prepr. Pap. Am. Chem. Soc., Div. Pet. Chem 1983, 28, (3), 633-639.
14. Rodriguez, J.; Tierney, J. W.; Wender, I., *In Situ* Evaluation of the Carbonization Behavior of Graphitizable Carbon Precursors. Am. Chem. Soc. Div. Fuel Chem. 1991, (36), 1081-1087.
15. Rahimi, P.; Gentzis, T.; Dawson, W. H.; Fairbridge, C.; Khulbe, C.; Chung, K.; Nowlan, V.; DelBianco, A., Investigation of Coking Propensity of Narrow Cut Fractions from Athabasca Bitumen Using Hot-Stage Microscopy. Energy Fuels 1998, 12, (5), 1020-1030.

16. Singer, L. S., The Mesophase in Carbonaceous Pitches. Faraday Discuss. 1985, 79, 265-272.

4. Influence of depressurization and cooling on the formation and development of mesophase

4.1. Introduction

Coke formation is a major problem in petroleum industry because of its effect on liquid yield and catalyst deactivation. In addition, it can foul reactor internals and downstream vessels and force shutdowns. These deposits are insoluble in the liquid phase at process conditions, but the most common definition of coke in laboratory studies is material insoluble in toluene[1]. Of particular interest is accumulation of such material as foulant inside process equipment. Brooks and Taylor[2] first observed that during the thermal cracking of petroleum and coal tar pitches, an intermediate phase is formed which is anisotropic. This intermediate phase, known as carbonaceous mesophase, is a discotic nematic liquid crystal state[3], while pitch is a convenient term for heavy liquid fractions that have been significantly altered by thermal cracking reactions. Carbonaceous mesophase appears during the heat treatment of pitch in the temperature range of 350 to 500°C as optically anisotropic spheres surrounded by an isotropic liquid matrix. Mesophase is believed to consist of a clusters of approximately planar aromatic molecules with significant orientational order but no long range positional order[4]. The onset of mesophase is of particular interest in hydroconversion processes, because this phase can give severe fouling of the reactor internals due to coalescence and adhesion[5, 6]. The formation of new phases, such as sediment or mesophase, can limit the conversion of the vacuum residue[7].

Formation of a new anisotropic phase requires a combination of chemical reaction, nucleation, and diffusion of material from the surrounding liquid to the new phase. Greinke et al.[8] studied the composition of coexisting mesophase and isotropic phase during the thermal cracking of petroleum pitch at 400°C with time. They suggested that the initial nucleation of mesophase was driven by removal of low-boiling components (< 400 Da) by distillation coupled with the polymerization of liquid-phase components in the 400 to 1100 Da range. Riggs and Diefendorf suggested that that pitches are solutions of large aromatic disc-like molecules (mesogens) in a solvent medium of smaller molecules (non-mesogen), preventing the ordering of mesogens to form the liquid crystalline mesophase [9]. Diefendorf and Riggs[10] patented the use of solvent extraction of pitch as an alternative to heat treatment to enhance mesophase formation. Extraction of the smaller components by solvents such as toluene gave an insoluble solid that rapidly formed 100% ordered mesophase upon melting [11],[12]. They demonstrated reversible formation of mesophase in mixtures of pitch and toluene insolubles [12], and proposed a pseudo-binary phase diagram for equilibrium between the mesophase and non-isotropic components of pitch[9].

Hu and Hurt[13] developed a thermodynamic model for mesophase formation by combining regular solution theory, Flory-Huggins theory, and statistical theories of liquid crystals. They suggested two distinct driving forces for mesophase formation: poor solubility of high molecular weight aromatic molecules in lower molecular weight fractions, and lowering of the system free energy by molecular

orientation of the large disk like molecules and expulsion of the smaller less-oriented molecules to a separate isotropic phase.

Wiehe's model[14] for toluene-insoluble coke formation in vacuum residue fractions of petroleum has some similarities to Riggs and Diefendorf's model. In this model asphaltenes are the major precursor for coke formation. Thermal cracking concentrates the large aromatics from the asphaltenes in the non-volatile liquid phase, and removes the attached pendant groups, eventually leading to a liquid-liquid-phase separation of asphaltene cores. This asphaltene-rich phase has little or no donor hydrogen to be abstracted by free radicals[15], therefore, combination reactions rapidly give insoluble coke. Wiehe reported that the portion of the coke that was insoluble in quinoline showed the presence of mesophase spheres, and suggested that the quinoline-soluble coke material could consist of sub-micrometer spheres of partially ordered structures[14].

Although mesophase forms spheres which can be recovered by dissolving the surrounding isotropic pitch[16], definitions based too rigidly on solubility of pitch in solvents can be misleading[17]. For example, Wang et al.[18] showed that in some cases the toluene-insoluble coke from thermal cracking can be completely soluble in quinoline. Mesophase can be exhaustive extracted with toluene to give limited solubility at extreme dilution[17].

Based on transmission-electron microscopy (TEM) studies of pitches, Oberlin proposed that mesophase forms when smaller molecular aggregates of order 1 nm diameter associate in suspension to form larger domains[19]. TEM images showed the presence of ellipsoids as small as 30 nm diameter which are entirely bright or

dark depending on the orientation of the aromatic layers[20]. The progression from randomly dispersed nano-aggregates to associated Brooks and Taylor mesophase spheres is driven by heat treatment and thermal reactions [19].

Marsh et al.[21] suggested that mesophase is not precipitated from pitch solution, and it does not occur because of insolubility of larger molecules within the pitch. Reactions at temperatures above 400°C drive an increase in molecular weight in the liquid phase, so that cohesive energy exceeds translational energy. In this view, as thermal reaction proceeds the molecules remain attached to each other after a collision, and these clusters collect more mesogen molecules until they become become observable by optical microscopy.

Since mesophase can be observed by its optical anisotropy, hot-stage microscopy is the most powerful technique for the characterization. Polarized-light hot-stage microscopy is used for the determination of both phase transition temperatures and phase type, and can also be used to observe the mesophase growth at the temperature of formation[22]. The first *in situ* observation of mesophase formation was by Lewis[23], using a modified hot-stage with a glass cover. The mesophase content did not change appreciably upon cooling of 400°C to room temperature[23]. Hoover et al.[24] confirmed these results using coal derived material. Several *in situ* studies of petroleum and bitumen fractions have been reported, at pressures up to 13.4 MPa[25],[26],[27],[28].. In every case, these studies used an upright reflective microscope, on very small samples of a few microliters under a sweep gas to keep the window clear of condensation. Lewis[23] used a

metal probe inserted into the hot-stage chamber to agitate the sample, but all studies on pressurized samples were conducted without agitation.

Hot-stage microscopy has rarely been used to study the effect of cooling and depressurization on the amount of visible mesophase. Azami et al.[29] studied the effect of cooling on petroleum-derived pitches. They observed no anisotropic spheres in rapidly quenched samples, while mesophase spheres of diameter less than 20 μm were observed in slowly cooled pitches. Yokono et al.[30] observed large mesophase spheres for the slowly cooled sample, but no anisotropy for the rapidly quenched samples. Forrest et al.[31] studied the effect of pressure on the carbonization of pitch, and reported that pressure can retard growth and coalescence of units of mesophase, thus reducing the size of the optical texture of the resultant coke. Marsh et al.[32] reported that higher pressures (circa 300 MPa) can prevent caoalescence of the mesophase. Santamaria-Ramirez et al.[33] studied the effect of depressurization on mesophase formation. They reported that as a result of depressurization, the spheres increase their diameter and there is less production of large domains of coalesced mesophase. These studies examined samples by microscopy after cooling and polishing; the effect of depressurization has never been studied by *in situ* hot-stage microscopy.

In this paper we report for the first time the use of a stirred hot-stage reactor to observe the effect of cooling and depressurization on mesophase onset and accumulation in Athabasca vacuum residue. The use of a stirred hot-stage allowed us to add heterogeneous catalyst to the reacting liquid. The experiments were conducted with and without catalyst under hydrogen and nitrogen atmospheres.

4.2. Experimental section

4.2.1. Materials

Athabasca vacuum residue supplied by Syncrude Canada Ltd. was used for observations (Table 4-1). The catalyst was a proprietary nanoparticulate material comprised of a transition metal sulfide.

Table 4-1. Properties of Athabasca vacuum residue.

Elemental analysis	C(wt%)	81.76
	H(wt%)	9.45
	S(wt%)	6.17
	N(wt%)	0.93
Asphaltene (wt%)		31.1
MCR (wt%)		14.9
Ash (wt%)		3.3
Solids (wt%)		0.22

4.2.2. Hot-stage reactor

A reactor equipped with a high-pressure optical cell was designed for use on a stage of an inverted reflective optical microscope. Before designing the hot-stage reactor, the type of microscope used for mesophase observations was determined. The transmission microscope is confined by the thickness of the sample. That is because vacuum residue is an opaque material which allows the light to pass through in very thin samples. In order to find the maximum thickness of sample

for a transmission microscope, a few samples of vacuum residue with deferent thicknesses were made, and theses samples were observed under a transmission microscope. From these observations, it was concluded that the maximum thickness of sample for a transmission microscope is approximately 50 microns, and a sample thicker than that will not pass the light (of course this depends on the power of the light source of the microscope. A tungsten light source as used, but using a halogen or xenon light source would allow for a greater maximum thickness for a transmission microscope). The practical problems of preparing such a thin sample led us to abandon the idea of using a transmission microscope, and select the reflective microscope as the best option for the hot-stage microscopy. In previous designs, samples in metal cups (stainless steel or aluminium) were placed into the hot-stage cell and covered by a glass[23], spinel[26] or YAG[28] (yttrium-aluminium-garnet) crystal as the viewport. In this particular configuration, there was a gap between the top surface of the sample and the viewport. The top surface of the sample is then observed with an upright reflective microscope during the heat treatment. This design has several limitations. First, the viewport is colder that the sampler during reaction, and condensation on the cold window makes the observations difficult. Secondly, to prevent condensation on the viewport, forced convection with sweep gas (hydrogen or nitrogen) is used throughout the experiments. The forced convection coupled with natural convection driven heat losses to the outer surface of the viewport resulted in temperature gradients in the sample. Additionally, and the thermal contact resistance between the cup and the cell walls makes the heat

transfer even worse. Thirdly, curvature of the liquid surface due to the surface tension affects the optical properties of the sample. Small samples form a thicker layer near the edges of the sample cup and a thinner layer in the center. As a result, the coke texture near the center of the cup is different than at the margins. Finally, heavy oil is an opaque substance and a reflective microscope is used in such experiments; however, with an upright microscope only the top surface of the sample can be observed. The mesophase particles are denser than the medium which surrounds them and tend to sediment after formation, so the top view is not a good representation of the whole sample.

In order to avoid these difficulties, we selected an inverted microscope to observe the liquid from underneath. A schematic design of the high-pressure optical hot-stage apparatus is shown in Figure 4-1.

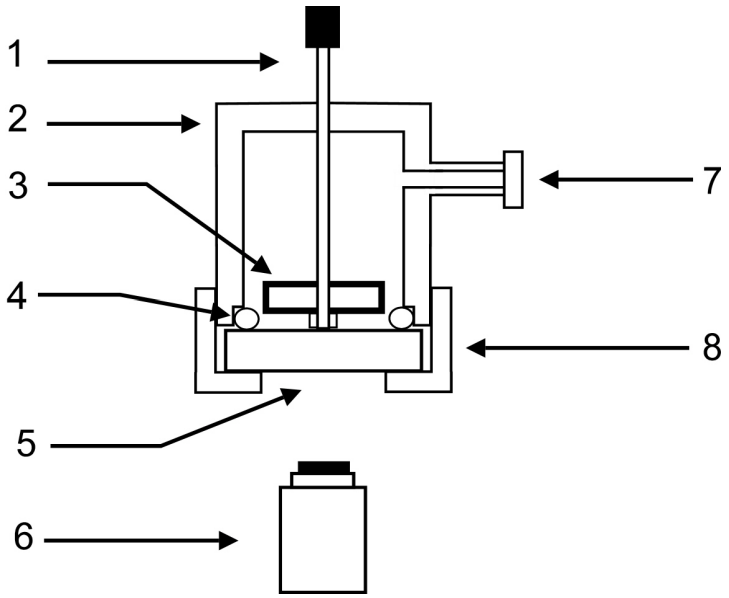

Figure 4-1. Schematic diagram of the hot-stage reactor. 1: thermocouple; 2: steel body; 3: magnet; 4: O-ring; 5: sapphire windows; 6: objective lens of microscope; 7: gas inlet; 8: bottom nut.

The chamber is made of stainless steel tubing of 0.5 inch in diameter and 0.1 inch in thickness, and the end is fitted with a sapphire window supplied by Meller Optics (Providence, RI) with diameter of 0.782 inch, at the bottom of the hot-stage. Swagelok fittings were to construct the reactor. The window is set in the hot-stage via a silver-plated stainless steel O-ring and a 0.001 inch thick brass ring, and it is fixed by a threaded steel nut.

Sapphire windows were used since sapphire is more suitable for high pressure-high temperature applications than YAG. In addition, sapphire is also a better thermal conductor than YAG which gives a more uniform temperature distribution across the window. The sample was placed directly on the sapphire window during the experiments. Normally, sapphire is a birefringent crystal material, and when used with polarized reflective light looks bright and doesn't allow the sample to be observed. A C-Axis sapphire window was used to minimize the birefringence. This approach works best for transmission microscopes in which the incident light is perpendicular to the window. In a reflective microscope, however, the incident light beam is not perpendicular to the window in order to give reflection back to the objective lens. As a result, the light beam is not parallel to the C-axis, and the sapphire crystal remains birefringent and cannot be used with an upright reflective microscope. By using an inverted microscope, we placed nearly opaque vacuum residue on the sapphire window. The liquid under observation significantly reduced the brightness of the sapphire window and enabled observation of the sample despite the birefringence. The hot-stage apparatus is heated by a heating tape, and thermally insulated by ceramic

covers. The temperature is monitored by an Omegaclad XL type K 1/16" thermocouple inserted into the top of the hot-stage, which is in direct contact with the inside surface of the sapphire window. The precision in temperature measurement was approximately 0.1°C. The operational temperature range is from room temperature to about 500°C, and pressures up to 20 MPa. The hot-stage reactor is connected to a hydrogen or nitrogen cylinder to purge and pressurize head space. We used an Alnico magnet stirrer inside the reactor. The stirrer is necessary for experiments which contain suspended catalyst. The stirrer is a block magnet (9.5*4*3 mm) with a 2 mm hole inside. The tip of the thermocouple passes through this hole and acts as shaft for the magnet stirrer (Figure 4-1). The magnet stirrer is coupled with an external rotating magnet to give stirring rates up to 150 rpm.

4.2.3. Polarized optical microscopy

The mesophase content was determined by polarized optical microscopy using a Zeiss Axio-Observer inverted reflective microscope equipped with crossed polarizers. A 3 megapixel camera was connected to the microscope to photographically record the progress of the reaction. Image analysis was performed on a personal computer using ImageJ program developed at National Institutes of Health. The images were analysed to determine the area fraction of mesophase particles in each photo.

4.2.4. Cooling experiments

Small samples, 0.4 g, of vacuum residue were charged in the reactor. It was premixed with 1.0 wt% catalyst. The experiment was done in three stages (experiment 1). In stage one, the sample was pressurized with hydrogen at 4.1 MPa and heated to 440°C. The mixing was started when the sample reached 350°C and was held at 120 rpm. The temperature was maintained until the first mesophase particles appeared after 47 min. The experiment was continued for another 17 min. In stage two, after the first observation of mesophase the stirrer was turned off. A random spot was chosen, and every 3 min, one photo was taken. The aim of this stage is to give enough time for sedimentation. This stage took 34 min. The photos were analyzed to check that sedimentation ended before starting the next stage. In stage three, the heater was turned off and the reactor was air cooled. The average cooling rate was 8.6 °C/min. Photos were taken of the same spot at specific temperatures. The photos were analyzed to compare the mesophase content before and after cooling.

4.2.5. Depressurization experiments

For experiments 2-6, 0.4 g of the vacuum residue was charged into the reactor. Experiments were conducted with either pure vacuum residue or with vacuum residue premixed with 1% catalyst. As with the cooling experiments, each run was conducted in three stages. In stage one, the sample was pressurized with hydrogen or nitrogen at a known pressure and heated up to 440°C. Mixing started at when the sample reached 350°C and was held at 120 rpm. The reaction temperature was maintained constant until the first mesophase particles appeared.

After this point, experiments were continued for another 8 to 45 min to allow mesophase to form in the liquid. In stage two, the stirrer was turned off. A fixed spot was chosen, and every 3 min, one photo was taken, to allow enough time for sedimentation (between 18 to 22 min). The photos were analyzed to check that sedimentation ended before starting the next stage. In stage 3, the reactor was depressurized to atmospheric pressure without changing the temperature. Photos were taken of the same spot after depressurization. The photos were analyzed to compare the mesophase content before and after depressurization. For samples 5 and 6, the depressurization was done before the onset of mesophase formation. The stirrer was turned off at the end of the stage one, and the reactor pressure and temperature were maintained constant for 2 min to allow for sedimentation if there was any suspended mesophase in the bulk liquid phase. Then the reactor was depressurized to observe the immediate results of depressurization on mesophase formation. For the sample 6, the stirrer was turned on again after depressurization; Mixing was turned off briefly whenever images were acquired to improve image quality. Table 4-2 shows all the experimental details for each experiment. To show the repeatability of the experiment for determining the onset of mesophase formation in experiments 2, 4 and 6 two more runs were carried out, and the average time for onset of mesophase formation and the standard deviation was calculated which is shown in Table 4-2.

Table 4-2. Summary of depressurization results for experiments on Athabasca vacuum residue at 440°C, agitated at 120 rpm.

Experiment	Atmosphere	Catalyst, Wt%	Initial Pressure, MPa	Reaction time for Stage 1 (at the initial pressure with agitation), min	Time for onset of mesophase, min	Average time for onset of mesophase formation / Number of replicates /Standard deviation	Total reaction time before depressurizing (Stage 1 with agitation + Stage 2 without agitation), min	Mesophase area fraction before depressurization, %	Mesophase area fraction after depressurization, %
2	H_2	1.0	4.1	67	45	43.67/3/ 4.16	85	6.3	19.5
3	H_2	1.0	6.5	92	50	--	110	0.4	6.0
4	N_2	0	4.8	49	41	45.33/3/ 3.79	70	27.1	57.5
5	N_2	0	4.8	33	35	--	35	0	6.3
6	N_2	0	4.8	19	24	22.67/3/ 1.53	21	0	0

4.3. Results

4.3.1. Effect of cooling on mesophase formation

The sample of vacuum residue was premixed with 1.0 wt % catalyst and then reacted at 440^{o}C. The first mesophase particles appeared 47 min after reaching the final temperature. After a total of 64 min of reaction, the stirrer was turned off to start the second stage where any suspended mesophase was allowed to settle. The reaction times were selected to enable observation of the onset of mesophase formation. After turning off the stirrer, the mesophase area fraction showed a linear increase with time (Figure 4-2). After a total reaction time of 81 min, the heater was turned off and the reactor cooled. Although the cooling rate was not linear, the average cooling rate was 8.6 °C/min. As the reactor cooled in stage three the mesophase area fraction still increased with the same linear trend that was observed in stage two until the temperature fell to 395°C. Below this temperature of 395°C the mesophase growth and formation stops.

4.3.2. Depressurization of hydroconversion product

The samples were premixed with 1.0 wt % catalyst, and then reacted at 440^{o}C under pressure (Table 4-2). When the hydrogen pressure was 4.1 MPa, the first mesophase particles appeared 45 min after reaching the final temperature. This time of onset was repeatable within ± 7 min for similar runs. The number of replicates and standard deviation for some of the results are given in Table 4-2. Increasing the pressure to 6.5 MPa increased the time for onset of mesophase

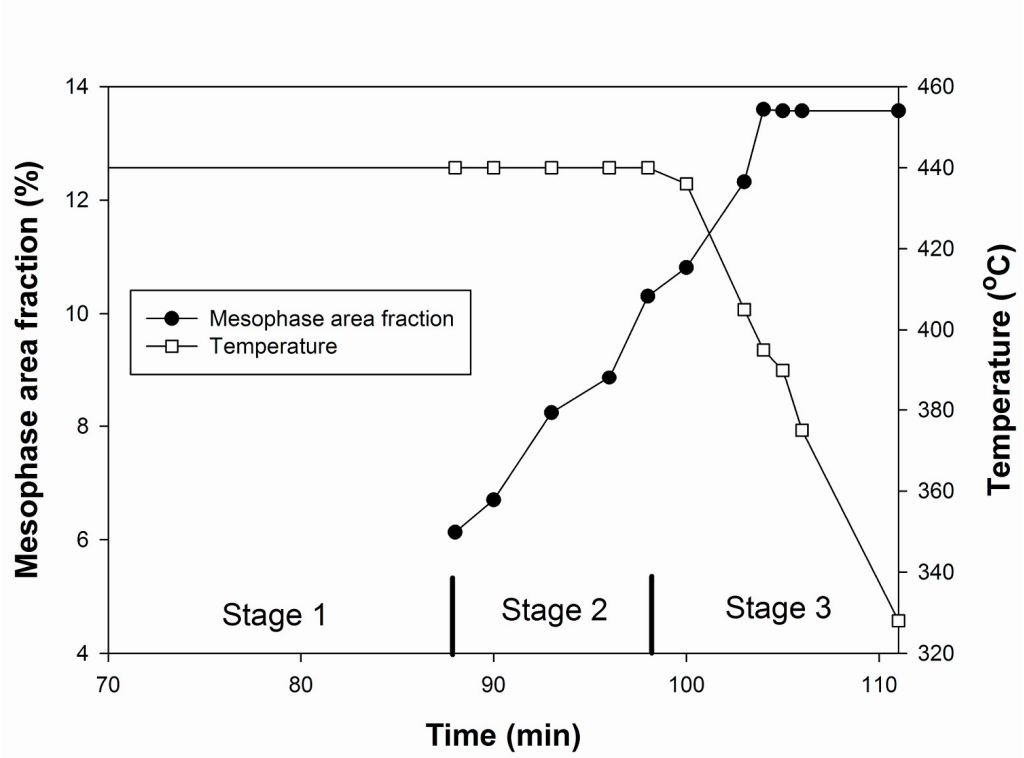

Figure 4-2. Growth and coalescence of mesophase before and after cooling under a nitrogen atmosphere (experiment 1). During stage 3 cooling, the amount of mesophase follows an increasing linear trend with time to 395°C, then it remained constant at lower temperatures.

slightly to 50 min. At both initial pressures, the release of pressure resulted in a significant increase in the amount of observable mesophase. When the H_2 gas pressure was reduced from 4.1 MPa to ambient a 13.2% increase in observable mesophase was measured and when the pressure was reduced from 6.5 MPa, a 5.6% reduction was observed (Table 4-2). Figure 4-3 shows the change in mesophase area fraction at 4.1 MPa, and after depressurization. The mesophase fraction continued to increase with time at the lower pressure due to the continued reactions in the liquid and sedimentation of the mesophase. The discontinuity due to the release of the pressure could not, therefore, be attributed solely to

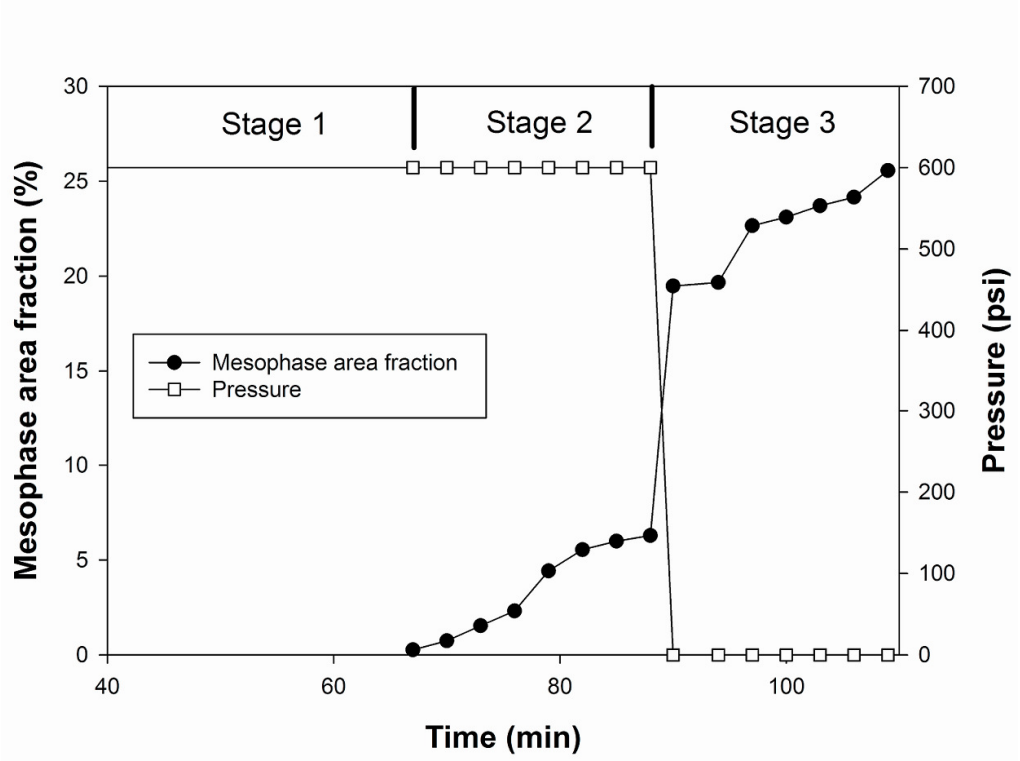

Figure 4-3. Growth and coalescence of mesophase before and after depressurization in catalytic hydroconversion (experiment 2). Depressurization of the reactor lead to an abrupt increase in the mesophase content.

sedimentation. The same trend was observed for the experiment at 6.5 MPa and for all other samples in this study. The micrographs of Figure 4-4 illustrate the appearance of the liquid phase immediately at 4.1 MPa before and after the release of the pressure. The field of view is the same in both images; the small domains in the upper left corner are visible in both images.

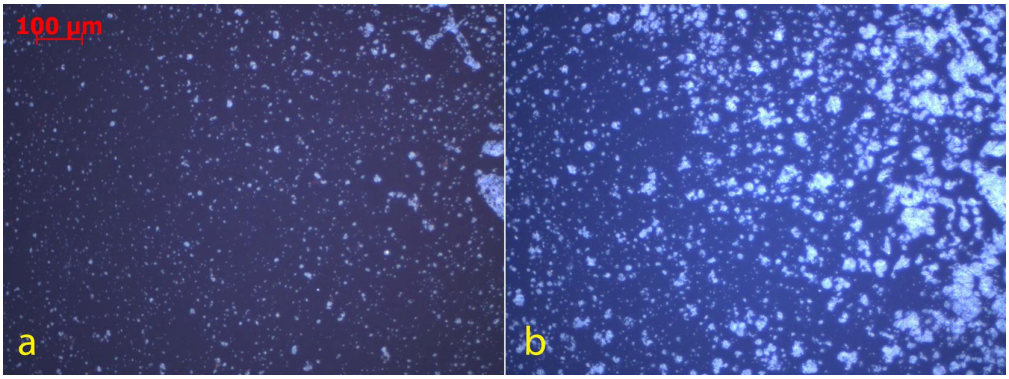

Figure 4-4. Polarized optical microphotograph showing the growth and coalescence of mesophase after depressurization in catalytic hydroconversion (experiment 2). (a) before depressurization; (b) after depressurization.

4.3.3. Depressurization of coking products

Cracking of vacuum residue under nitrogen and in absence of catalyst was examined to ensure that the results from hydroconversion conditions were not due to sedimentation of the catalyst. When the sample was cracked under nitrogen at 4.8 MPa and 440°C without catalyst, the first mesophase particles appeared 41 min after reaching the final temperature (Table 4-2, experiment 4).. Eight minutes later, the stirrer was turned off to start the stage 2. At this stage, the reactor was left without agitation at the same pressure and temperature for 21 min, and then the hot-stage reactor was depressurized from 4.8 MPa to atmospheric pressure. Again, there was a sudden 31% increase in the mesophase area fraction after depressurization.

The results of the above experiments showed that depressurization can increase the mesophase growth after the onset of mesophase formation. To investigate its effect on the onset of mesophase formation, in experiment 5 the reactor was

depressurized before the onset point. This experiment was done in the absence of catalyst under nitrogen (Table 4-2). The stirrer was turned off 33 min after reaching the final temperature, when there was no observable mesophase in the sample, and after 2 min the reactor was depressurized from 4.8 MPa to atmospheric pressure. After depressurizing the reactor, mesophase particles appeared immediately. Figure 4-5 shows the sample before and after depressurization. One minute after the depressurization, the mesophase area fraction at the same spot was 6.27%. Consequently, the depressurization led to immediate mesophase formation in an isotropic mixture.

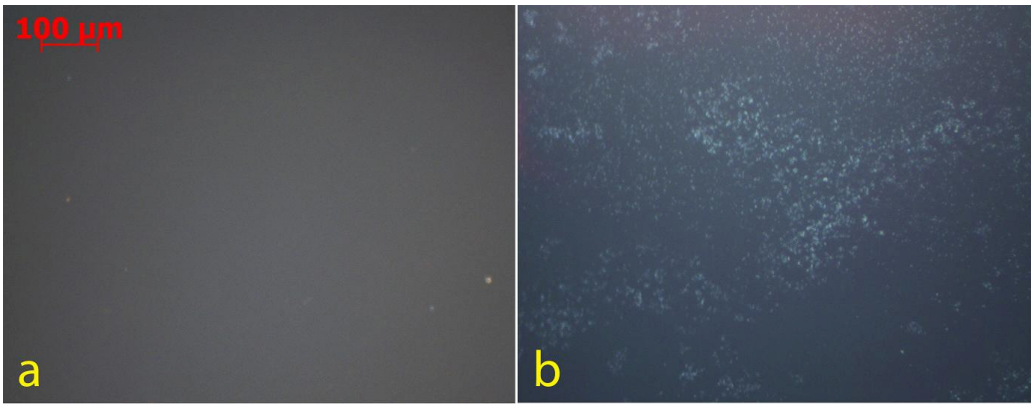

Figure 4-5. Polarized optical microphotograph showing the immediate mesophase formation after depressurization in experiment 5. (a) before depressurization; (b) after depressurization.

In order to determine the effect of earlier depressurizing of the reactor, experiment 6 was conducted with operating conditions similar to that of the sample 5 (Table 4-2), except that the reactor was depressurized sooner. The stirrer was turned off 19 min after reaching the final temperature, and after 2 min

the hot-stage was depressurized from 4.8 MPa to atmospheric pressure, again with no observable mesophase in the sample. At first, the sample did not show any sign of mesophase formation, so the stirrer was turned on again, and the experiment continued at the same conditions (atmospheric pressure). 5 min after depressurization, the first mesophase particles appeared in this sample. In the first stage of the heat treatment of sample 4, mesophase formed 41 min after reaching the final temperature under similar operating conditions. In this case, mesophase was observed after 24 min at low pressure. These results showed that depressurization did not cause immediate mesophase formation during the early stages of cracking, but could accelerate its onset.

4.3.4. Submicron mesophase

One important aspect of mesophase observation is the limit of detection. Mesophase domains smaller than 0.5 μm in diameter appear isotropic under the optical microscope[32]. Domains of mesophase smaller than 0.1 μm in size have been detected using scanning electron microscopy (SEM)[34] and TEM[19, 35]. For example, when a sample of Athabasca vacuum residue was cracked at 440°C under nitrogen at 4.1 MPa for 90 min and then cooled down to the room temperature, mesophase spheres were observed on the surface of this sample using polarized optical microscopy (Figure 6). A selected region of this sample (marked by the rectangle a in Figure 4-6) was also observed with SEM using backscattered mode as shown in Figure 4-6 (marked by the rectangle b). The larger mesophase spheres match in both photos, but the dark isotropic parts of rectangle a in Figure 4-6 (under polarized light) are now observed in the rectangle

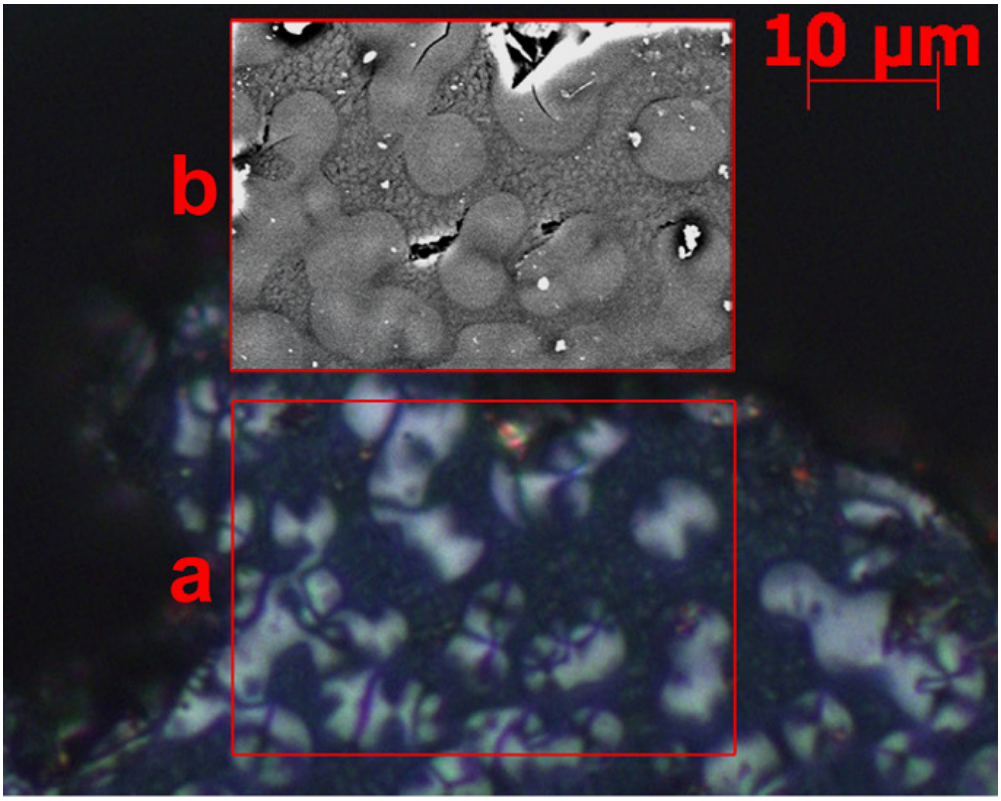

Figure 4-6. Polarized optical microphotograph showing the mesophase spheres formed in Athabasca vacuum residue under nitrogen at 4.8 MPa, 440°C after 90 min. The region marked by rectangle *a* in this photo was also observed under SEM which is shown in rectangle *b*. The bigger mesophase particles can be matched in both photos, but there are many mesophase particles in the sample which cannot be detected by the optical microscope due to their small size.

b (under SEM) to be formed of a dense array of what are most likely mesophase spheres. As a result, a sample which appears largely isotropic at the observable length scale of optical microscopy can contain abundant anisotropic domains which are too small to be detected by an optical microscope. The mechanism for the transformation of these submicron domains into micron-scale mesophase is not well understood.

4.4. Discussion

The results of this study demonstrate that cooling of a high temperature liquid did not change the amount of observable mesophase. When the cooling rate is slow, the mesophase content will increase with time as long as the liquid is above the cracking temperature, due to the ongoing thermal cracking reactions. Quenching the liquid stopped the formation of mesophase, consistent with previous studies[23, 29, 30].

In contrast, depressurization resulted in a significant and immediate increase in the mesophase content when the second phase was already present or about to form (Experiments 4 and 5). At low extent of conversion, a reduction in pressure reduced the time for the onset of mesophase. Both of these observations are consistent with a larger driving force for mesophase formation at low pressure.

In a pressurized batch reactor, as in these experiments, the closed head space prevents the complete loss of volatile materials formed during the reactions; instead these components are in equilibrium between the vapor and the liquid phase. Depressurization during the course of cracking reduces the partial pressure of cracked products in the vapor phase, which drives the rapid loss of volatile cracked products and hydrogen gas from the liquid phase. This devolatilization increases the viscosity of the remaining isotropic phase and decreases the mobility of mesophase spheres. Based on this reasoning, Santamaria-Ramirez et al.[33] suggested that depressurization should decrease the coalescence of mesophase spheres. They investigated the effect of depressurization on the cracking of petroleum pitch and, reported that as a result of depressurization, the mesophase

spheres increase their diameter, and there is less production of bulk (coalesced) mesophase. The total amount of mesophase (spheres plus coalesced regions) was almost the same (within 0.5%) and sometimes a little lower for the depressurized samples. These observations are not consistent with our results. One possible reason for the difference is that Santamaria-Ramirez et al.[33] did not use *in situ* polarized microscopy to measure the mesophase area, rather at the end of all the experiments (the ones that carried on at a constant pressure and the other ones which depressurized to a lower pressure in the middle of reaction) the reactor was depressurized at the reaction temperature and then cooled down to room temperature. These cooled samples were then prepared for microscopy analysis to determine the mesophase area[33]. Based on our results, this protocol based on analysis of ex-situ samples cannot be used to explore the role of the vapor phase, either through pressure or composition. The lower molecular weight components in a pitch are known to inhibit mesophase formation[36]. For example, Kershaw et al.[37] studied the mesophase formation in petroleum pitch using nitrogen sparging and vacuum, and found that the removal of the lower molecular weight species using vacuum allows mesophase formation to commence earlier and proceed more rapidly than with sparging. Rahimi et al.[28] reported that a more volatile sample fraction had a shorter mesophase induction time than expected, which they attributed to the evaporation of low molecular weight species into the flowing sweep gas under hot-stage conditions.

The increase in visible mesophase domains with depressurization is consistent with the solubility model of Riggs and Diefendorf[9]. The loss of volatiles which

act as the disordering non-mesogen species can promote the ordering of mesogens to form mesophase. Similarly, the models of Oberlin[19] and Marsh[21] suggest that evaporation of low-molecular weight species from the liquid phase due to depressuring the reactor should promote growth of mesophase domains. Under hydroconversion conditions, hydrogen gas comprises a significant mole fraction in the liquid phase. The depressurization of sample 2 under hydrogen increased the mesophase content (Figure 4-3). The removal of hydrogen alone should increase the solubility parameter of the light liquid phase, and make it closer to that of the heavy phase-separated liquid, whereas the loss of low-molecular weight aromatic products to the vapour phase will decrease the solubility parameter. The observed results are consistent with available models based on phase behavior, such as Riggs and Diefendorf[9], Hu and Hurt[13], and Wiehe's models[14], as long as the loss of volatiles decreases the solubility parameter of the liquid phase.

The removal of volatiles can promote the nucleation of and coalescence of submicron mesophase domains. The smaller particles which were not visible before would grow and coalesce and form bigger observable particles which can now be detected by the optical microscope as shown in Figure 4-7. When the liquid mixture is far from the onset of mesophase formation (as in experiment 6), the submicron mesophase domains may not be formed yet. The depressurization would promote the nucleation of these submicron domains, and increase their size, giving a reduction in the time for onset of visible mesophase as in experiment 6.

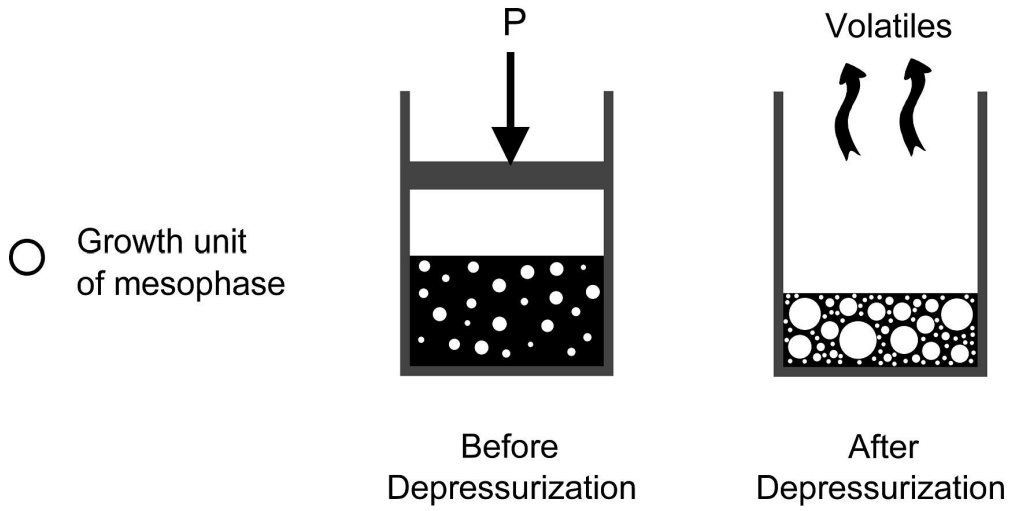

Figure 4-7. A Schematic diagram showing the effect of depressurization on mesophase formation. Depressurization leads to the removal of volatiles form the liquid which results in the growth and coalescence of mesophase particles.

One important implication of this study is that sampling reactors in order to define mesophase content requires quenching of samples at the reactor pressure, in order to prevent the loss of volatiles from the isotropic liquid phase and increasing the mesophase content. This effect would be most pronounced when the liquid phase is rich in volatile components, which would depend on the level of conversion and the gas flow rate.

4.5. Conclusions

The results of this study demonstrate the use of a stirred reactor for *in situ* observation of mesophase formation during thermal cracking and catalytic hydroconversion of heavy oil. Rapid cooling of the sample stopped the formation

of mesophase, but did not change the amount observed. Depressurization can either increase the observed mesophase content or decrease the time needed for onset of mesophase formation, depending on the extent of reaction; consequently, the mesophase content at the actual high-pressure reactor conditions does not correlate with the measurement of the mesophase content in the depressurized reactor product at ambient conditions.

4.6. References

1. Gray, M. R., Upgrading Petroleum Residues and Heavy Oils. Marcel Dekker Inc.: New York, 1994.
2. Brooks, J. D.; Taylor, G. H., Formation of Graphitizing Carbons from Liquid Phase. Nature 1965, 206, (4985), 697-699.
3. Bisoyi, H. K.; Kumar, S., Discotic Nematic Liquid Crystals: Science and Technology. Chem. Soc. Rev. 2010, 39, (1), 264-285.
4. Hurt, R. H.; Hu, Y., Thermodynamics of Carbonaceous Mesophase. Carbon 1999, 37, (2), 281-292.
5. Nandi, B. N. Microscopic studies for the structure of coke formed during thermal hydrocracking of Athabasca bitumen; ERP/ERL 76-176(OP)(J); Natural Resources Canada: Ottawa, 1976; pp 76-176.
6. Lott, R.; Cyr, T. J., Study of mechanisms of coking in heavy oil processes. In Proc. - Int. Symp. Heavy Oil Residue Upgrading Util.: Beijing Peop. Rep. China., 1992; pp 309-315.

7. Mochida, I.; Zhao, X. Z.; Sakanishi, K., Suppression of Sludge Formation by Two Stage Hydrocracking of Vacuum Residue at High Conversion. . Ind. Eng. Chem. Res. 1990, 29, 2324-2327.
8. Greinke, R. A., Early Stages of Petroleum Pitch Carbonization - Kinetics and Mechanisms. In Chemistry and Physics of Carbon, Vol 24, Marcel Dekker: New York, 1994; Vol. 24, pp 1-43.
9. Riggs, D. M.; Diefendorf, R. J., A Phase Diagram for Pitches. In Carbon '80. , Baden-Baden 1980; pp 326-329.
10. Diefendorf, R. J.; Riggs, D. M. Forming optically anisotropic pitches , U.S. Patent No. 4208267, 1980.
11. Venner, J. G.; Diefendorf, R. J., Pitch –Solvent Interaction and Their Effects on Mesophase Formation. In Polymers for Fibers and Elastomers : Based on a Symposium Sponsored by the Macromolecular Secretariat at the 186th Meeting of the American Chemical Society, Washington, D.C., 1983; pp 219-234.
12. Diefendorf, R. J., Mesophase Formation in Polymer Aromatic Compounds a Route to Low Cost Carbon Fibers. In Polymers for Fibers and Elastomers : Based on a Symposium Sponsored by the Macromolecular Secretariat at the 186th Meeting of the American Chemical Society, ACS: Washington, D.C., 1983; pp 209-218.
13. Hu, Y.; Hurt, R. H., Thermodynamics of Carbonaceous Mesophase - II. General Theory for Nonideal Solutions. Carbon 2001, 39, (6), 887-896.

14. Wiehe, I. A., A Phase-Separation Kinetic-Model for Coke Formation. Ind. Eng. Chem. Res. 1993, 32, (11), 2447-2454.

15. Gould, K. A.; Wiehe, I. A., Natural Hydrogen Donors in Petroleum Resids. Energy Fuels 2007, 21, (3), 1199-1204.

16. Brooks, J. D.; Taylor, G. H., The Formation of Graphitizing Carbons from the Liquid Phase. Carbon 1965, 3, (2), 185-193.

17. Chwastiak, S.; Lewis, R. T.; Ruggiero, J. D., Quantitative Determination of Mesophase Cnotent in Pitch. Carbon 1981, 19, (5), 357-363.

18. Wang, S.; Chung, K.; Masliyah, J. H.; Gray, M. R., Toluene-Insoluble Fraction from Thermal Cracking of Athabasca Gas Oil: Formation of a Liquid-in-Oil Emulsion that Wets Hydrophobic Dispersed Solids. Fuel 1998, 77, (14), 1647-1653.

19. Oberlin, A., High Resolution TEM Studies of Carbonization and Graphitization. In Chemistry and Physics of Carbon, Marcel Dekker: New York, 1989; Vol. 22, pp 1-143.

20. Lafdi, K.; Bonnamy, S.; Oberlin, A., Mechanism of Anisotropy Occurrence in a Pitch Precursor of Carbon-Fibers .1. Pitches-A and Pitches-B. Carbon 1991, 29, (7), 831-847.

21. Marsh, H.; Menendez, R., Mechanisms of Formation of Isotropic and Anisotropic Carbons. In Introductio to Carbon Science, Marsh, H., Ed. Butterworths: London, 1989; pp 37-73.

22. Dierking, I., Textures of Liquid Crystals. Wiley-VCH: Weinheim, 2003.

23. Lewis, R. T., Hot-Stage Microscopy of Mesophase Pitches. Ext. Abstr. 12th Bienn. Am. Conf. Carbon, Am. Carbon Soc. 1975, 215-216.

24. Hoover, D. S.; Davis, A.; Perrotta, A. J.; Spackman, W., The Use of Cinematography in a Study of Mesophase Formation. Ext. Abstr. 12th Bienn. Am. Conf. Carbon, Am. Carbon Soc. 1979, 393.

25. Perrotta, A. J.; McCullough, J. P.; Beuther, H., Pressure-Temperature Microscopy of Petroleum-Derived Hydrocarbons. Prepr. Pap. Am. Chem. Soc., Div. Pet. Chem 1983, 28, (3), 633-639.

26. Rodriguez, J.; Tierney, J. W.; Wender, I., *In Situ* Evaluation of the Carbonization Behavior of Graphitizable Carbon Precursors. Am. Chem. Soc. Div. Fuel Chem. 1991, (36), 1081-1087.

27. Lafdi, K.; Bonnamy, S.; Oberlin, A., Mechanism of Anisotropy Occurrence in a Pitch Precursor of Carbon-Fibers .3. Hot Stage Microscopy of Pitch--B and Pitch-C. Carbon 1991, 29, (7), 857-864.

28. Rahimi, P.; Gentzis, T.; Dawson, W. H.; Fairbridge, C.; Khulbe, C.; Chung, K.; Nowlan, V.; DelBianco, A., Investigation of Coking Propensity of Narrow Cut Fractions from Athabasca Bitumen Using Hot-Stage Microscopy. Energy Fuels 1998, 12, (5), 1020-1030.

29. Azami, K.; Yokono, T.; Sanada, Y.; Uemura, S., Studeis on the Early Stage of Carbonization of Petroleum Pithch by Means of High-Temperature H-1-NMR and ESR. Carbon 1989, 27, (2), 177-183.

30. Yokono, T.; Oka, N.; Sanada, Y., Mesophase Generation during Cooling Process of Isotropic Melt of Pitch Investigated by Electron-Spin-Resonance Spin Probe Method. Carbon 1984, 22, (6), 614-616.

31. Forrest, M. A.; Marsh, H., The Effects of Pressure on the Carbonization of Pitch and Pitch Carbon-Fiber Composites. J. Mater. Sci. 1983, 18, (4), 978-990.

32. Marsh, H.; Latham, C. S., The Chemistry of Mesophase Formation. Am. Chem. Soc., Symp. Ser. 1986, 303, 1-28.

33. Santamaria-Ramirez, R.; Romero-Palazon, E.; Gomez-de-Salazar, C.; Rodriguez-Reinoso, F.; Martinez-Saez, S.; Martinez-Escandell, M.; Marsh, H., Influence of Pressure Variations on the Formation and Development of Mesophase in a Petroleum Residue. Carbon 1999, 37, (3), 445-455.

34. Qian, Z.; Clarke, D. E.; Marsh, H., Structure in Cokes from Coals of Different Rank. Fuel 1983, 62, (9), 1084-1089.

35. Lafdi, K.; Bonnamy, S.; Oberlin, A., TEM Studies of Coal Tars Influence of Distillation Process at Increasing Temperature. Carbon 1990, 28, (5), 631-640.

36. Lewis, I. C., Chemistry of Pitch Carbonization. Fuel 1987, 66, (11), 1527-1531.

37. Kershaw, J. R.; Black, K. J. T.; Jaeger, H. K.; Willing, R. I.; Hanna, J. V., A Comparison of Mesophase Formation under Sparging and Vacuum. Carbon 1995, 33, (5), 633-643.

5. *In situ* observation of mesophase formation and coalescence in catalytic hydroconversion of vacuum residue

5.1. Introduction

The use of hydrogen in catalytic processes was one of most important advances in refining technology during the twentieth century[1]. This process uses the fact that the presence of hydrogen during a thermal reaction of petroleum feedstocks prevents many of coke-forming reactions and improves the yields of the lower boiling components such as gasoline, kerosene, and jet fuel[2]. The cracking and hydrogenation of heavy hydrocarbon molecules and the removal of heteroatoms result in a product with lighter oil fractions and a lower level of contaminants with an increased commercial value and less pollution[3]. The formation of coke during the upgrading of heavy oil is an area of significant importance because of its effect on reducing the liquid yield, catalyst deactivation and fouling of reactor internals and downstream vessels[4]. Coke is usually defined in petroleum industry as toluene insoluble material[4], and coke formation is triggered by reactions such as cracking, polymerization, and condensation which results in the formation of coke as a new carbonaceous phase. Phase behavior also plays an important role in the formation of coke[5].

Carbonaceous mesophase is an intermediate phase which can form during the cracking of heavy oil, as a subset of toluene-insoluble, or coke phases, which is distinguished by its optical anisotropy[6]. During the thermal cracking of heavy

petroleum and coal tar fractions, Brooks and Taylor[7] observed the formation of an intermediate condensed phase which is anisotropic when viewed under polarized light. This carbonaceous mesophase is now classified as a discotic nematic liquid crystal[8]. Carbonaceous mesophase appears during the thermal conversion of heavy oil, in the temperature range of 350 and 500°C, as optically anisotropic spheres surrounded by an isotropic liquid matrix. Cracking of heavy oil gives formation of polycondensed aromatic hydrocarbons, by polymerization, cyclization, dealkylation, and dehydrogenation reactions. The mesophase spherules form as a result of the accumulation of layers of oriented polycondensed aromatic hydrocarbons[9]. Important factors in the mesophase formation process are the heating rate, temperature, residence time, gas flow rate, and stirring rate[9]. Once mesophase spheres begin to form, they can coalesce to form larger mesophase domains. These larger domains eventually deposit as coke on the interior surfaces of process equipment. If the coalescence process can be hindered or ideally prevented, the size of mesophase domains would be smaller and, consequently, be carried out of the process lines and vessels without fouling the equipment[10].

The Slurry hydroconversion processes utilize finely dispersed catalysts which can be introduced into the feed as water-soluble or oil-soluble precursors or as finely divided powders[11]. Several slurry hydroconversion demonstration plants have been built so far, including the CANMET process at the Petro-Canada Montreal Refinery (constructed in the mid 1980's)[12]. Currently, these technologies are still at the demonstration scale. Typically in the hydroconversion

of heavy oils, the main reaction is thermal cracking that produces lower boiling point products. The role of catalyst and hydrogen is to inhibit coke formation by hydrogenating reactive products such as olefins and removing heteroatoms[13, 14]. Kennepohl and Sanford[15] and Panariti et al.[16] showed that dispersed catalysts such as molybdenum sulfide or molybdenite have the ability to prevent coke formation at low catalyst concentrations. At higher concentrations, however, catalyst can promote coke formation. In addition to a chemical role, the catalyst particles act as a supporter or nucleation site for coke and, hence, reduces coking of the reactor walls[17].

The formation of mesophase can be studied by various methods, but polarized-light microscopy is generally the most useful method, because carbonaceous mesophase was discovered and defined by its optical anisotropy[7]. In hot-stage microscopy, a heated microreactor is placed on the optical stage of a polarized light optical microscope to enable the *in situ* observation mesophase growth at the conditions of formation[18]. The first *in situ* observations of mesophase formation was done by Lewis[19] in 1975 using a modified hot-stage apparatus with a glass cover. Perrotta *et al.*[20] observed the *in situ* mesophase formation in petroleum and coal tar pitch at elevated temperatures and pressures. They used a custom reactor for high pressure observations. Rodriguez *et al.*[21] also designed a high pressure and high temperature hot-stage to observe the *in situ* mesophase formation in petroleum fractions. Lafdi *et al.*[22] used hot-stage microscopy to study anisotropic pitches, and Rahimi *et al.*[23] studied the incipient mesophase formation of 10 fractions from Athabasca bitumen vacuum bottoms using hot-

stage microscopy under flowing hydrogen at 5.2 MPa. All these studies used an upright reflective microscope, and samples in the hot-stage were not subjected to stirring. Lewis[19] used a metal probe inserted into the hot-stage chamber to agitate the sample, but not an effective stirrer or agitator. All other studies on pressurized samples were conducted without agitation.

The effect of catalyst on mesophase formation has been studied previously. Braun *et al.*[24] studied iron-catalyzed pyrolysis of coal-tar pitch using iron benzoate and naphthoate as catalyst precursors. They showed that with iron benzoate, the nucleation and growth of mesophase spheres is strongly influenced by the catalyst, with a reduced tendency for coalescence to form large mesophase domains. Bernhauer *et al.*[25] reported similar results when ferrocene was used as a catalyst precursor. However, these results were based on the examination of cooled products, not *in situ* observations. *In situ* study of mesophase formation during catalytic hydroconversion using hot-stage microscopy has not been previously reported, mainly due to the inability of the previous designs to stir the fluid under observation in a hot-stage microscope.

In this paper we report for the first time the use of a stirred hot-stage reactor to observe the effect of stirring on mesophase formation and growth in Athabasca vacuum residue. The experiments were conducted with and without stirring to be able to compare the results. The use of a stirred hot-stage apparatus allowed us to suspend heterogeneous catalyst in the reacting liquid and study the effect of catalyst on mesophase formation and growth. The resulting cokes were observed

with scanning electron microscopy (SEM) to reveal the possible interactions between mesophase and catalyst particles.

5.2. Experimental section

5.2.1. Materials

Athabasca vacuum residue supplied by Syncrude Canada was used for observations, and its properties are shown in Table 5-1. The catalyst was a proprietary nanoparticulate material consisting of transition metal sulfides.

Table 5-1. Properties of Athabasca Vacuum Residue.

Elemental analysis	C(wt%)	81.76
	H(wt%)	9.45
	S(wt%)	6.17
	N(wt%)	0.93
Asphaltene (wt%)		31.1
MCR (wt%)		14.9
Ash (wt%)		3.3
Solids (wt%)		0.22

5.2.2. Characterization of catalyst

BET surface area of catalyst was determined from N_2 adsorption–desorption isotherms measured at 77 K using a Micromeritics ASAP 2020 analyzer. Sample

was degassed in 523 K under vacuum (500 μm) for 8 hours before being analyzed. Eight N_2 uptake measurements made in the range of $0.06 < P_{N2} / P0_{N2} < 0.2$ were used to calculate the BET surface area.

5.2.3. Hot-stage microscopy

Reactions were carried out in a new hot-stage reactor which has been discussed in details elsewhere[26]. A schematic design of the hot-stage is shown in Figure 5-1. The hot-stage reactor was configured to interface with an inverted reflective microscope. is the reaction chamber was made of stainless steel Swagelok fittings and a sapphire window at the bottom to facilitate the observation of the sample inside it. The temperature of the hot-stage is maintained by a heating tape connected to a temperature controller, and thermally insulated by ceramic covers. Reaction temperature is monitored by an Omegaclad XL type K 1/16" thermocouple inserted into the top of the hot-stage which is in direct contact with the sapphire window. The tip of the thermocouple acts as shaft for the magnet stirrer (Figure 5-1). A custom built Alnico magnet stirrer was used in this hot-stage reactor to mix the reactor contents. The stirrer is a block magnet (9.5*4*3 mm) with a 2 mm hole at the center for the thermocouple. The stirrer is coupled with an external magnet rotating at 140 rpm. A stainless steel (thickness 0.13 mm, diameter 2.7 mm) washer (provided by Boker's Inc, Minniapolis) is used to raise the magnet from the window (Figure 5-1).

A mass of 0.4 g of each sample was heated in the reactor to 440°C under continuous stirring at 140 rpm (For the non-stirred experiment the initial mass

was 0.25 g). Experiments were conducted under hydrogen atmosphere that was maintained at 4.8 MPa. The onset of mesophase formation was determined for all

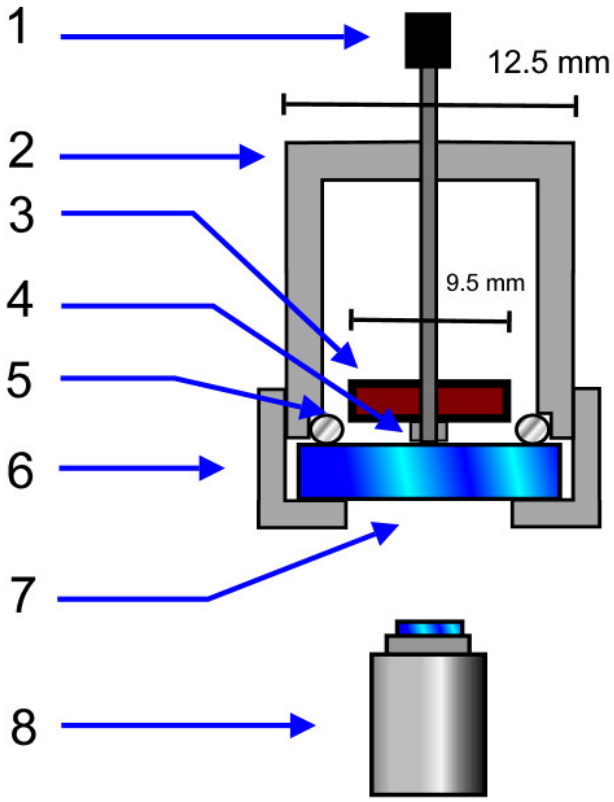

Figure 5-1. Schematic diagram of the hot-stage reactor. 1: thermocouple; 2: steel body; 3: magnet; 4: Metal washer; 5: O-ring; 6: bottom nut; 7: sapphire windows; 8: objective lens of microscope.

the samples by using a Zeiss Axio-Observer inverted reflective microscope (Zeiss, Germany) equipped with crossed polarizers. A Zeiss 3 megapixel camera was connected to the microscope to photographically record the progress of the reaction. Image analysis was performed on a personal computer using ImageJ, a program developed at National Institutes of Health (USA). The images were analysed to determine the area fraction of observable mesophase particles and

their mean area in each photo. In the image analysis, particles with areas smaller than 3 μm^2 were excluded from the results because such small domains could not be accurately identified.

To follow the progress of the non-stirred experiment, one random spot was chosen, and the formation and growth of mesophase at this spot was followed by taking images at different times. For the experiments with the stirred-reactor, the experimental procedure for taking the photos was as follows: before taking the photos the stirrer was turned off for 4 min to give enough time for sedimentation; after sedimentation, seven photos were taken, at random locations, showing the mesophase visible on the window; stirring was turned on again, and the same procedure was repeated. The time of reaction shown for all the graphs in this paper begins when the reactor is heated to the set-point temperature and the reported time for each set of data was the average of the times at which all seven photos were taken. Acquiring seven photos under *in situ* conditions took approximately 3 min. The total area covered by the seven photos was 6.34 mm^2. The photos were analysed using ImageJ, and the results of the all images combined to determine the observable mesophase area fraction in the hot-stage at each time. Ideally, an estimate of the volume fraction of mesophase would be used to follow the progress of the reactions. Calculating the mesophase volume from images was not practical, however, due to the limitations of the hot-stage microscope technique and therefore the data is reported as area coverage of the viewable area (μm^2). Due to the presence of a bimodal distribution of mesophase particles, the image analysis was done separately for the upper and lower modes

of the distribution (the upper mode generally began for particles with areas above 2000 μm^2).

5.2.4. SEM and EDX

Samples were observed using a high resolution JEOL 6301F field emission scanning electron microscope. EDX analysis was done via a PGT X-ray analysis apparatus (res. 135 eV). In addition, some samples were freeze-fractured in liquid nitrogen and the cross-section was observed by SEM. Samples were sputter-coated with carbon before the observation.

5.3. Results and discussion

5.3.1. Cracking of vacuum residue under hydrogen in absence of stirrer

A mass of 0.25 g of Athabasca vacuum residue was cracked under hydrogen at 4.8 MPa and 440°C without catalyst. In this set of experiments, it was important that hydrogen should diffuse into the bitumen film and reach the interface between bitumen film and sapphire window. Therefore, it was important that the sample should be thin enough to provide the required concentration of hydrogen throughout the liquid layer. Fortunately, at the reaction conditions used in this study, the cracking and hydrogenation reactions are relatively slow, with residence times of order 1 h or more[11], and solubility of hydrogen is significant on a molar basis[27]. Using these data and an estimated diffusion coefficient of $1.13x10^{-8}$, m^2/s, we calculated that a liquid film thickness of up to 1.7 mm would ensure that that the dissolved hydrogen concentration was at least 80% of

saturation. This thickness corresponded to a sample mass of 0.25 g in our reactor. The reacting fluid in the non-stirred sample could have an average temperature that is higher than the set-point temperature. The thermocouple is placed in the centre of the sapphire window (Figure 5-1), which is the coldest part of the sample because of the thermal convection from the window. As a result, the fluid closer to the wall of the reactor would be hotter than the temperature shown by the thermocouple. With this provision, mesophase was first observed 27 min after reaching the nominal set-point temperature of 440°C. The initial domains were very small and the areas of the biggest domains were around 5 μm^2. In this unmixed mixture, mesophase did not form uniformly in the field of view through the window, and at some spots mesophase was not observed at all during the experiment. Figure 5-2 shows the mesophase area fraction of this reacting mixture versus time of reaction. The time course follows a sigmoid-shape curve, which is commonly observed in phase transformations like solidification and crystallization[28]. The sigmoid-shape curve is consistent with a nucleation growth process in which the new phase forms by random nucleation in the bulk of the fluid or continuous phase, and then these nuclei grow. The growth occurs at the interface between the old and new phases. As the reaction proceeds, the interface increased constantly, giving an acceleration of rate of formation of mesophase up to an inflection point. Given the low area fraction of mesophase in the micrographs, two reasons are likely responsible for the reduction in rate at long reaction times: depletion of the mesophase precursors in the liquid (the MCR of the sample is 14.9% which means there is a finite amount of coke that can be

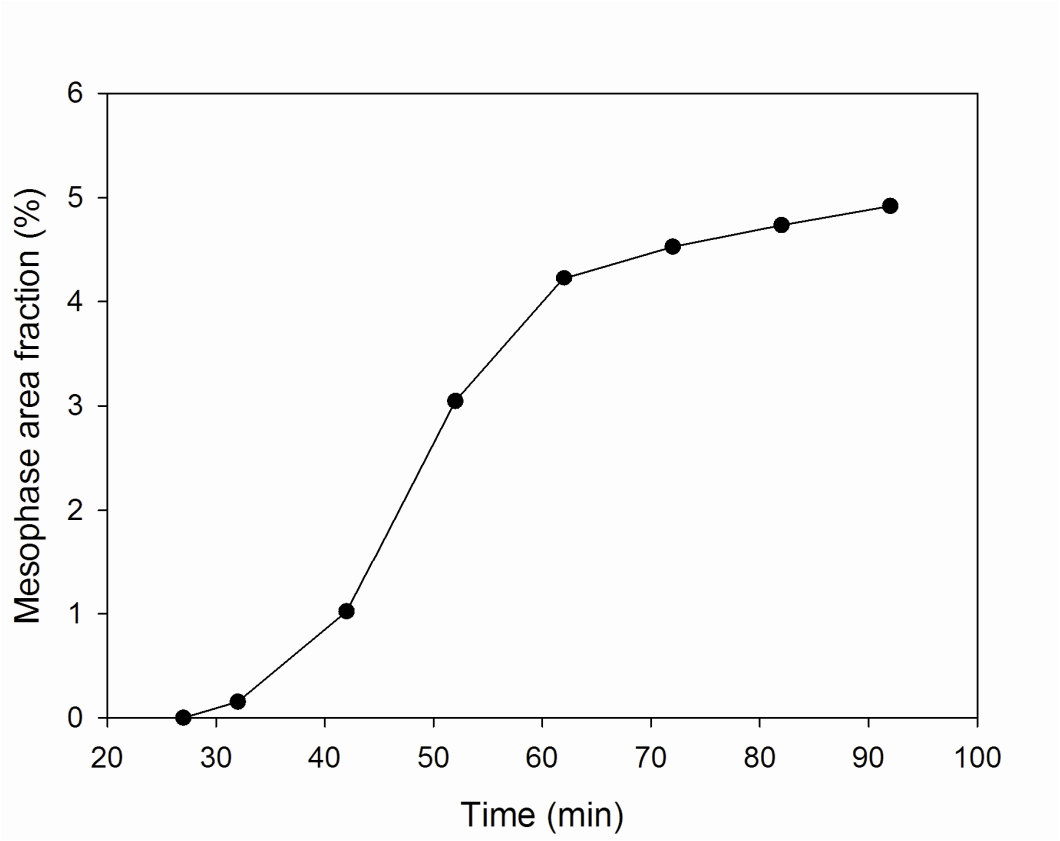

Figure 5-2. Mesophase area fraction versus time during the cracking of Athabasca vacuum residue under hydrogen at 4.8 MPa and 440°C without stirring. Zero time was defined as the point when the reactor was heated to the final temperature. Data points are shown only when detectable mesophase was observed. Prior to the onset time no mesophase was detected, and no data points are shown.

made during thermal reactions), or increased viscosity in the liquid due to the progressive thermal alteration of the feed (the bulk liquid viscosity will decrease but the viscosity of mesophase will increase with time). Fig 3 shows the particle area distribution in this mixture 92 min after reaching the set-point temperature. An important feature that should be noted is the monomodal nature of the particle

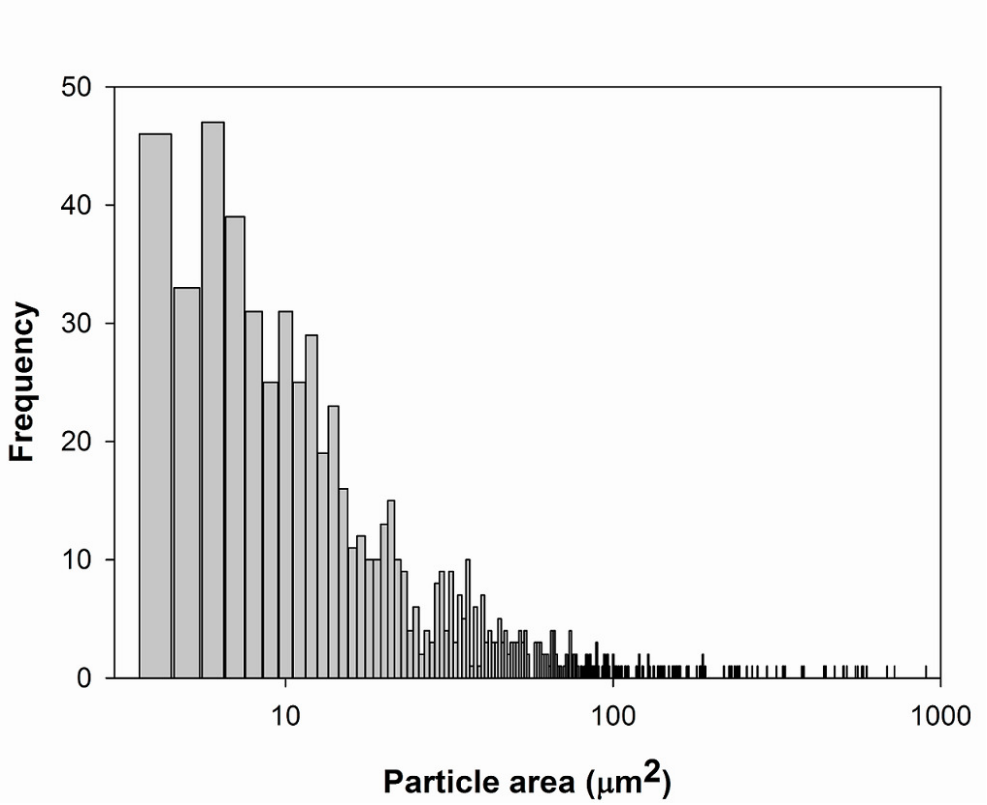

Figure 5-3. Particle area distribution for mesophase particles after 92 min during cracking of Athabasca vacuum residue under hydrogen without stirring at 4.8 MPa and 440°C.

area distribution. This type of distribution was only observed in the absence of mixing.

5.3.2. Cracking of vacuum residue under hydrogen with stirring

A sample of Athabasca vacuum residue was cracked under hydrogen at 4.8 MPa without catalyst. The stirrer was turned on when temperature reached 300°C. Unfortunately, mesophase particles can not be observed while the hot-stage reactor is being stirred. Therefore, after reaching the final temperature, the stirrer was turned off every 2 min to check for the onset of mesophase formation.

Mesophase was first observed in this experiment at 46.0 ± 1.7 min (n=3) after reaching the set-point temperature. With mixing, the temperature of the reacting fluid should be much more uniform and closer to the set-point, 440 °C, than in the case of the unmixed reactor. Since the kinetics of mesophase formation is known to be sensitive to temperature, the on-set times for the mixed and unmixed reactions should not be compared.

Notably, the distributions of mesophase domain sizes are different between the stirred and unstirred cases. As mentioned previously, a monomodal size distribution was observed in the unmixed case. When the reactor contents were mixed, a bimodal distribution of mesophase domains was observed. The initial mesophase observed when the reactor was agitated was characterized by a few large domains formed in the bulk, and the areas of the largest domains were around 4500 μm^2, as shown in Fig 4.

At the same time a, few smaller domains (4-60 μm^2) were also observed, but the total area fraction of these smaller domains (0.01%) was much smaller than that of the large domains (0.2%). The large regions were probably the result of the coalescence of smaller mesophase domains, and we call this material "bulk mesophase". Bulk mesophase is usually defined as a continuous anisotropic phase formed by coalescence of mesophase spheres[29]. This definition of bulk mesophase is qualitative, however, and in this paper we define bulk mesophase as any domains in the larger mode of the bimodal distribution (generally bigger than 2000 μm^2). With this operational definition, the majority of the domains observed at the onset of mesophase formation were characterized as bulk mesophase. This

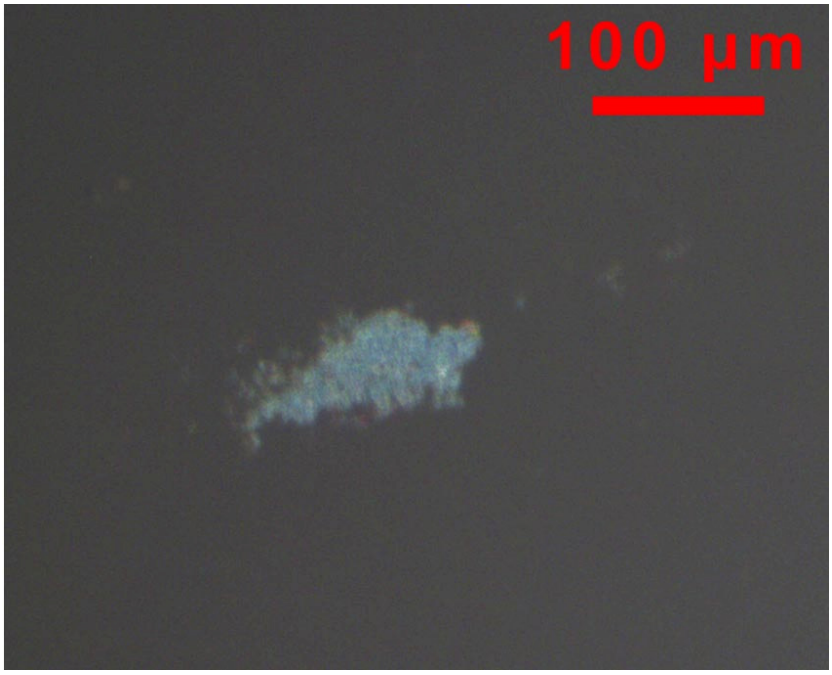

Figure 5-4. Photomicrograph of initial mesophase observed during cracking Athabasca bitumen under hydrogen at 4.8 MPa and 440°C with agitation at 140 rpm as an aggregated domain.

observation was completely different from with what observed in the non-stirred reactor in which all the initial detectable domains were smaller than 2 μm^2. In the mixed case, smaller mesophase domains were observed 8 min after the observance of large bulk domains, and these domains grew with time. Consequently, the reactor contained both mesophase spheres (small domain) and bulk mesophase (large domain) at the same time as shown in Figure 5-5. Both the large domains and the small domains were mobile, in that they were suspended in the fluid phase and were easily moved by the action of the stirrer.

As noted, mixing of the reacting fluid resulted in the formation of a bimodal distribution of mesophase in the reactor. To show this bimodal distribution, the

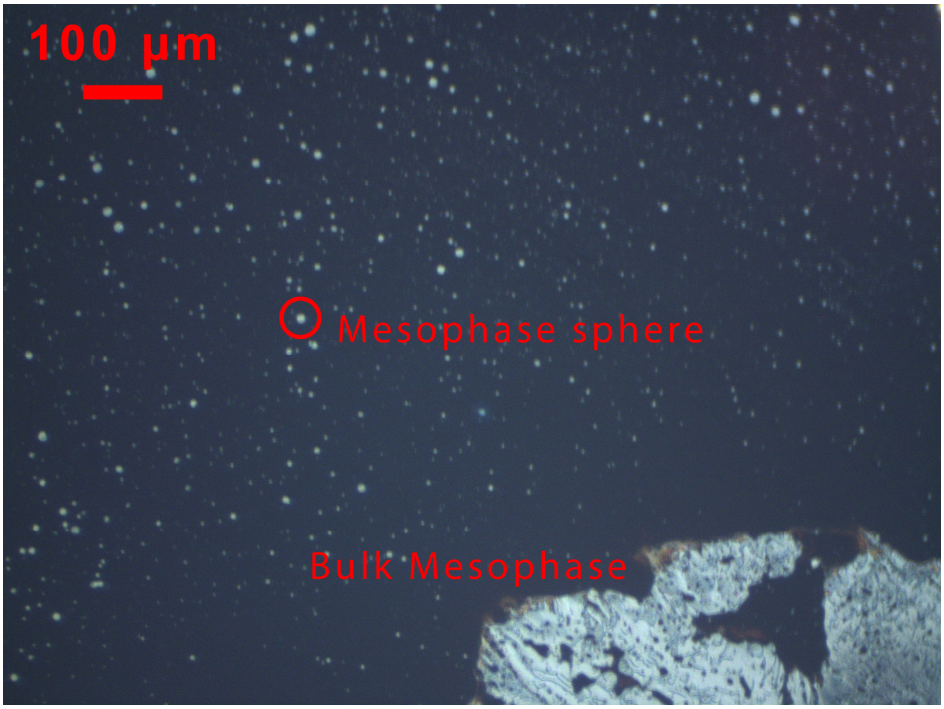

Figure 5-5. Photomicrograph of mesophase formed during cracking Athabasca vacuum residue under hydrogen at 4.8 MPa and 440°C stirred at 140 rpm, showing coexistence of mesophase spheres (small domain) and bulk mesophase (large domain) formed by stirring after 85 min.

particles were divided into two groups: the lower mode of the distribution was comprised of particles with area below 2000 μm^2 which formed the small mesophase particles, and the upper mode of the distribution included particles with area above 2000 μm^2 which formed the large mesophase regions (bulk mesophase). The total number of mesophase particles per unit area in the field of view was calculated at different times for both groups and is shown in Table 5-2 and the area fraction of both groups is shown in Figure 5-6. Each of the data points is calculated from seven images that were taken over a period of 3 minutes, during which time the reactions were proceeding.

Table 5-2. Number of mesophase domains per area (mm^2) with and without the addition of catalyst. Small domains have an area below 2000 μm^2, and large domains have an area above 2000 μm^2.

No catalyst			With 1.0 wt% catalyst		
Time (min)	Number of small domains per area (mm^{-2})	Number of large domains per area (mm^{-2})	Time (min)	Number of small domains per (mm^{-2})	Number of large domains per area (mm^{-2})
45	3.15	0.47	55	4.10	0.00
53	$1.46x10^2$	0.16	71	$5.05x10$	0.47
69	$9.00x10^2$	0.95	87	$5.28x10^2$	1.73
85	$8.39x10^2$	3.78	103	$1.02x10^3$	3.31
101	$9.69x10^2$	3.63	119	$1.62x10^3$	2.84
117	$5.03x10^2$	8.67	135	$1.97x10^3$	1.73

The results of Figure 5-6 show that the total mesophase area fraction increased 1.7% over approximately the 3 min time span. This change limits the number of photos that can be used to calculate each data point. The area fraction of bulk mesophase regions (area above 2000 μm^2) was much larger, but from a much smaller number of particles. In spite of their limited number, the size of the bulk mesophase domains grew rapidly, and soon they became too big to fit into the field of view of the microscope, so it is possible that the total area of these regions was much greater than the reported value. These large domains were not observed in the absence of the mixing, so it is likely that these domains were the result of the forced coalescence caused by turbulence. Figure 5-7 shows a typical distribution of the particle area in the reaction mixture at different times. The distributions for particles below and above 2000 μm^2 were drawn separately due

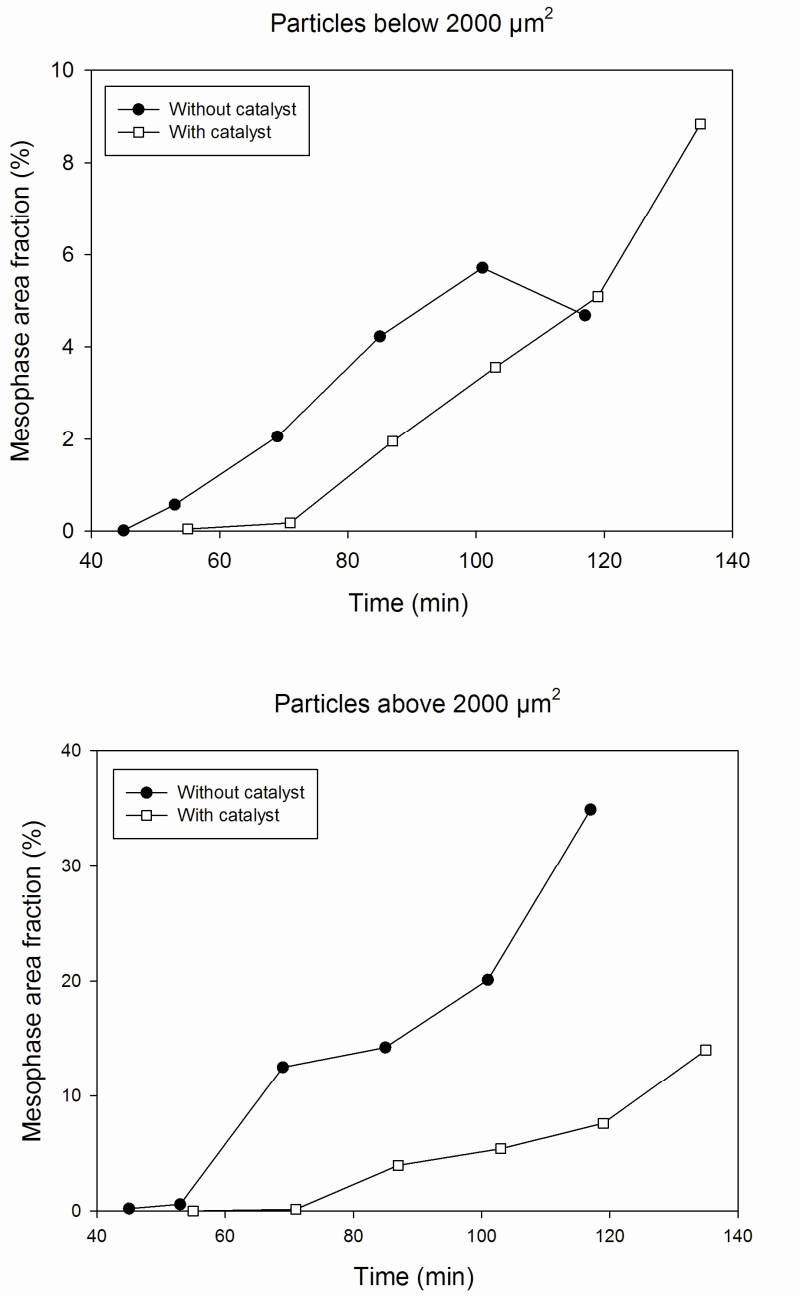

Figure 5-6. Mesophase area fraction during cracking of Athabasca vacuum residue under hydrogen at 4.8 MPa and 440°C stirred at 140 rpm without catalyst and with 1.0 wt % catalyst for (a) small domains with area below 2000 μm^2 versus time, (b) large domains with area above 2000 μm^2 versus time of reaction. Data points are shown only when detectable mesophase was observed. Prior to the onset time no mesophase was detected, and no data points are shown.

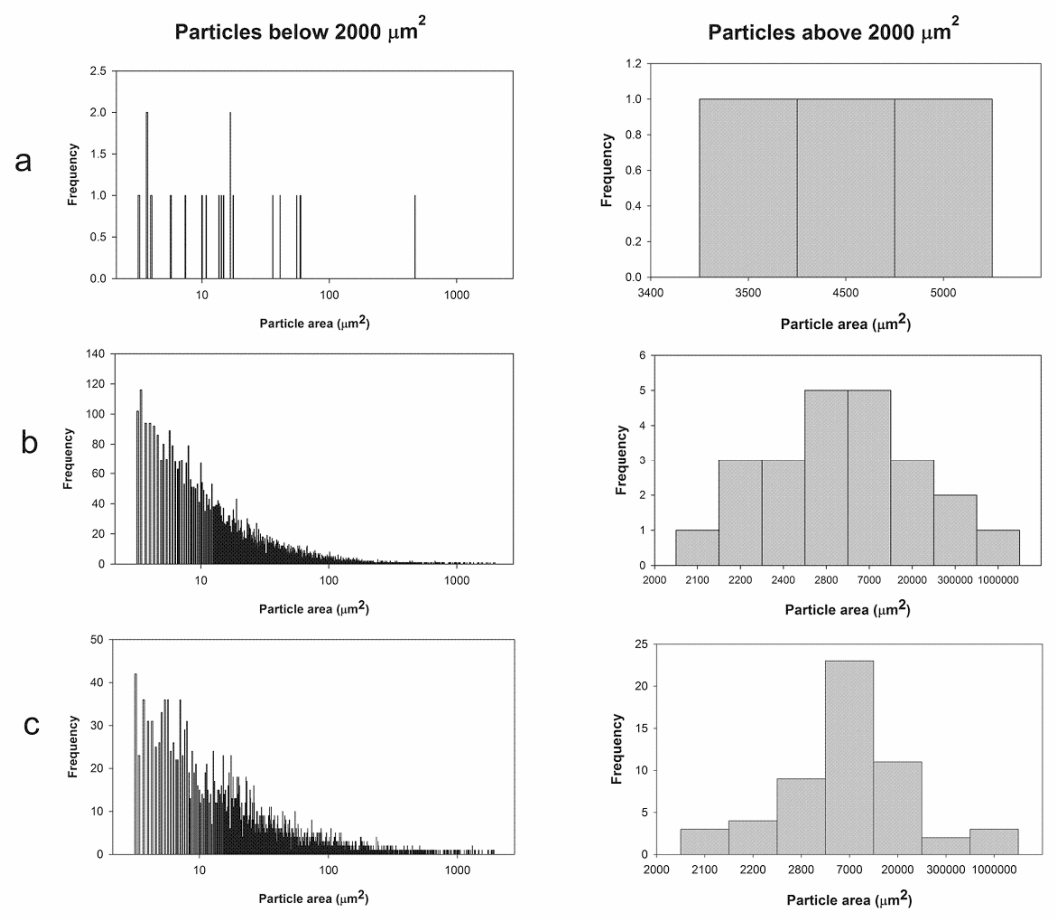

Figure 5-7. Particle area distribution for particles with area below and above 2000 μm^2 at different time of reaction in cracking of Athabasca vacuum residue under hydrogen at 4.8 MPa and 440°C stirred at 140 rpm.

to the very different range of particle size and frequency in each group. The data from the experiments with mixing clearly show a bimodal distribution of particle areas, and implicitly particle sizes. Given the mild agitation in the reactor and the fluid properties, turbulent eddies are unlikely to break up the mesophase domains, except perhaps the very largest over 2000 μm^2 which did not fit in the field of view of the microscope[30]. Mixing clearly alters the coalescence of the mesophase particles, giving a bimodal distribution, but how does this distribution arise, and

why are the domains found at the onset of mesophase observation so large? One way to answer these questions is to study the effects of turbulence on other two-phase mixtures in the nature. An analogous example is the turbulent interaction of particles in atmospheric clouds which results in the formation of raindrops.

Rain droplet growth is initially dominated by condensation which results in a narrow distribution of small particles. The formation of larger drops is the result of collision and subsequent coalescence which is called "collection"[31]. While initial rain droplet growth is dominated by condensation in the earliest stages of cloud development, subsequent growth is dominated by collisions and coalescence of the fraction of larger droplets. A large droplet can absorb a very large number of smaller droplets. The result is an explosive growth which results in a bimodal distribution of droplet size[32]. The computations of Berry and Reinhardt[33] showed that a monomodal narrow size distribution can change into bimodal distribution. They proposed three phases of growth of cloud droplets by collision–coalescence. They divided the size spectrum into small cloud droplets (S1) which were smaller than 50 μm and larger drops (S2) which were larger than 50 μm. They showed that the initial growth is governed by S1–S1 "autoconversion" phase in which the self-collections of the small cloud droplets near the peak of the initial size distribution can result in the mass transfer to the larger drops. After that, an "accretion" phase starts in which accretion dominates over the autoconversion and results in the mass transfer from the initial peak (S1) to the newly formed secondary peak of larger size (S2) domains. The final stage is the "large hydrometeor self collection" phase in which the self-collections of

large droplets near the second peak will dominate over the accretion mode. This results in shrinkage of the initial peak (S1) and the growth of the second peak (S2)[34]. A clear separation between the modes of the size distribution persists, after the formation the bimodal distribution by the collection process for long times, and the larger drops tend to retain their identity[35]. The study of Carlos de Almeida[36] demonstrated at small scale that cloud turbulence can significantly enhance the growth of particles by the collection process. In addition the turbulence could decrease the initial mean mass radius which was necessary for the collection process to commence growth and change the monomodal distribution into a bimodal distribution.

By analogy to the behavior of water droplets, we can suggest an explanation for our observations. Figure 5-8 shows our suggested size distribution of mesophase domains, consistent with the area distribution in Figure 5-7. When the mesophase domains form, they initially are submicron in size, and form a monomodal narrow size distribution that is below the resolution of an optical microscope. The mode of this distribution can shift to larger particles with time, but the peak of the distribution always remains at submicron-scale below the resolution of an optical microscope. When measured optically, the results appear as a truncated Gaussian distribution, which now looks like an exponential distribution (Figures 5-3 and 5-7). In absence of turbulence, the distribution remained monomodal at all times (Figure 5-3). The addition of stirring can enhance the collision-coalescence process and change this initially monomodal distribution into a bimodal distribution (Figure 5-7). Apparently when the second mode of larger mesophase

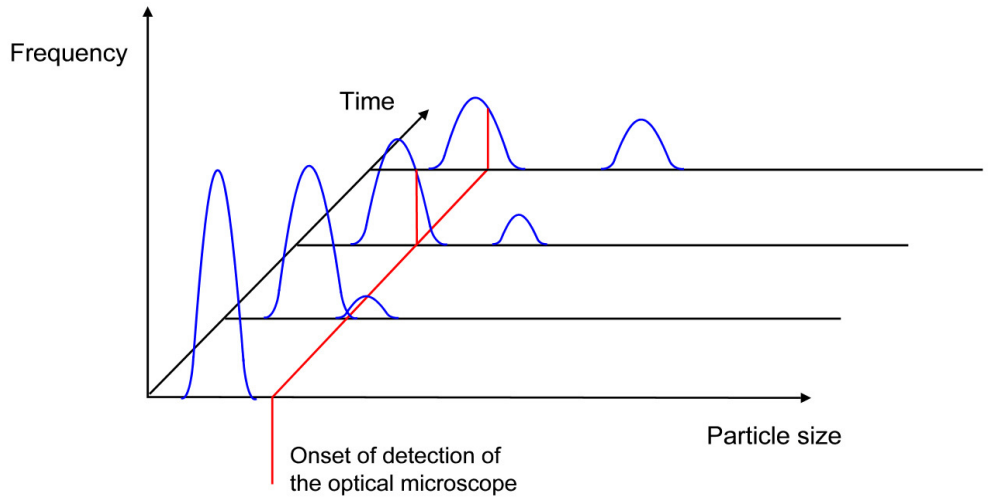

Figure 5-8. Time evolution of particle size distribution during mesophase formation in a stirred reactor.

particles initially forms, the lower mode of the particle size distribution is just below the resolution of the optical microscope (with the exception of a few large domains) and is not observed (Figure 5-8). As a result, the initial domains which were observed at the onset of mesophase formation were composed of a few large domains (from the second mode) accompanied with a few small domains (from the first mode) (Figure 5-8). After formation, the number and size of domains in the second mode continually grows at the expense of diminishing first mode's domains (Figure 5-8).

In order to understand how stirring affects the observed size distribution, first we suggest in Figure 9 a series of reactions and physical changes which are responsible for the formation and growth of mesophase. The combination of thermal cracking, addition, and condensation reactions in the vacuum residue leads to the formation of high molecular weight planar polyaromatic molecules.

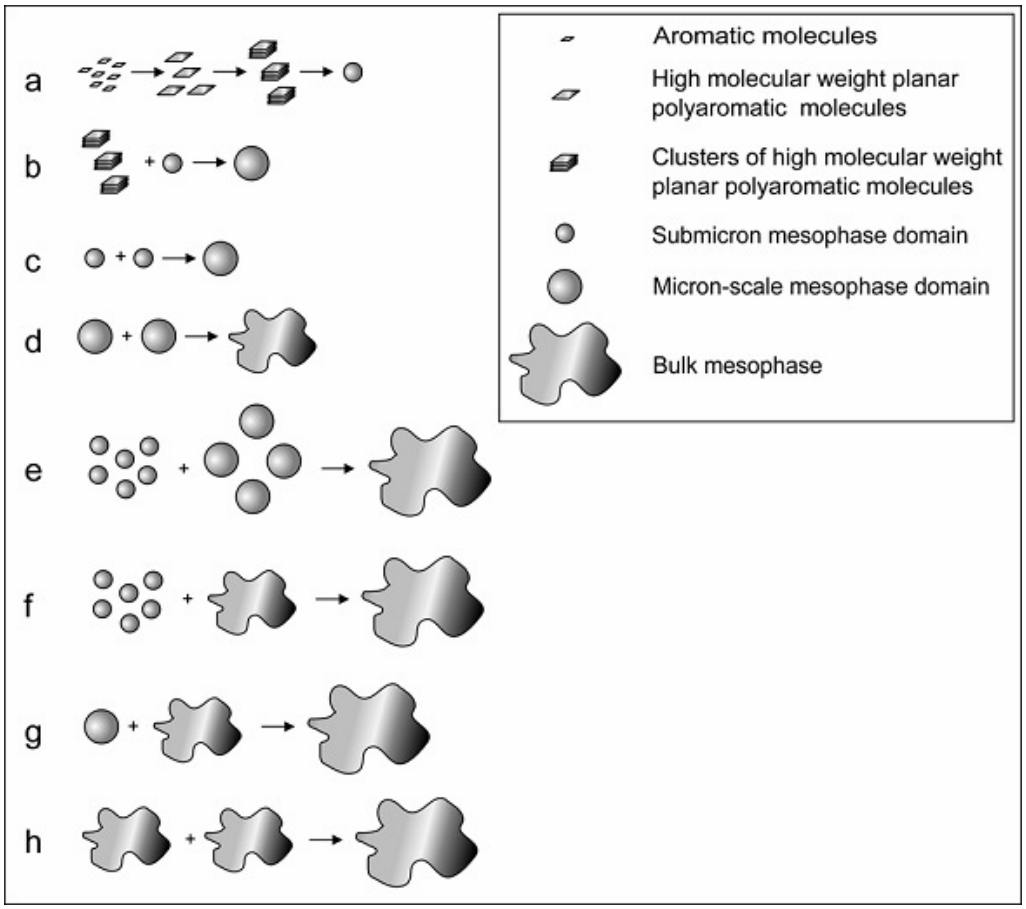

Figure 5-9. Different mechanisms for the formation and growth of mesophase.

These molecules can stack and to give mesophase domains, which are initially too small to be detected by an optical microscope (Figure 5-9a). As conversion of vacuum residue proceeds, these mesophase domains can grow by the addition of molecular clusters resulting from addition reactions and condensation of more polyaromatic aromatic molecules (Figure 5-9b). The mesophase domains, when contacted with each other, can also coalesce instantaneously to form larger mesophase domains[37] (Figure 5-9c). The growth and coalesce of mesophase domains continue until they become observable with an optical microscope as

micron-scale mesophase spheres. The further coalescence of these micron-scale mesophase spheres can result in the formation of bulk mesophase (Figure 5-9d). The combination of steps a, b, c, and d in Figure 5-9 would give rise to the initial monomodal distribution, and results in the formation of a large number of submicron mesophase domains with or without mixing. Stirring forces the coalescence of the submicron domains with each other (Figure 5-9e) to form the second mode of size distribution for bulk mesophase. The formed bulk mesophase can also grow by collecting more submicron domains (Figure 5-9f). When the population of these large domain increases, however, they can coalesce both with each other and with smaller micron-scale mesophase spheres to form even larger domains (Figure 5-9g and h).

5.3.3. Cracking of vacuum residue under hydrogen with the stirrer and catalyst

A sample of Athabasca vacuum residue was premixed with 1.0 wt% of catalyst and reacted under hydrogen at 4.8 MPa. The stirrer was turned on when temperature reached to 300 °C. After reaching the set-point temperature, the stirrer was turned off every 2 min to identify the onset time of mesophase formation. Mesophase formed 60.3 ± 6.1 min (n=3) after reaching the set-point temperature. As expected, the addition of catalyst, gave a longer time to onset; in this case 14 min longer than the experiments with only hydrogen and mixing. Similar to the experiments without catalyst, the first observed mesophase particles were the larger bulk type mesophase particles and they could be moved easily by the motion of the stirrer.

The initial mesophase observed when the reactor was agitated without catalyst was dominated by a few large domains formed in the bulk, and the areas of the largest domains were around 4500 μm^2, as shown in Fig 4. In contrast, the initial mesophase domains observed in the presence of catalyst consisted of smaller domains of bulk mesophase, with areas of around 950 μm^2. Some smaller domains, as small as 3 μm^2, were also observed at the same time. Initially, the total area fraction of these smaller domains (0.006% for domains between 3-100 μm^2), however, was much smaller than that of the larger domains (0.044% for domains larger than 100 μm^2). Note that with the addition of catalyst, the median size of upper mode of the particle size distribution, or bulk mesophase, was smaller than in the case of the stirred uncatalyzed reactions. The majority of the initial domains were still much larger than in the case of the unmixed reaction. The spherical domains of mesophase were observed in large numbers 16 min after the onset of mesophase observation and grew with time, so at this time the reactor fluid contained significant amounts of both small mesophase spherules and bulk mesophase. As in the experiment without catalyst, the stirring resulted in the formation of a bimodal distribution of mesophase. The area fractions and total number of mesophase particles per unit area were calculated at different times for particles in both modes of the bimodal particle size distribution and are shown in Figure 5-6 and Table 5-2. The particle areas for particles in the lower mode of the distribution again had a truncated Gaussian or exponential distribution like the previous experiment. As in the previous experiment, the area of the bulk

mesophase domains grew rapidly to become and too large to fit into the field of view of the microscope.

The addition of catalyst increased the time for onset of mesophase formation as expected. The slope of the curves for the middle points in Figure 5-6a was very close, which indicated that the rates of growth for the small particles in the lower mode of the distribution, below 2000 μm^2, were almost the same with and without catalyst. However, the addition of catalyst significantly suppressed the rate of formation of the large particles with area above 2000 μm^2, as shown in Figure 5-6b. The addition of catalyst apparently suppressed the driving forces for coalescence of spheres to form bulk mesophase, which resulted in a lower area fraction of bulk mesophase. This observation was also consistent with the previous study by Braun *et al.*[24] who showed that iron sulfide catalysts derived from ferrocene and especially iron benzoate could significantly reduce the coalescence of mesophase domains, giving a much longer time to form bulk mesophase. Their SEM analysis showed that catalyst particles were located at the surface of mesophase spheres, therefore, they suggested that the surface coverage of the spheres could be responsible for the hindrance of coalescence[24, 25].

In this study, the coke that remained in the reactor after the cracking of vacuum residue under hydrogen with stirring and catalyst was collected after finishing the experiment. Figure 5-10 shows the surface of this coke by SEM microscopy. The mesophase particles were easily detectable due to their higher density giving brighter domains and the catalyst particles were also detectable as even brighter particles in the photo. This analysis was confirmed by EDX analysis of the sample

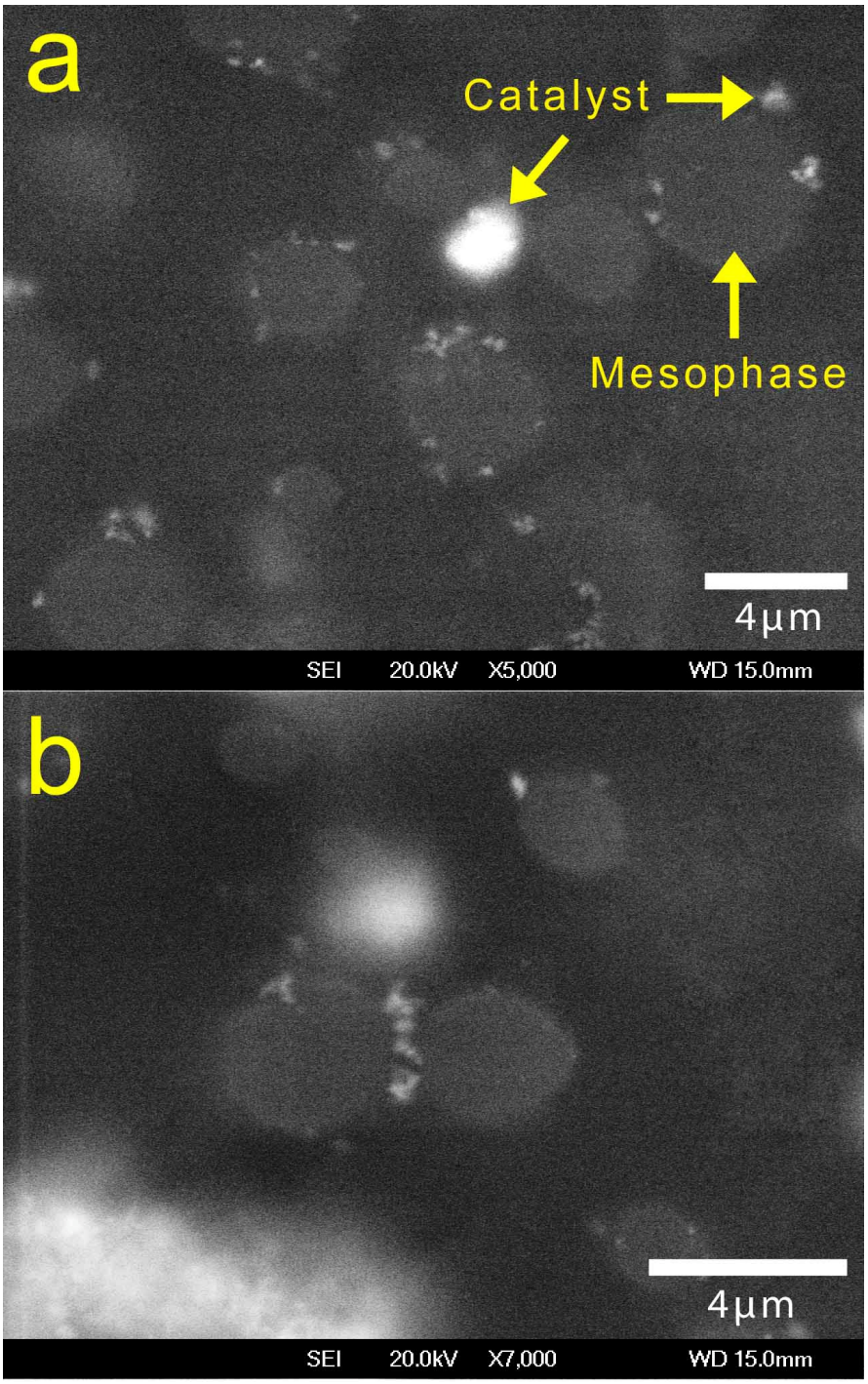

Figure 5-10. SEM photograph of the coke formed after cracking of Athabasca vacuum residue with 1.0 wt % catalyst under hydrogen at 4.8 MPa and 440°C stirred at 140 rpm. Sample was heated for 90 min in the hot-stage reactor. (a) The catalyst attaches to the outer surface of mesophase domains. (b) the catalyst can prevent the coalescence of mesophase domains.

(Figure 5-10a). The image showed that the catalyst only attached to the outer surface of mesophase and did not penetrate into mesophase domains as suggested by previous studies[24,38]. With the catalyst collected on the surface of the mesophase domains, there are two possible mechanisms by which the catalyst could reduce the formation of bulk mesophase: a chemical mechanism and a physical mechanism.

Chemically, it is well known that the addition of hydrogen and an active hydrogenation catalyst can reduce the formation of coke during the thermal cracking of heavy oil. One possible role of the catalyst is to reduce the addition reactions that are thought to precede mesophase formation (Fig 9a). Gray and McCaffrey[39] suggested that the key role of the catalyst is preventing olefin addition reactions by promoting direct olefin conversion and partial hydrogenation of polynuclear aromatic hydrocarbons to form donor species. Polymerization of olefins has the potential to build higher molecular weight molecules which result in the formation of coke. The condensation of these molecules can result in the formation of aggregates of planar polyaromatic molecules in mechanism a. As a result the addition of catalyst can suppress the formation or growth of submicron mesophase domains. This mechanism can explain the delay in on-set time of observable mesophase in Figure 5-6 when catalyst is present.

In addition to the expected chemical effect, the dispersed catalyst had an important physical effect by inhibiting the coalescence of the submicron domains. Any adhesion of catalyst particles to the exterior of the mesophase domains could

hinder coalescence (Figure 5-10b). Stabilization of the small particles by steric repulsion can explain the smaller area fraction of the larger bulk mesophase domains in the experiments with catalyst. The freeze-fractured surface of the collected coke (coke which remained in the hot-stage after the cracking of vacuum residue under hydrogen) was observed by SEM as shown in Figure 5-11.

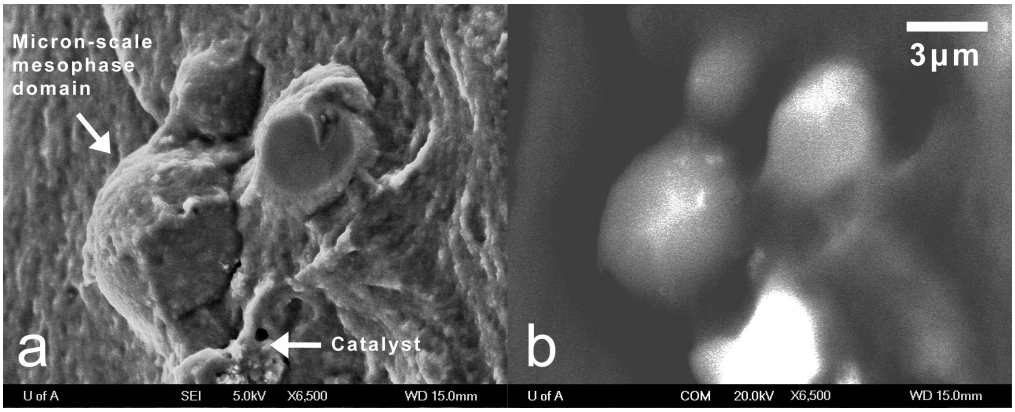

Figure 5-11. The freeze-fractured surface of coke from Athabasca vacuum residue premixed with 1 wt% of catalyst under SEM. Sample was heated for 90 min in the hot-stage reactor at 440°C under hydrogen at 4.8 MPa and 440°C stirred at 140 rpm. (a) the secondary mode image. Some micron-scale mesophase spheres are detectable. The surface is also completely covered with submicron domains. (b) the backscattered mode image shows the presence some catalyst particles at the outer surface of mesophase micron-scale domains.

The micron-scale mesophase domains are easily detectable in Fig 11a; however, the sample is covered with many submicron mesophase domains. This was also consistent with our hypothesis that the first mode of the size distribution contains a large amount of submicron scale domains which are not detectable with optical

microscopy, and the peak of this mode probably lies at a size below the resolution of an optical microscope. The catalyst particles were detected in the backscattered image (Figure 5-11b), and the presence of catalyst metal on the surface of the domains was confirmed by EDX analysis. The catalyst particles are again attached to the outer surface of mesophase domains.

The literature on dispersed catalysts emphasizes the nano-size of the particles. In practice, nano-sized particles invariably cluster together under reactor conditions[40]. At low catalyst concentrations, the clustering of the catalyst particles is not extensive and the resulting agglomerates are still very small, as can be seen in Fig 10. Due to the limited agglomeration of catalyst particles at low concentration, they were apparently more effective for preventing the growth of larger mesophase domains, i.e. preventing 570 μm^2 domains from growing to over 2000 μm^2.

As previously discussed, the initial submicron mesophase domains are not detectable by optical microscopy[41, 42]. While a nano-sized catalyst which is well dispersed in the reactor should be able to prevent submicron mesophase domains from further coalescence by steric repulsion, the micrographs indicate small-scale agglomeration of the catalyst at low concentrations. In theory, well dispersed nano-sized catalyst particles could inhibit the coalescence of the submicron domains. Agglomeration of catalyst particles, which increases their size and reduces their exterior surface area, makes them less effective at suppressing the coalescence of these submicron mesophase domains (Figure 5-12a). They are, however, still effective at stabilizing larger micron-scale mesophase domains

(Figure 5-12b). This role is consistent with the data of Figure 5-6. For small particles with area below 2000 μm^2, mesophase formation started sooner without catalyst, but

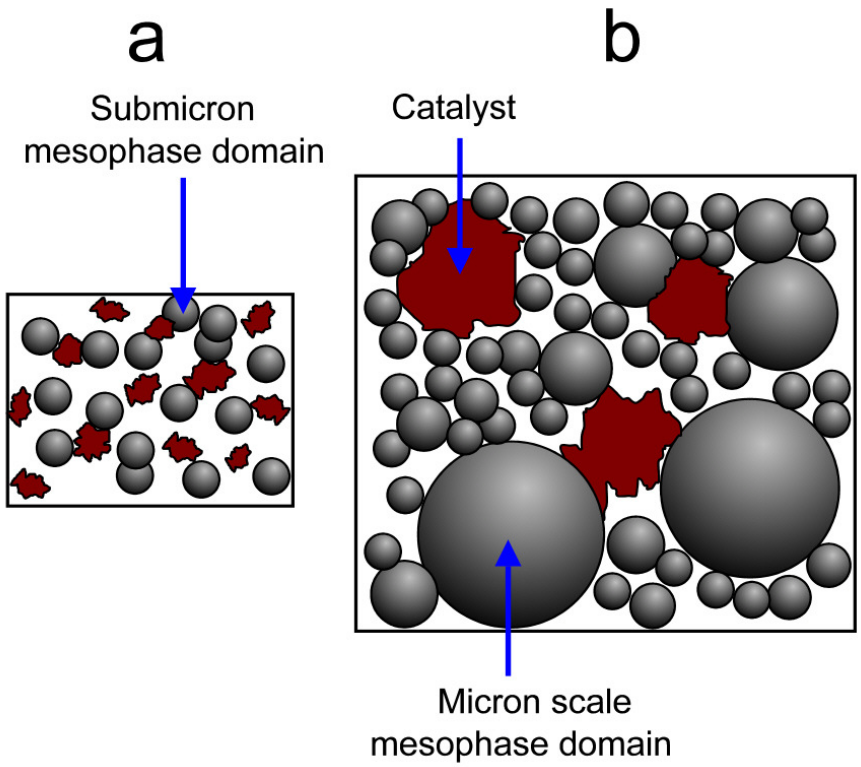

Figure 5-12. Schematic representation of the interaction of catalyst with mesophase domains. (a) the nano size catalyst prevents the coalescence of submicron mesophase domains, but (b) the agglomerated catalyst particles are not effective in suppressing the coalescence of submicron mesophase domains anymore; however, they can prevent the coalescence of larger (multi-micron scale) mesophase domains.

the area fraction increased almost at the same rate with and without catalyst. Conversely, for big particles with areas above 2000 μm^2, the area fraction increased at a significantly lower rate with the addition of catalyst. Mechanisms b and c in Figure 5-9 would be mainly responsible for the formation mesophase

particles with area below 2000 μm^2. These steps would not be affected by catalyst since catalyst could not suppress the coalescence of submicron domains and molecular clusters. Catalyst also could not prevent the formation of the bimodal distribution, since it was not effective on mechanisms e and f in Figure 5-9. However, catalyst was apparently very effective in suppressing the growth of bulk mesophase by influencing mechanisms d and g and h in Figure 5-9, since larger domains were involved in these mechanisms and agglomerated catalyst particles can attach to the outer surface of these large domains and suppress their coalescence.

5.3.4. Effect of catalyst concentration on mesophase formation

The catalyst used in this study was supplied as a fine power. Figure 5-13 shows the effect of catalyst concentration on the onset of mesophase observation at 4.8 MPa and 450°C. The results show that the most effective concentration of catalyst, as measured by the maximum time for the onset of mesophase formation, was 1 wt% of catalyst. At higher catalyst loading, the effectiveness of the catalyst decreased significantly.

Very few studies have looked at the effect of the dispersed catalyst concentration on coke yield. Bearden and Aldridge[43] studied the effect of metal sulphide catalyst on the coke yield. They found that initially the coke yield decreased with molybdenum concentration and reached a minimum when molybdenum concentration was 500-800 ppm. Above that concentration the coke yield slowly increased with increasing the molybdenum concentration. The work of Kennepol and Sanford[15] showed the same effect on coke yield for micro-

dispersed molybdenum sulphide catalyst, and the work of Panariti *et al.*[16] showed similar results for dispersed molybdenite. These results suggest that dispersed catalysts at low concentrations are effective in suppressing mesophase and coke formation, but this efficiency decreases at higher concentrations. This

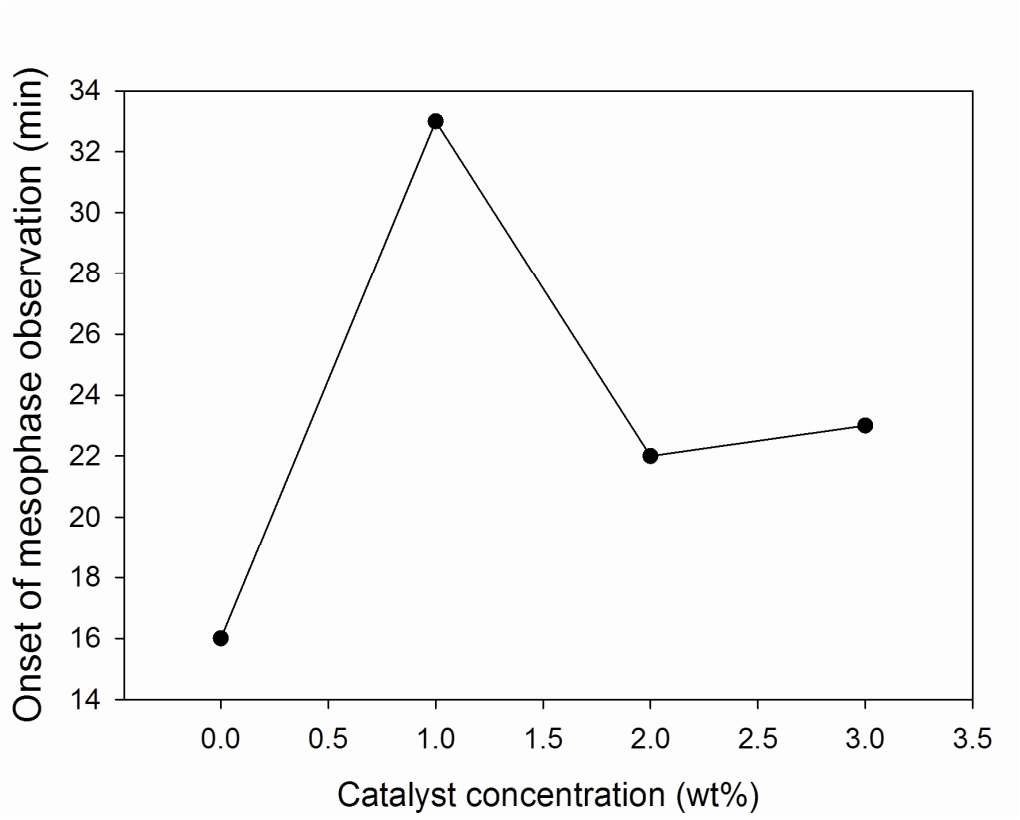

Figure 5-13. Onset of mesophase observation versus the concentration of catalyst during cracking of Athabasca vacuum residue under hydrogen at 4.8 MPa and 450°C stirred at 140 rpm.

effect is not limited to catalyst but can be extended to include other noncatalytic solids. Liu[44] studied the effect of the addition of vacuum residue solids to solid-free vacuum residue on coke yield. A minimum ultimate coke yield was observed at an intermediate concentration of solids. These results suggest that this

behaviour can be attributed to the physical role of catalyst in suppressing mesophase and coke formation. As we mentioned before, a nano-dispersed catalyst has both a chemical and physical role in suppressing the coalescence of submicron mesophase domains. In addition, the chemical effect is much more effective with highly dispersed catalyst particles due to the higher surface area. At high concentrations, large scale agglomeration of the catalyst can significantly decrease the efficiency of catalyst in terms of both the physical and chemical effects.

To demonstrate this large-scale agglomeration, the coke which remained in the hot-stage after the cracking of vacuum residue under hydrogen with 3 wt% at 4.8 MPa and 450°C was collected and observed by SEM, as shown in Figure 5-14. Rather than the finely distributed catalyst particles and small aggregates that were observed at an initial concentration of 1%, the catalyst particles in this sample were highly agglomerated. Catalyst agglomeration in this case resulted in a decrease in the onset time of observable mesophase formation.

5.4. Conclusions

The *in situ* mesophase formation in Athabasca vacuum residue was investigated using a novel stirred hot-stage reactor. Mesophase formation was studied in vacuum residue under hydrogen atmosphere with and without the addition of catalyst. Stirring forced coalescence which results in the formation of large bulk mesophase regions in the pitch which coexisted with a large number of small mesophase domains. Turbulence resulted in the formation of a bimodal

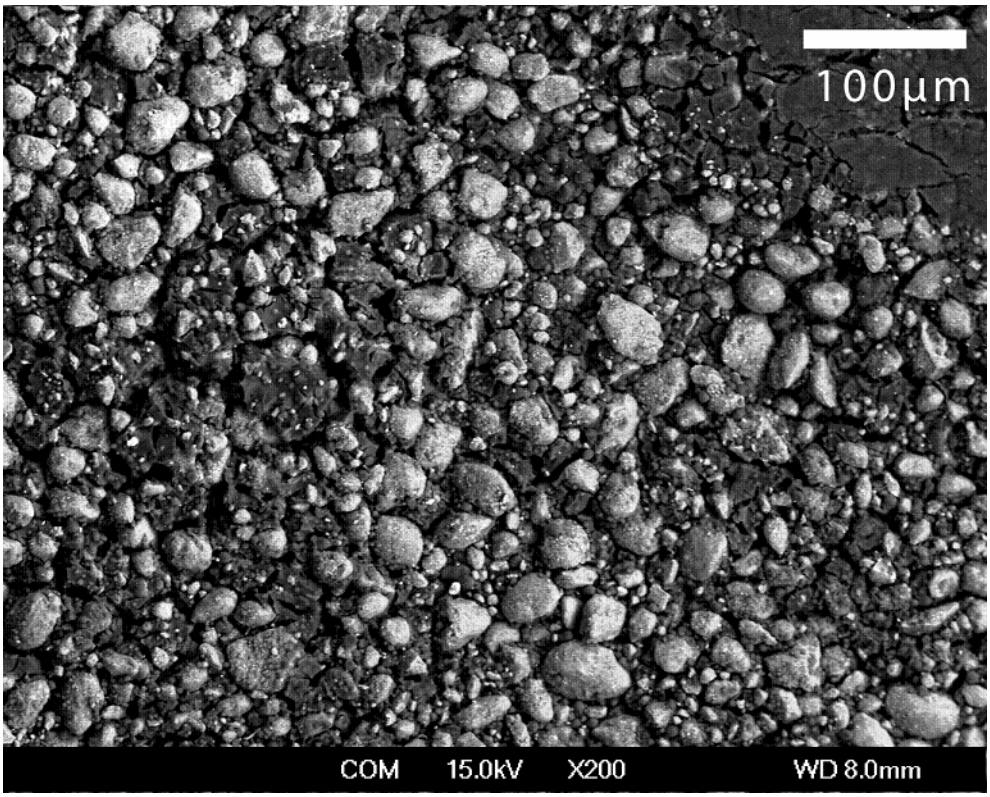

Figure 5-14. SEM photograph of the coke formed after cracking of Athabasca vacuum residue with 3.0 wt % catalyst under hydrogen at 4.8 MPa and 450°C stirred at 140 rpm. Sample was heated for 35 min in the hot-stage reactor. Using a higher concentration of catalyst led to significant agglomeration of catalyst particles.

distribution of mesophase particles in the reacting fluid resulting in a bimodal distribution comprised of a large number of small spherical mesophase domains and a small number of very large bulk mesophase domains. The addition of catalyst had both chemical and physical effects on mesophase formation. The chemical effect increased the time of onset of mesophase formation and the physical effect decreased the tendency of mesophase spheres to form bulk mesophase. SEM analysis showed that catalyst particles agglomerated and stuck

to the outer surface of mesophase domains and prevented their coalescence. Although the agglomeration of catalyst particles likely decreased its efficiency for suppressing the formation of small mesophase domains of a few microns in diameter, the agglomerated material was still effective in suppressing the formation of bulk mesophase. The results showed that there was a maximum for the onset of mesophase observation versus catalyst concentration. As a result, increasing the concentration of catalyst does not necessarily increase its efficiency for suppressing mesophase formation due to the extensive large-scale agglomeration of catalyst particles at high catalyst concentrations.

5.5. References

1. Dolbear, G. E., Chapter 7. In Petroleum Chemistry and Refining, Speight, J. G., Ed. Taylor & Francis: Washington, DC, 1998.
2. Speight, J. G., The Chemistry and Technology of Petroleum. 4th ed.; CRC Press: Boca Raton, 2006.
3. Carbonell, M. M.; Guirardello, R., Modelling of a Slurry Bubble Column Reactor Applied to the Hydroconversion of Heavy Oils Chem. Eng. Sci. 1997, 52, 4179-4185.
4. Gray, M. R., Upgrading Petroleum Residues and Heavy Oils. Marcel Dekker Inc.: New York, 1994.
5. Rahmani, S.; McCaffrey, W.; Elliott, J. A. W.; Gray, M. R., Liquid-Phase Behavior during the Cracking of Asphaltenes. Ind. Eng. Chem. Res. 2003, 42, (17), 4101-4108.

6. Marsh, H.; Latham, C. S., The Chemistry of Mesophase Formation. Am. Chem. Soc., Symp. Ser. 1986, 303, 1-28.
7. Brooks, J. D.; Taylor, G. H., Formation of Graphitizing Carbons from Liquid Phase. Nature 1965, 206, (4985), 697-699.
8. Bisoyi, H. K.; Kumar, S., Discotic Nematic Liquid Crystals: Science and Technology. Chem. Soc. Rev. 2010, 39, (1), 264-285.
9. Honda, H., Carbonaceous Mesophase-History and Prospects. Carbon 1988, 26, (2), 139-156.
10. Rahimi, P.; Gentzis, T., The Chemistry of Bitumen and Heavy Oil Processing. In Practical Advances in Petroleum Processing Hsu, C. S.; Robinson, P. R., Eds. Springer: New York 2006.
11. Delbianco, A.; Panariti, N.; Dicarlo, S.; Beltrame, P. L.; Carniti, P., New Developments in Deep Hydroconversion of Heavy Oil Residues with Dispersed Catalysts .2. Kinetics Aspects of Reaction. Energy Fuels 1994, 8, (3), 593-597.
12. Pruden, B.; Denis, J. M.; Muir, G., Upgrading of Cold Lake Heavy Oil in the CANMET Hydrocracking Demonstration Plantprocess. In 4th ITAR/UNDP Conf. Heavy Crude Tar Sands, Edmonton, 1989.
13. Miki, Y.; Yamadaya, S.; Oba, M.; Sugimoto, Y., Role of Catalyst in Hydrocracking of Heavy Oil. J. Catal. 1983, 83, (2), 371-383.
14. Gray, M. R.; Khorasheh, F.; Wanke, S. E.; Achia, U.; Krzywicki, A.; Sanford, E. C.; Sy, O. K. Y.; Ternan, M., Role of Catalyst in Hydrocracking of Residues from Alberta Bitumens. Energy Fuels 1992, 6, (4), 478-485.

15. Kennepohl, D.; Sanford, E., Conversion of Athabasca Bitumen with Dispersed and Supported Mo-Based Catalysts as a Function of Dispersed Catalyst Concentration. Energy Fuels 1996, 10, (1), 229-234.

16. Panariti, N.; Del Bianco, A.; Del Piero, G.; Marchionna, M.; Carniti, P., Petroleum Residue Upgrading with Dispersed Catalysts Part 2. Effect of Operating Conditions. Appl. Catal., A 2000, 204, (2), 215-222.

17. Zhang, S.; Liu, D.; Deng, W.; Que, G., A Review of Slurry-Phase Hydrocracking Heavy Oil Technology. Energy Fuels 2007, 21, (6), 3057-3062.

18. Dierking, I., Textures of Liquid Crystals. Wiley-VCH: Weinheim, 2003.

19. Lewis, R. T., Hot-Stage Microscopy of Mesophase Pitches. Ext. Abstr. 12th Bienn. Am. Conf. Carbon, Am. Carbon Soc. 1975, 215-216.

20. Perrotta, A. J.; McCullough, J. P.; Beuther, H., Pressure-Temperature Microscopy of Petroleum-Derived Hydrocarbons. Prepr. Pap. Am. Chem. Soc., Div. Pet. Chem 1983, 28, (3), 633-639.

21. Rodriguez, J.; Tierney, J. W.; Wender, I., *In Situ* Evaluation of the Carbonization Behavior of Graphitizable Carbon Precursors. Am. Chem. Soc. Div. Fuel Chem. 1991, (36), 1081-1087.

22. Lafdi, K.; Bonnamy, S.; Oberlin, A., Mechanism of Anisotropy Occurrence in a Pitch Precursor of Carbon-Fibers .3. Hot Stage Microscopy of Pitch--B and Pitch-C. Carbon 1991, 29, (7), 857-864.

23. Rahimi, P.; Gentzis, T.; Dawson, W. H.; Fairbridge, C.; Khulbe, C.; Chung, K.; Nowlan, V.; DelBianco, A., Investigation of Coking Propensity

of Narrow Cut Fractions from Athabasca Bitumen Using Hot-Stage Microscopy. Energy Fuels 1998, 12, (5), 1020-1030.

24. Braun, M.; Kramer, J.; Huttinger, K. J., Kinetics of Mesophase Formation in a Stirred-Tank Reactor and Properties of the Products .6. Catalysis by Iron Benzoate and Naphthoate. Carbon 1995, 33, (10), 1359-1367.
25. Bernhauer, M.; Braun, M.; Huttinger, K. J., Kinetics of Mesophase Formation in a Stirred-Tank Reactor and Properties of the Products .5. Catalysis by Ferrocene. Carbon 1994, 32, (6), 1073-1085.
26. Bagheri, S. R.; Gray, M. R.; McCaffrey, W. C., Influence of Depressurization and Cooling on the Formation and Development of Mesophase. Energy Fuels 2011, 25, (12), 5541-5548.
27. Cai, H. Y.; Shaw, J. M.; Chung, K. H., Hydrogen Solubility Measurements in Heavy Oil and Bitumen Cuts. Fuel 2001, 80, (8), 1055-1063.
28. Callister, W. D.; Rethwisch, D. G., Fundamentals of Materials Science and Engineering : An Integrated Approach. 7th ed.; Wiley: 2007.
29. Fitzer, E.; Kochling, K. H.; Boehm, H. P.; Marsh, H., Recommended Terminology for the Description of Carbon as a Solid - (IUPAC Recommendations 1995). Pure Appl. Chem. 1995, 67, (3), 473-506.
30. Paul, E. L.; Atiemo-Obeng, V. A.; Kresta, S. M., Handbook of Industrial Mixing: Science and Practice Wiley-Interscience: Hoboken, N.J., 2004.
31. Berry, E. X., Cloud Droplet Growth by Collection. J. Atmos. Sci. 1967, 24, (6), 688-701.

32. Shaw, R. A., Particle-Turbulence Interactions in Atmospheric Clouds. Annu. Rev. Fluid Mech. 2003, 35, 183-227.

33. Berry, E. X.; Reinhard.Rl, Analysis of Cloud Drop Growth by Collection: Part 1. Double Distributions. J. Atmos. Sci. 1974, 31, (7), 1814-1824.

34. Xue, Y.; Wang, L. P.; Grabowski, W. W., Growth of Cloud Droplets by Turbulent Collision-Coalescence. J. Atmos. Sci. 2008, 65, (2), 331-356.

35. Lamb, D., Rain Production in Convective Storms. In Severe Convective Storms, Meteorol. Monogr., Doswell III, C. A., Ed. Am. Meteorol. Soc.: Boston, MA, 2001; Vol. 28, pp 299–321.

36. Carlos de Almeida, F., Effects of Small-Scale Turbulent Motions on the Growth of a Cloud Droplet Spectrum. J. Atmos. Sci. 1979, 36, (8), 1557-1563.

37. Marsh, H.; M.A., D., Mesophase of Graphitizable Carbons. In Liquid Crystalline and Mesomorphous Polynzers, Shibaev, V. P.; Lam, L., Eds. Springer: New York, 1993; pp 231-257

38. Marsh, H.; Martinez-Escandell, M.; Rodriguez-Reinoso, F., Semicokes from Pitch Pyrolysis: Mechanisms and Kinetics. Carbon 1999, 37, (3), 363-390.

39. Gray, M. R.; McCaffrey, W. C., Role of Chain Reactions and Olefin Formation in Cracking, Hydroconversion, and Coking of Petroleum and Bitumen Fractions. Energy Fuels 2002, 16, (3), 756-766.

40. Chianelli, R. R.; Siadati, M. H.; De la Rosa, M. P.; Berhault, G.; Wilcoxon, J. P.; Bearden, R.; Abrams, B. L., Catalytic Properties of Single

Layers of Transition Metal Sulfide Catalytic Materials. Cat. Rev. - Sci. Eng. 2006, 48, (1), 1-41.

41. Oberlin, A., High Resolution TEM Studies of Carbonization and Graphitization. In Chemistry and Physics of Carbon, Marcel Dekker: New York, 1989; Vol. 22, pp 1-143.

42. Qian, Z.; Clarke, D. E.; Marsh, H., Structure in Cokes from Coals of Different Rank. Fuel 1983, 62, (9), 1084-1089.

43. Bearden, R.; Aldridge, C. L., Novel Catalyst and Process to Upgrade Heavy Oil. Energy Prog. 1981, 1, (1-4).

44. Liu, L., Effect of Solids on Coke Formation from Athabasca Bitumen and Vacuum residue. Ph.D. Thesis, University of Alberta, Edmonton, 2002.

6. Depolarized light scattering for study of heavy oil and mesophase formation mechanisms

6.1. Introduction

One of the operational problems of upgrading heavy feeds is the formation of an undesirable carbon-rich material known as coke, which either limits the extent of conversion or represents a significant cost in terms of hydrogen loss to low value coke product. Coke formation is a major problem in petroleum industry because of its effect on liquid yield and catalyst deactivation. In addition, it can foul reactor internals and downstream vessels and force shutdowns[1]. Heat exchangers and other refinery units must be shut down for the mechanical removal of coke which results in a significant loss of output and revenue. Coke is usually defined in petroleum industry as toluene insoluble material[1]. The carbonaceous mesophase is an intermediate phase which can form during the cracking of thermally altered high-boiling fractions from petroleum or coal tar, commonly called pitch. Mesophase can be regarded as a as a subset of coke phases (toluene insolubles) which is distinguished by its anisotropy[2].

Carbonaceous mesophase, first observed by Brooks and Taylor[3], is an intermediate condensed phase which forms during the thermal cracking of heavy petroleum and coal-derived liquids. This intermediate phase which is characterized by its optical anisotropy is a discotic liquid crystal[4]. Carbonaceous mesophase has important technological applications in producing pitch-based carbon fibers[5], carbon microbeads[6], and battery anodes[7], however, in petroleum

upgrading it is an unwanted by-product of cracking reactions which contributes to the yield of coke[8].

Formation of mesophase occurs through a combination of chemical reaction, and phase separation to give the observed anisotropic domains. Riggs and Diefendorf proposed a pseudo-binary phase diagram for mesophase, analogous to a nematic liquid crystal, based on the assumption that pitches are solutions of disk-shaped molecules, or mesogens, in a solvent phase of smaller molecules[9]. The phase diagram includes regions of isotropic, nematic, and nematic-isotropic coexisting phases. Evaporation or solvent extraction of non-mesogenic molecules moves the overall composition toward the nematic region, and mesophase forms as a result of the phase transition of the isotropic phase into nematic phase. To confirm this mechanism, Mochida et al.[10] separated coal tar pitch into benzene soluble and benzene insoluble fractions and recombined them in various weight ratios. These mixtures were observed on a hot-stage microscope at different temperatures to obtain a partial phase diagram for mesophase formation. The assumption in these experiments was that the rate of reactions in the highly aromatic mixture, such as cracking or addition, was extremely slow. Shishido et al.[11] used the statistical theory of liquid crystalline mixtures to model the experimental phase diagram reported by Mochida et al.[10]. Later Hu et al.[4] used the Flory-Huggins theory and statistical theory of liquid crystals to develop a phase diagram for mesophase formation in pitches. Although Marsh and coworkers suggested that conventional phase equilibrium was unsuitable for mesophase

formation because of a lack of equilibrium conditions[12], the work on phase diagrams contradicts this proposition.

At the molecular level, Mochida et al.[13] and Marsh et al.[12] suggested that a self-assembly mechanism was important in aligning and stacking the planar molecules. Mochida et al.[13] proposed that the planar molecules stack due to van der Waals forces to form clusters, and these clusters gather to form domains up to 100 nm in diameter. The microdomains then coalesce to form the larger domains with visible anisotropic texture which are visible by optical microscopy.

While coal derived materials such as anthracene oil can give liquids with very low reactivity that enable observation of apparent phase equilibrium, petroleum derived streams are much more reactive, and can form coke with little visible mesophase. Although domains of mesophase can be detected in coke from cracking of vacuum residue, a significant fraction of the solid is either mesophase in domains too small for observation of optical anisotropy, or is not mesophase at all[14, 15]. Consequently, models for coke formation from vacuum residue have focussed on the toluene-insoluble material, rather than the detectable mesophase. For example, Wiehe[14] combined chemical reaction with a solubility limit model to describe the formation of coke during cracking of petroleum fractions. In this model, asphaltenes are the major contributor to coke. Cracking reactions remove the pendant groups from the asphaltenes, leaving large aromatic cores in the liquid phase. A phase separation occurs when the concentration of these asphaltene cores exceed their solubility limit in the remaining liquid phase[14]. After phase separation, the formation of coke is rapid. This model was successful

in modeling the delay between the start of cracking and the onset of coke formation. Due to the rapid cracking and addition reactions in petroleum-derived materials, the phase diagrams for coke or mesophase were not developed in this model beyond the concept of a solubility limit. Although Marsh and coworkers suggested that mesophase is removed from the isotropic liquid phase not because of solubility limitations, but because of the higher stability of mesophase[16], the distinction makes no difference in the context of a practical kinetic model.

At least of portion of the asphaltenes fraction is present in crude oil as aggregated nanoparticles at ambient temperature, based on X-ray scattering and other methods[17]. Storm et al.[18] proposed that these asphaltene nano-aggregates are dispersed in the oil by a layer of absorbed non-asphaltene molecules. This layer will dissipate at elevated temperatures which leads to the flocculation asphaltenes as mesophase. However, Thiyagarajan et al.[19] used small angle neutron scattering (SANS) to study the structural changes of asphaltenes at elevated temperatures, and found that the asphaltene aggregates at ambient temperatures tend to dissociate into individual molecules at elevated temperatures which is in contradiction with Storm's hypothesis. Furthermore, this process is reversible as the temperature is reduced. Without modification by chemical reaction, petroleum fractions do not exhibit mesophase behavior.

The exact behavior of pitches during pyrolysis which leads to mesophase formation is not still well understood, especially for the more reactive petroleum-derived materials. One reason is the lack of methods to track the process *in situ*. Mesophase was discovered and characterized by its optical anisotropy[3], so

polarized optical microscopy is a very useful tool to study mesophase formation. This method is limited, however, by the optical resolution of microscope. If the mesophase is present in domains of less than 0.5 micron, then the pitch would appear to be isotropic to the optical microscope[2]. Transmission electron microscopy (TEM) has been used to detect units of mesophase of size of less than 0.1 micron[2]; however, TEM techniques cannot be used to study the *in situ* mesophase formation inside a reactor. A technique which can show the *in situ* interaction of molecules during the early stages of pyrolysis is needed to reveal the mechanisms of mesophase formation.

Light scattering is a useful method for studying mixtures composed of very small particles. A parallel monochromatic beam of light propagates in a vacuum without any change in its intensity or polarization state, but a small particle interposed into the beam can extract some of the incident energy and scatter it in all directions at the frequency of the incident beam. This phenomenon is called elastic scattering and, in general, changes the polarization state of the incident beam[20]. The scattering of sunlight in the atmosphere was one of the earliest examples of scattering which was studied by Tyndall, Rayleigh, and others at the end of the nineteenth century[21]. The wavelength dependence of scattering by the atmosphere is the reason for the blue color of the sky and red color of sunset[22]. Formal light scattering theory can be categorized in terms of two theoretical frameworks. One is the theory of Rayleigh scattering which is applicable to dielectric (non-absorbing), spherical particles that are much smaller than the wavelength of the light. The second is the theory of Mie scattering that

encompasses the general spherical scattering solution (absorbing or non-absorbing) without a particular bound on particle size. Mie scattering theory has no size limitations and can be used for describing most spherical particle scattering systems, including Rayleigh scattering. However, due to the complexity of the Mie scattering formulation, the Rayleigh scattering theory is preferred if applicable to the size of particles.

Light scattering has been applied to the study of the structure and dynamics of molecular fluids[23], two dimensional imaging for temperature and mixture fraction measurements in flames[24], and the characterization of solutions of polymers and macromolecules[25]. Depolarized light scattering is a powerful remote sensing technique for characterizing the contrail and aerosol particles in atmospheric science[26-28]. Light-scattering has been used to study nematic and lyotropic chromonic liquid crystals[29-31]; however, this technique has never been applied to the study the formation of carbonaceous mesophase.

In this paper, we introduce for the first time an *in situ* method of probing mesophase formation in pitches, based on light scattering with polarized light. The method makes it possible to track the interaction of molecules within pitch during thermal cracking, and the mixture moves toward the onset of mesophase formation. The formation and growth of mesophase domains can be studied using this technique before they are observable with an optical microscope, in order develop a mechanism for mesophase formation.

6.2. Theory of depolarized light scattering

Depolarization light scattering is a useful method for distinguishing between the spherical and non-spherical particles[32]. This method (used as depolarization LIDAR) has been widely used in atmospheric science to characterize contrail particles[33, 34]. A light source, usually a laser, transmits a narrow, fully polarized beam of light in which light waves all oscillate in the same plane. The receiver measures the polarization of light scattered in the backward direction by scattering particles[34].

The Stokes parameters given in a 4×1 vector can be used to describe the of properties of the incident and the scattered light[35]:

$$\mathrm{I}=\begin{bmatrix} I \\ Q \\ U \\ V \end{bmatrix} \tag{6-1}$$

where I is the net monochromatic energy flux. Q and U express the state of linear polarization and V describes the state of circular polarization. The Stokes parameters should be defined with respect to a reference plane. If we define the scattering plane with reference to the fully linearly polarized light beam, the Stokes vector of the incident light ($\mathbf{I}^{\mathbf{inc}}$) source will be

$$\mathbf{I}^{\mathbf{inc}}=\begin{bmatrix} 1 \\ 1 \\ 0 \\ 0 \end{bmatrix} \tag{6-2}$$

The scattering of light by particles can be described by a 4*4 real scattering matrix which transforms the Stokes parameters of the incident light into those of

the scattered light[36] (assuming that the scattering plane is the reference plane for defining the Stokes parameters of the incident and scattered light). For an assembly of randomly oriented particles, and each particle has a plane of symmetry and/or particles and their mirror particles are present in equal number, then the scattering matrix can be given by[36]

$$\mathbf{F(\theta)} = \begin{bmatrix} F_{11}(\theta) & F_{12}(\theta) & 0 & 0 \\ F_{12}(\theta) & F_{22}(\theta) & 0 & 0 \\ 0 & 0 & F_{33}(\theta) & F_{34}(\theta) \\ 0 & 0 & -F_{34}(\theta) & F_{44}(\theta) \end{bmatrix} \tag{6-3}$$

The scattering matrix for the exact backscattering direction (θ=180) from the polarized light source can be given by[37]

$$\mathbf{F(180^0)} = \begin{bmatrix} F_{11}(180^0) & 0 & 0 & 0 \\ 0 & F_{22}(180^0) & 0 & 0 \\ 0 & 0 & F_{33}(180^0) & 0 \\ 0 & 0 & 0 & F_{44}(180^0) \end{bmatrix} \tag{6-4}$$

The quantity to describe the degree of polarization of the backscattered light is the linear depolarization ratio (δ). The linear depolarization ratio is defined as the ratio of the perpendicular to the parallel polarization components of backscattered light[38] and is equal to

$$\delta = \frac{I_{\perp}}{I_{\parallel}} \tag{6-5}$$

where $I_{\perp}$ and $I_{\parallel}$ are the measured perpendicular and parallel backscatter intensities in respect to the transmitter polarization axis. The depolarization ratio can also be written as[37]

$$\delta = \frac{F_{11}(180^0) - F_{22}(180^0)}{F_{11}(180^0) + F_{22}(180^0)} \tag{6-6}$$

For spherical (isotropic) particles we will have, $F_{11}(180^0) = F_{22}(180^0)$ so $\delta = 0$[37]. For a spherical particle, like a water droplet in a cloud, the backscattered light is fully polarized in the same direction as the transmitted beam ($\delta = 0$)[39], however, for non-spherical particles like the non-spherical ice crystals in a cloud, the backscattered light can be partially depolarized; i.e., it can have a "cross-polarized" component which vibrates perpendicularly to the transmitted polarization. The power of the scattering methods lies in its sensitivity to very small particles. For example, even anisotropic molecules (like the molecules in the air) can depolarize the backscattered light[40].

Depolarized light scattering was also used to study the molecular anisotropy of pure liquids. In this method a monochromatic linearly-polarized light beam traverses a liquid sample, and the depolarized component of the scattered light form the sample is isolated and measured. For a pure sample, the intensity of the depolarized light scattered by the unit volume of the sample is equal to

$$R_i = \frac{i}{VE^2/2} = \frac{32\pi^4}{135\lambda^4} p(n^2+2)\gamma^2 \tag{6-7}$$

where i is the measured intensity of the depolarized light scattered by the ensemble of molecules in the sample, p is the number of molecules in each unit of scattering volume (V), n is the index of refraction of the sample at wavelenghth of the light beam (λ), E is the electric field of the incident light beam. The variable γ is called the molecular optical anisotropy, which is an invariant property of the

tensor of polarizability that does not depend on the orientation of the molecule[41]. The depolarized intensity should be proportional to the square of the molecular anisotropy for the same number of molecules per volume and similar indices of refraction. In this method only the depolarized component is measured, and the parallel component and depolarization ratio are not taken into account in Equation 6-7. In addition, the intensity of the depolarized component is measured at 90° with respect to the incident beam. However, for an isotropic molecule the perpendicular component of the scattered light and the depolarization ration should be essentially zero at 90°[42]. The molecular anisotropy of many pure samples has been measured in this way from depolarized Rayleigh scattering. For spherical molecules like CCl_4, the value of the molecular optical anisotropy is very small[43]. The molecular optical anisotropy of aromatics is usually higher than alkanes[43], and the anisotropy increases dramatically with the number of rings[44].

6.3. Experimental section

6.3.1. Materials

Athabasca vacuum residue supplied by Syncrude was used for observations (Asphaltene content: 31 wt %, MCR: 14.9 wt%, Ash: 3.9 wt%, Solids: 0.22 wt%). Asphaltenes C5 (or C7) was precipitated from Athabasca vacuum residue by dilution in n-pentane (or n-heptane). Athabasca asphaltenes were precipitated from the oil by the addition of 40 ml of n-pentane (or n-heptane) per gram of oil. The mixture was agitated overnight at 400 RPM at room temperature and atmospheric pressure. After that, the mixture was filtered using a 0.22 μm

Millipore mixed cellulose ether membrane. In order to eliminate any residual oil, the filtration membranes and the flask were washed with small volumes of n-pentane (or n-heptane) until the filtrate was colorless. The resultant filter cake was placed overnight until all pentane (or n-heptane) was evaporated. The pentane (or n-heptane) in the resultant filtrate was evaporated in a rotary evaporator to recover the maltenes. The elemental analysis of the samples is shown in Table 6-1.

Table 6-1. Elemental analysis of Athabasca Vacuum Residue, asphaltenes and maltenes

Sample	C(wt%)	H(wt%)	S(wt%)	N(wt%)
Athabasca vacuum residue	81.76	9.45	6.17	0.93
Athabasca C5 asphaltenes	82.0	7.6	7.6	1.4
Athabasca C7 asphaltenes	81.5	7.5	8.1	1.5
Athabasca C7 Maltenes	82.6	10.1	5.2	0.6

6.3.2. Hot-stage reactor

A new hot-stage reactor was used for the *in situ* observation of samples during the heat treatment which has been discussed in details elsewhere[15]. The reactor was made to work with an inverted reflective microscope, and a schematic design of the high-pressure optical hot-stage apparatus is shown in Figure 6-1. It is made of stainless steel Swagelok fittings and a sapphire window to observe the sample inside it. The sample sits on the sapphire window, and covers it after melting. A magnet stirrer was used in this hot-stage reactor to mix the reactor contents, have a better heat transfer, and avoid surface effects of sapphire window on the sample.

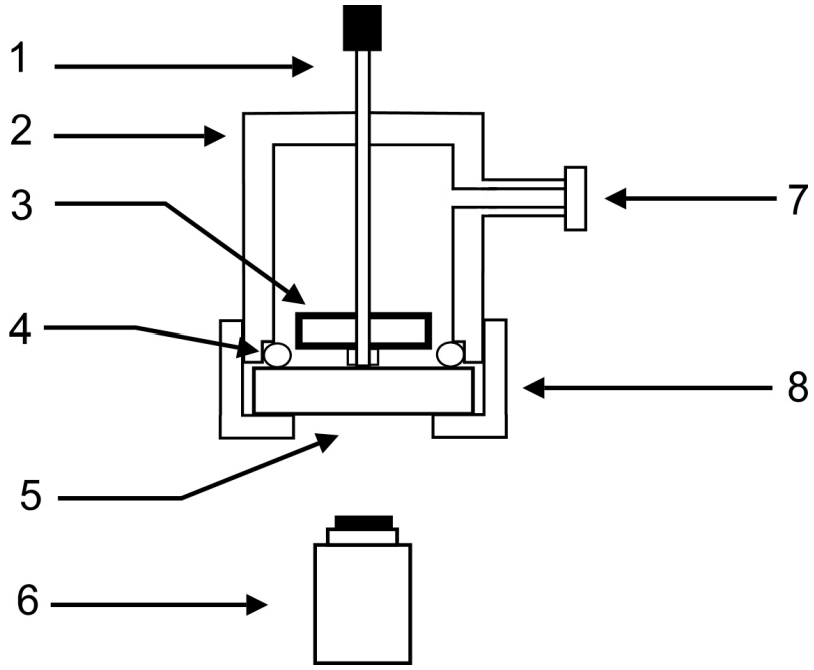

Figure 6-1. Schematic diagram of the hot-stage reactor. 1: thermocouple; 2: steel body; 3: magnet; 4: O-ring; 5: sapphire windows; 6: objective lens of microscope; 7: gas inlet; 8: bottom nut.

A mass of 0.4 g of each sample was heated in the reactor under continuous stirring at 120 rpm and pressurized with nitrogen at 4-5 MPa. A Zeiss Axio-Observer inverted reflective microscope equipped with crossed and parallel polarizers was used to take photos of the sample during heat treatment. The cross polarizer set up was used to get the perpendicular component of the back scattered light, and the parallel polarizers set up was used to get the parallel component of the backscattered light. A combined magnification of 50X was used to take photos used in this study. However a magnification of 200X was used to check for the onset of mesophase formation. A halogen bulb was used as the light source of the microscope, and its intensity could be changed by changing the voltage. The intensity of the light source of the microscope was constant for all the images

taken in each experiment. Table 6-2 shows the voltage of the light source for each experiment.

Table 6-2. Light source intensity (voltage) for different experiments in this study.

Microscope light source intensity	Cross polarizers set-up	Parallel polarizers set-up
Unreacted vacuum residue (Figure 6-3)	9.5	6.5
Unreacted vacuum residue fractions (Figure 6-4)	10	6.5
Mixture of asphaltene and vacuum residue (Figures 6-5 and 6-6)	12	6.5
Reacting vacuum residue (Figures 6-7, 6-8)	8.7	6.5
Reacting asphaltenes (Figure 6-9)	11.8	6.5
Depressurization of vacuum residue (Figure 6-10)	11.5	6.5

6.3.3. Image analysis

The images taken by the microscope (with either cross polarizers or parallel polarizers set-up) were analyzed to measure their brightness which was proportional to the intensity of the (perpendicular or parallel components of) backscattered light. In image processing, a grayscale image is an image in which each pixel carries only intensity information. Images of this sort, also known as black and white, are composed exclusively of shades of gray, varying from black at the weakest intensity to white at the strongest. The intensity of a pixel is

expressed within a given range between a minimum and a maximum, inclusive. For 8-bit grayscale images, this range is represented as a range from 0 (total absence, black) to 255 (total presence, white).

In computers, "color" is produced on the screens using a similar system of 3 very particular wavelengths of "red", "green", and "blue" light (usually abbreviated together as RGB) in an attempt to imitate what our eyes see. With RGB images, the grayscale image can be produced by calculating the gray value of each pixel using the formula gray=(red+green+blue)/3. To find the brightness of each image, the software calculates the gray value of all the pixels and then computes the average of these values (Mean Gray value). The image analysis was performed on a personal computer using ImegeJ program developed at National Institutes of Health. The images were analysed to determine the mean gray value of the photos.

6.3.4. Light scattering analysis

In situ hot-stage microscopy is usually used to determine the onset of observable mesophase, and the growth or coalescence of mesophase after formation. The interaction of the sample with linear polarized light before the start of mesophase observation has never been studied as far as the authors are aware. The main question is that whether any useful information can be gained by the observation of sample under polarized light before the observation of mesophase.

Figure 6-2 illustrates how the cross polarized arrangement of an optical reflective microscope can be used to measure the depolarized light scattering of

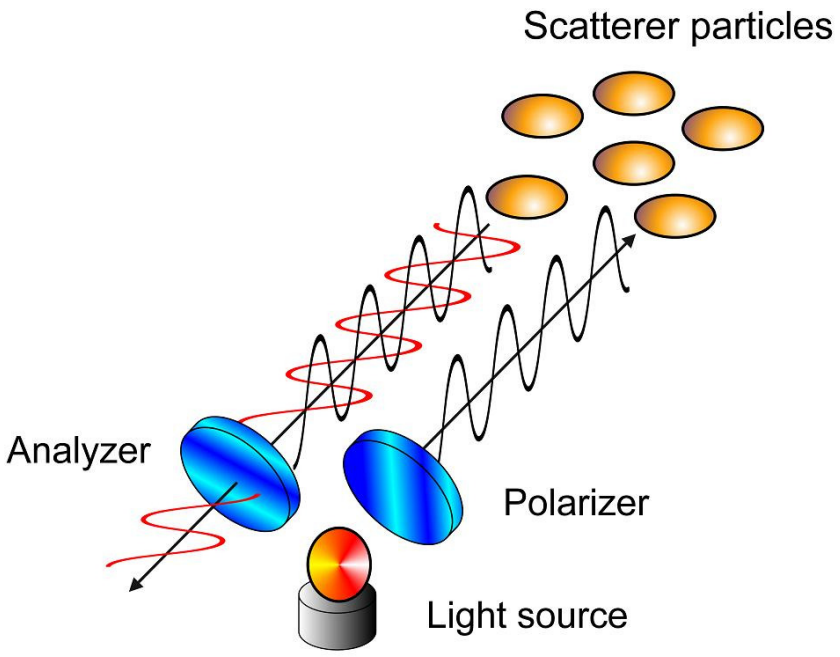

Figure 6-2. Depolarized light scattering by anisotropic particles. By using a cross polarizers set-up the parallel component of the backscattered light can be eliminated, and only the perpendicular components will be passed through the analyzer.

the sample. The first polarizer turns the natural light of the microscope light bulb into a linear polarized beam. The light beam hits the sample, and backscatters into the objective lens of microscope. Then the second polarizer (analyzer) filters the component of this backscattered light which has a polarization state parallel to that of the incident light. In other words, it leaves the component with the polarization state perpendicular to that of the incident beam. So what you see with the microscope is the depolarized backscattered light coming from the sample. Of course to calculate the depolarization ratio by Equation 6-6, the parallel component of backscattered light is required. We achieved this requirement by

changing to microscope setup to making the optical axes of the polarizers parallel to each other. This was not a traditional set-up for light scattering analysis. The light source used was not coherent, and we were not able to use a beam splitter and measure the perpendicular and parallel components of the backscattered light simultaneously. In addition we did not use a detector to measure the intensities of these components and relied on image analysis of *in situ* photos taken by the microscope to measure the backscattered light intensities.

6.3.5. Scanning electron microscopy (SEM)

Samples were observed using a high resolution JEOL 6301F field emission scanning electron microscope. Samples were freeze-fractured in liquid nitrogen and the cross-section was observed by SEM. All these samples were sputter-coated with carbon before the observation.

6.4. Results

6.4.1. Light scattering from unreacted vacuum residue

In this experiment 0.4 g of Athabasca vacuum residue was heated in the hot-stage reactor under nitrogen at 4.1 MPa stirred at 120 rpm. The sample was heated up to 305°C and held at that temperature for 41 min. The sample was observed under both cross polarizers (to obtain the perpendicular component of the backscattered light) and parallel polarizers (for the parallel component of the backscattered light) at 50X, and a series of photos were taken of the sample with the same light intensity of the microscope (9.5V). The mean gray values of the images versus time are shown in Figure 6-3. This graph shows that by fixing the

temperature at 305°C, the mean gray values of both the perpendicular and parallel components of the backscattered light remained almost constant. Below the cracking temperature, in the absence of any reaction, the depolarization ratio of the sample (Equation 6-5) remained constant at constant temperature.

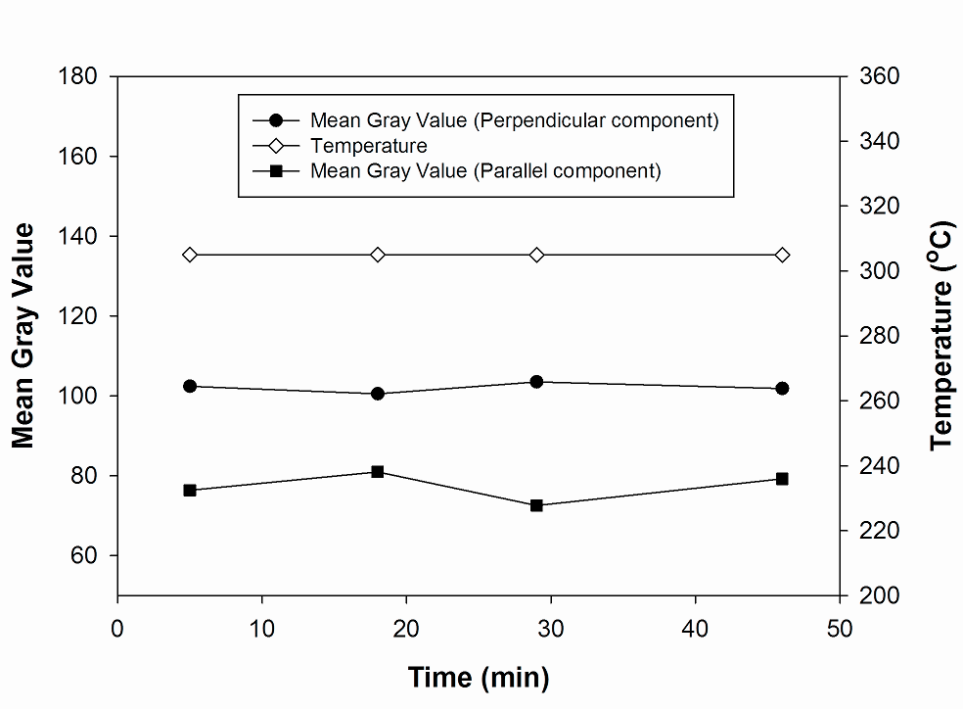

Figure 6-3. Changes in mean gray values of Athabasca vacuum residue under nitrogen at 305°C and 4.1 MPa and stirred at 120 rpm. By heating the sample at a constant temperature below the cracking temperature the mean gray values of parallel and perpendicular components of the backscattered light remained constant.

6.4.2. Light scattering from unreacted vacuum residue fractions

Athabasca vacuum residue, Athabasca C7 asphaltenes, and Athabasca C7 maltenes were heated separately in the hot-stage from the room temperature up to 350°C. A series of images were taken (with both cross and parallel polarizers set-up) of each sample inside the hot-stage at different temperature, and the light

intensity of microscope was the same for all these 3 samples (10V). Figure 6-4 shows the mean gray values of these samples versus temperature. For all 3 samples the mean gray values of the perpendicular component of the backscattered light increased with temperature. The mean gray value of this component for asphaltenes was much smaller than that of vacuum residue and maltenes, at the same temperature, e.g. 168 for maltenes, 122 for vacuum residue, and 49 for asphaltenes at 250°C.

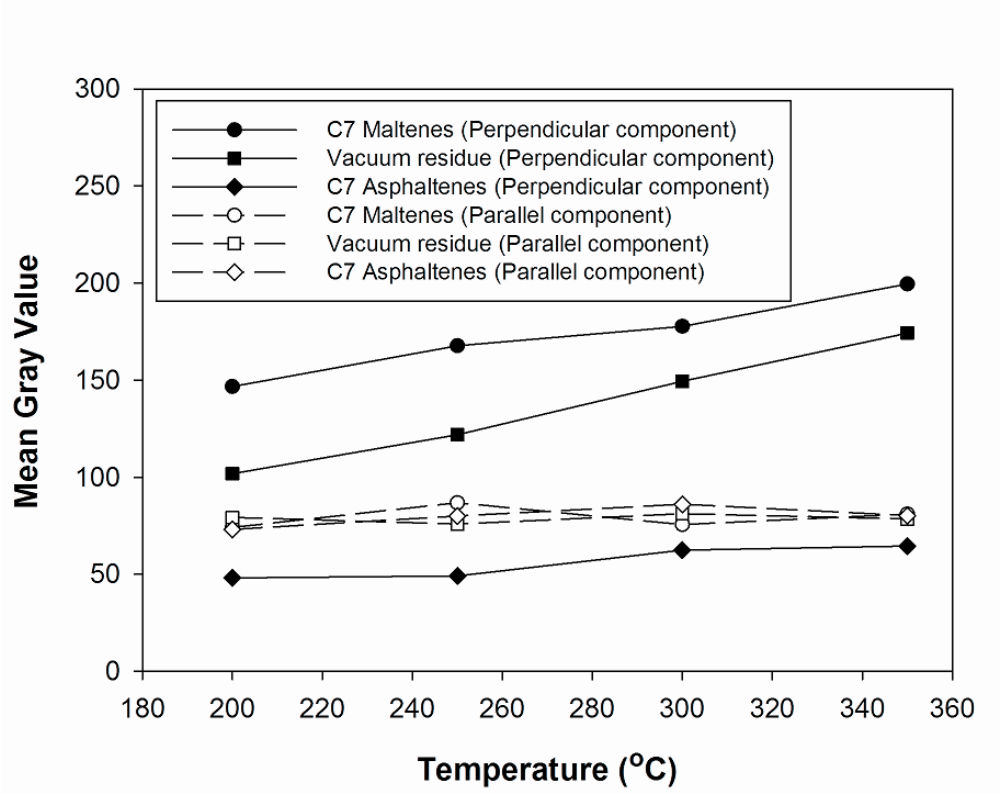

Figure 6-4. Mean gray values of the perpendicular and parallel components of the backscattered light as a function of temperature from Athabasca vacuum residue, Athabasca C7 maltenes, and Athabasca C7 asphaltenes.

The mean gray value of the parallel component was, however, almost the same for all these fractions, 86.8 for maltenes, 75.9 for vacuum residue, 79.9 for

asphaltenes at 250°C. We cannot use Equation 6-5 to directly calculate the depolarization ratio, since we did not measure the perpendicular and parallel components simultaneously with the same light source intensities; we used 10v for the perpendicular component and 6.5v for parallel component. The depolarization ratios are proportional to the intensities of the perpendicular component, since the change in the parallel components was negligible. Consequently, we can calculate the changes in the depolarization ratio on a relative basis, using only the perpendicular components. On this basis, the value of $\delta_{asphaltene}/\delta_{maltene}$ at 250°C was 0.3, so that the difference in scattering can distinguish between these fractions. The brightness of all the samples under cross polarized light increased with temperature (Figure 6-4), which was probably due to changes in the birefringent behaviour of sapphire window with increasing temperature, so in subsequent experiments we only report results under isothermal conditions.

In another experiment 0.135 g of Athabasca C5 asphaltenes and 0.27 g of Athabasca vacuum residue were placed in the hot-stage reactor without premixing. The sample was heated under nitrogen at 4.1 MPa to 290°C without stirring. The image in Figure 6-5a shows the coexistence of asphaltenes and vacuum residue at this temperature. Asphaltenes (marked by 2) were darker than vacuum residue (marked by 1), indicating that they can distinguished under cross-polarized light (Figure 6-5a). In the same image under normal light (Figure 6-5b), and the image with parallel alignment of polarizers (parallel component of backscattered light) (Figure 6-5c) these phases could not be distinguished at all.

Figure 6-5. A mixture of Athabasca vacuum reside and Athabasca C5 asphaltenes at 290°C under nitrogen at 4.1 MPa before mixing: (a) under cross polarized light. The vacuum residue is (marked by 1) distinguishable from asphaltenes (marked by 2). (b) under normal light at 4.7 v the phase are not distinguishable. (c) under polarized light with parallel alignment of polarizers at 6.5 V. Again the phases are not distinguishable.

The stirrer was then turned on for 15 min, at a constant temperature of 290°C. As illustrated in Figure 6-6b, mixing gave a homogeneous phase and the asphaltenes and maltene phases were no longer distinguished from each other. The light intensity of microscope light source was constant at 11.5 V in both Figures 6-6a and 6-6b. The mean gray values of vacuum residue at point 1 (the points inside the circle) and asphaltenes at point 2 in Figure 6-6a were 196 and 104 respectively, while the mean gray value of Figure 6-6b was 137. The weighted average of mean gray values of asphaltene and vacuum residue in Figure 6-6a can be calculated as (0.135*104+0.27*196)/(0.135+0.27) which results in 142, which is close to the mean gray value of Figure 6-6b (137). These results indicate that the mean gray value of the mixture was close to the arithmetic average of that of the asphaltene and vacuum residue phases.

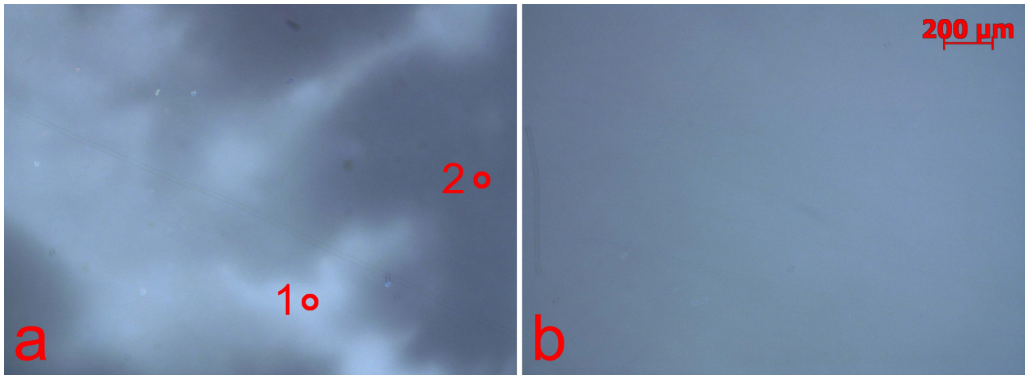

Figure 6-6. The same mixture of Athabasca vacuum reside and Athabasca C5 asphaltenes shown in Figure 5 under cross polarized light. (a) before mixing the vacuum residue is (marked by 1) distinguishable from asphaltenes (marked by 2). (b) after stirring for 15 min the mixture becomes homogeneous.

6.4.3. Light scattering from reacting vacuum residue

In this experiment, vacuum residue was cracked until domains of mesophase were visible in the fluid under the optical microscope. A sample of 0.4 g of Athabasca vacuum residue was cracked under nitrogen at 4.1 MPa and 435°C stirred at 120 rpm. Images were recorded after the temperature was constant to within one degree of the set point. The images taken from this sample under cross polarizers (perpendicular component) are shown in the Figure 6-7 as a series with time of reaction. The first images are bright green, but the brightness decreases with time so that the final images are rather dark. The first mesophase particles were observed after 47 min. The first mesophase particles formed in the bulk of the sample and could be moved easily by the stirrer. Even after the formation of the mesophase particles, the images of the dark background could be recorded when the stirrer was on. As the mesophase domains grew, they began to cover the

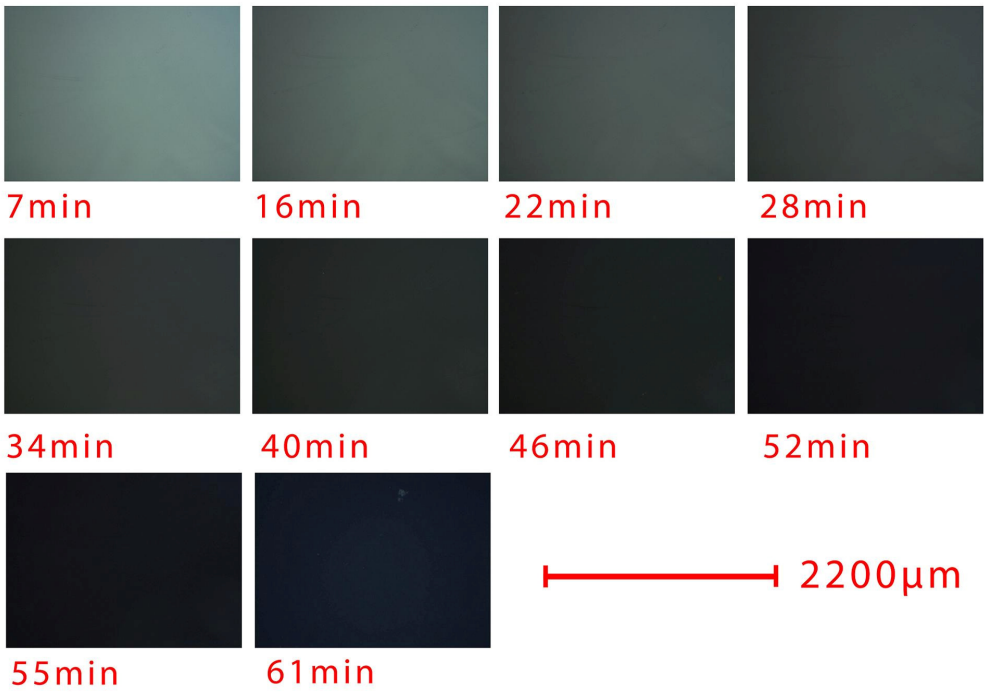

Figure 6-7. Images of Athabasca vacuum reside under cross polarized light versus time showing changes in the mean gray value. The sample was cracked under nitrogen at 435°C and 4.1 MPa and stirred at 120 rpm.

window and changed the brightness significantly, so that images of the background could no longer be recorded.

The mean gray value of the images under cross polarizers and parallel polarizers was calculated by using ImageJ, and the results are plotted versus time in Figure 6-8. For the perpendicular component of the backscattered light, the values tend to decrease with time. The increase in the gray value after 55 min was due to the brightness of the growing mesophase domains. On the other hand, the gray values of the parallel component remained almost constant (82.45+/-4.24), which means that the depolarization ratio (Equation 6-5) was proportional to the intensity of the perpendicular component of the backscattered light and decreased

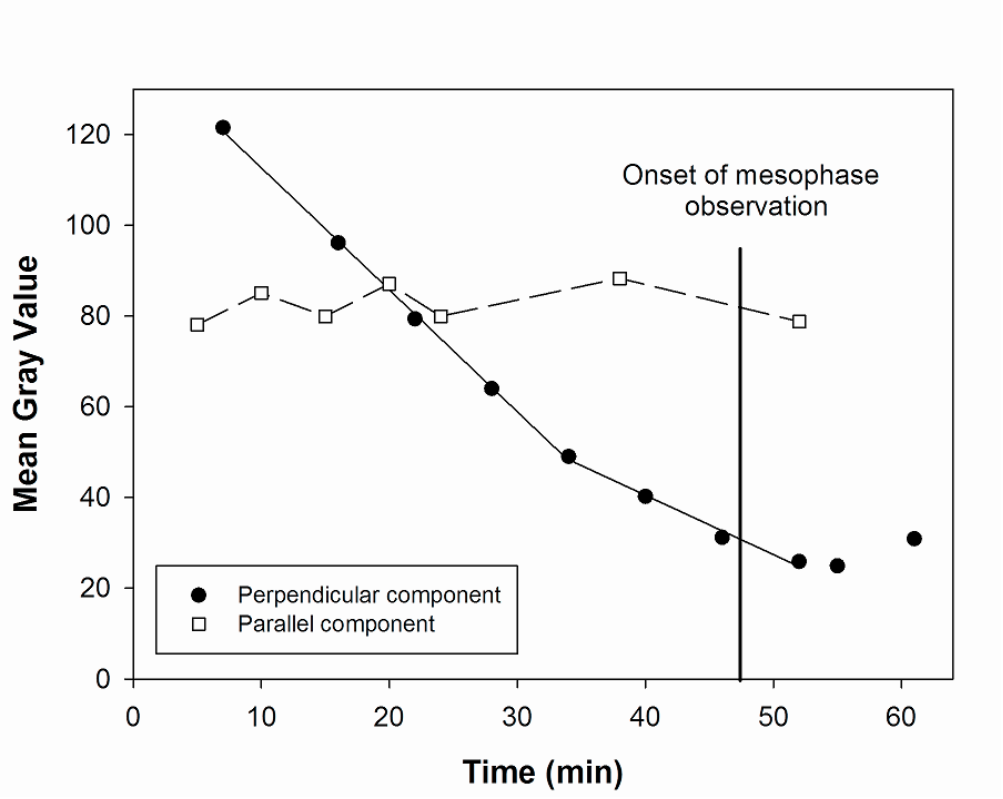

Figure 6-8. Mean gray values of the backscattered light from Athabasca vacuum residue versus time cracked at 435°C under nitrogen at 4.1 MPa.

during 52 min of reaction by a factor of 4.7. The data of Figure 6-8 shows two regions; the first 5 points up to 34 min after reaching the final temperature followed a highly linear trend (especially at lower intensities of the light source of microscope). However after that the slope of the line increased from -2.688+/-0.145 (95% confidence) with R^2=0.999 to -1.308+/-0.443 with R^2=0.989. This slope change happened 13 min before the observation of mesophase in this experiment.

The mean gray values of the points for consecutive runs, taken at the same time and operating conditions and the same type of sample, were reproducible to

within 30% which was comparable with some previous studies[45]. These variations were likely due to imprecise horizontal alignment of the hot-stage reactor (which changes the alignment of the c-axis sapphire window and its birefringence.), variations in temperature within 1°C (which has a significant effect on the birefringence of the window), and the incoherent light source which used for the experiments. However, the trend of change of the mean gray values was reproducible for all the samples used in this study.

6.4.4. Light scattering from reacting asphaltenes

A sample of 0.4 g of C5 Athabasca asphaltenes was cracked under nitrogen at 4.1 MPa and 430°C stirred at 120 rpm. Images were taken of the sample inside the hot-stage before the start of mesophase observation. The first mesophase particles were observed 21 min after reaching the final temperature. The data of Figure 6-9 show the mean gray values of the images of this sample under cross polarizers. The gray values again can be divided into two linear zones similar to Figure 6-8 The first 4 points during the initial 20 min of reaction, after reaching the final temperature, followed a highly linear trend (R^2=0.999), then the slope of the line increased from -1.443 ± 0.123 (95% confidence) to -0.624 ± 1.150 (R^2=0.980). It is important to note that the slope confidence interval is overlapped with the first line. This can be attributed to the fact that the last two points of the second line represent images taken after observation of mesophase, which grows faster in asphaltenes than in vacuum residue and affects the brightness of the images. This artefact and the lower number of images were possibly responsible for the higher P value for the second line. This slope change happened 1 min

before the observation of mesophase in this experiment. The mean gray values of the parallel component remained constant (not shown in Figure 6-9); therefore, the depolarization ratio (Equation 6-5) decreased by a factor of 2.

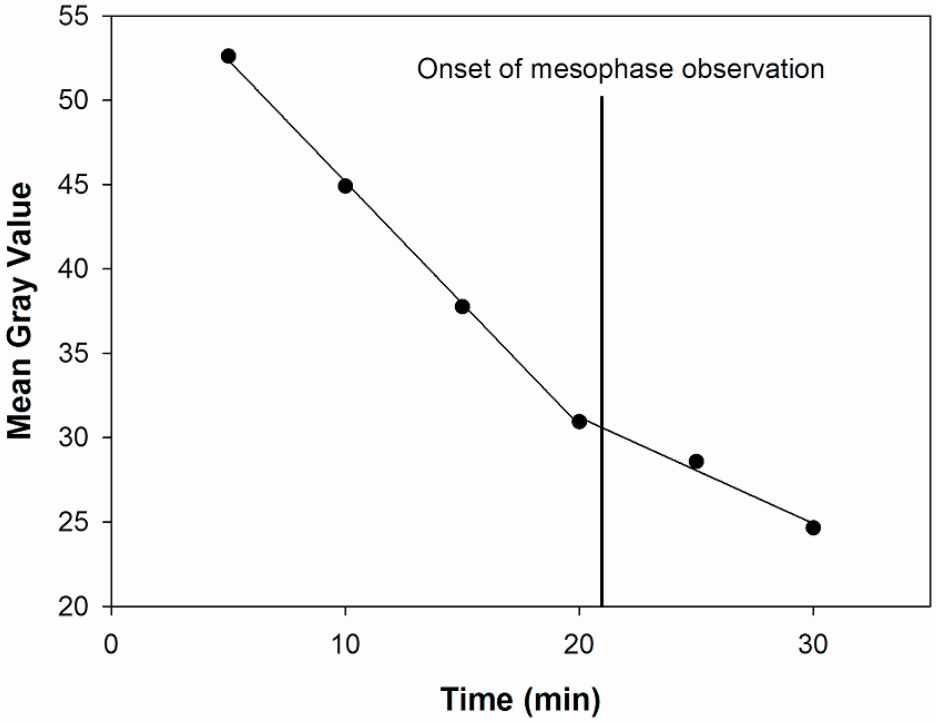

Figure 6-9. Mean gray value of Athabasca C5 asphaltenes under cross polarized light (perpendicular component) versus time. The sample was cracked under nitrogen at 430°C and 4.1 MPa and stirred at 120 rpm.

6.4.5. Depressurization during cracking of vacuum residue

The results of a previous study showed that depressurization had a significant effect on formation and growth of mesophase[15]. Depressurization before the onset of mesophase formation induced the formation of observable mesophase earlier than if the reactor had been maintained at pressure. The light scattering method was applied to this experiment to study the mechanisms responsible for

mesophase formation upon depressurization. A sample of 0.4 g of Athabasca vacuum residue was cracked under nitrogen at 4.9 MPa and 440°C stirred at 120 rpm. The hot-stage reactor was depressurized to atmospheric pressure 19 min after reaching to the final temperature. Before depressurization no mesophase had been observed in this sample. The depressurization from 4.9 MPa to atmospheric pressure led to a significant decrease in the brightness of the sample under cross polarized light as shown in Figure 6-10. After 2 min, the first mesophase particles were observed in this sample. Compared to an experiment with similar operating conditions and without depressurization, mesophase formed 20 min sooner. Images were taken of the sample inside the reactor before and after depressurization. Figure 6-10 shows the mean gray values versus time. The initial 5 points before depressurization followed a linear trend; however, the slope of the points suddenly changes after depressurization. The slope changes significantly from -5.059 ± 0.960 (95% confidence) with R^2=0.989) to -1.433 ± 0.617. (R^2=0.980). The mean gray values of the parallel component (not shown in Figure 6-10) remained constant as in previous experiments, therefore, the depolarization ratio (Equation 6-5) decreased by a factor of 2 after depressurization. The general trend of the graph in Figure 6-10 is similar to that of Figure 6-8, but due to the depressurization, the liquid phase suddenly jumps into the second line with the less negative slope. This result is consistent with the fact that mesophase was observed earlier than usual in this sample. The depressurization of sample below the cracking temperature (e.g. 300°C) did not change the brightness and mean gray values of either of the components of the backscattered light.

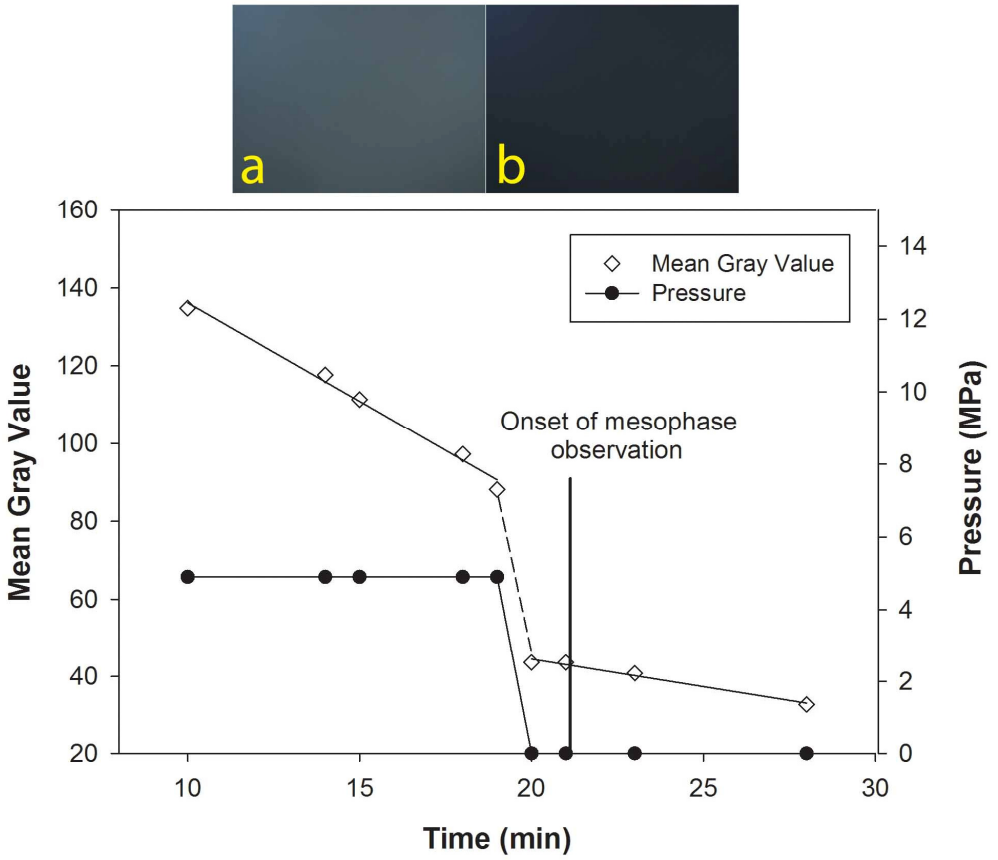

Figure 6-10. Mean gray value of Athabasca vacuum reside under cross polarized light (perpendicular component) versus time. The sample was Athabasca vacuum residue being cracked under nitrogen at 440°C and 4.9 MPa and stirred at 120 rpm which was suddenly depressurized to atmospheric pressure. The slope of the curve changes after depressurization from 4.9 MPa to atmospheric pressure. Top: The change in brightness due to depressurization. (a) Before depressurization. (b) Immediately after depressurization.

6.4.6. SEM observations

The light scattering analysis showed significant changes in the sample before the microscopic observation of mesophase. However, the resolution of an optical microscope is limited, so SEM was used to examine whether any structural

changes in the sample (before the formation of microscopic mesophase) can be detected to be connected to light scattering results. A sample of 0.4 g of Athabasca vacuum residue was heated in the hot-stage reactor at 440°C under nitrogen at 4.1 MPa and stirred at 120 rpm, then the heater was turned off after reaction times of 20, 35, and 65 min. These times were chosen to study the samples both before and after the microscopic observation mesophase. After each experiment the remaining sample was removed from the hot-stage reactor, and dried in an oven at 70°C for a few hours. Part of this sample was polished and observed under polarized like to check for mesophase formation. The freeze-fractured surface of the other part was observed with SEM. The sample heated for 20 min was completely isotropic and no mesophase was observed under optical microscope. Figure 6-11 shows the freeze-fractured surface of the sample heated for 18 min, which was essentially smooth and featureless. The sample heated for 35 min was still isotropic, but SEM showed the formation of small more or less spherical domains on the freeze-fractured surface of this sample as shown in Figure 6-12. Domains as small as 30 nm was observed under SEM which were certainly below the resolution of an optical microscope. The sample heated for 65 min was cooled down after the formation of mesophase and showed mesophase spheres as larger than 10 μm under optical microscope with polarized light as shown in Figure 6-13.

The micrograph of Figure 6-14 show the freeze-fractured surface of the sample heated for 65 min. This surface is far different from the previous sample which was reacted for 35 min. The number of submicron domains has been increased

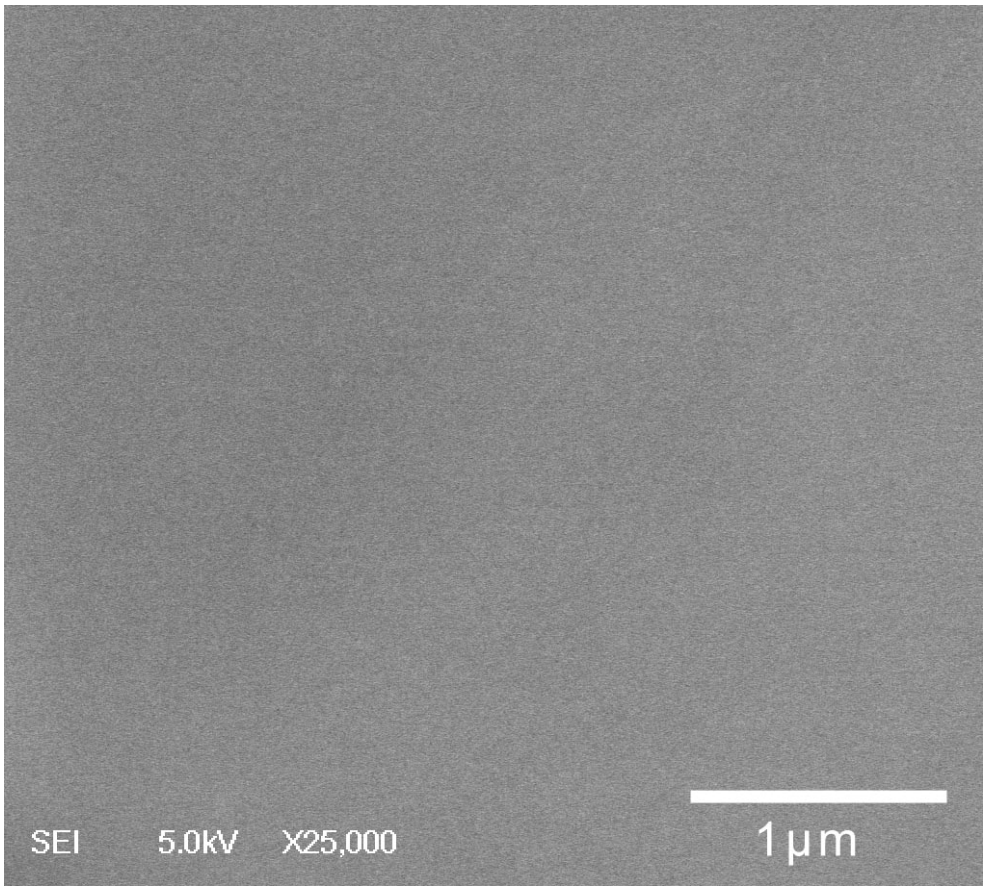

Figure 6-11. The freeze-fractured surface of coke from Athabasca Vacuum residue reacted for 20 min under SEM (secondary mode). The sample reacted under nitrogen at 435°C and 4.1 MPa and stirred at 120 rpm. The surface is smooth and featureless.

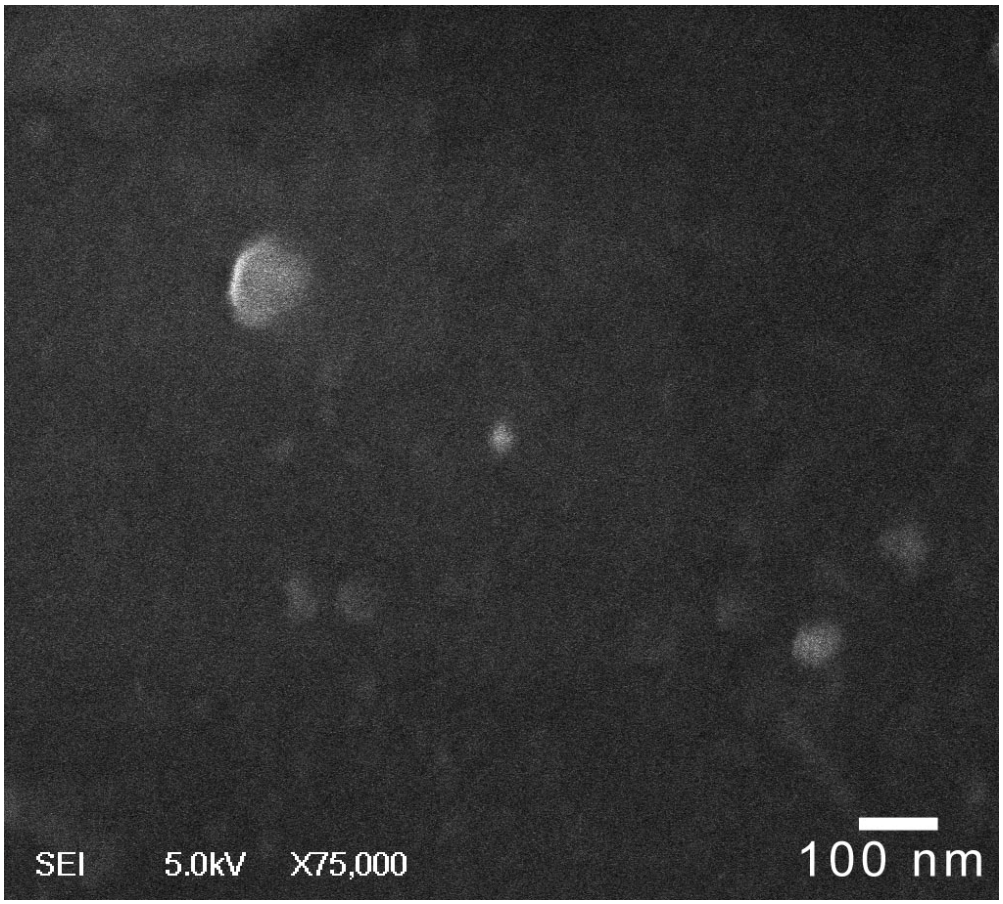

Figure 6-12. The freeze-fractured surface of coke from Athabasca Vacuum residue heat treated for 35 min under SEM (secondary mode). The sample was heat treated under nitrogen at 435°C and 4.1 MPa and stirred at 120 rpm. The surface contains many submicron domains.

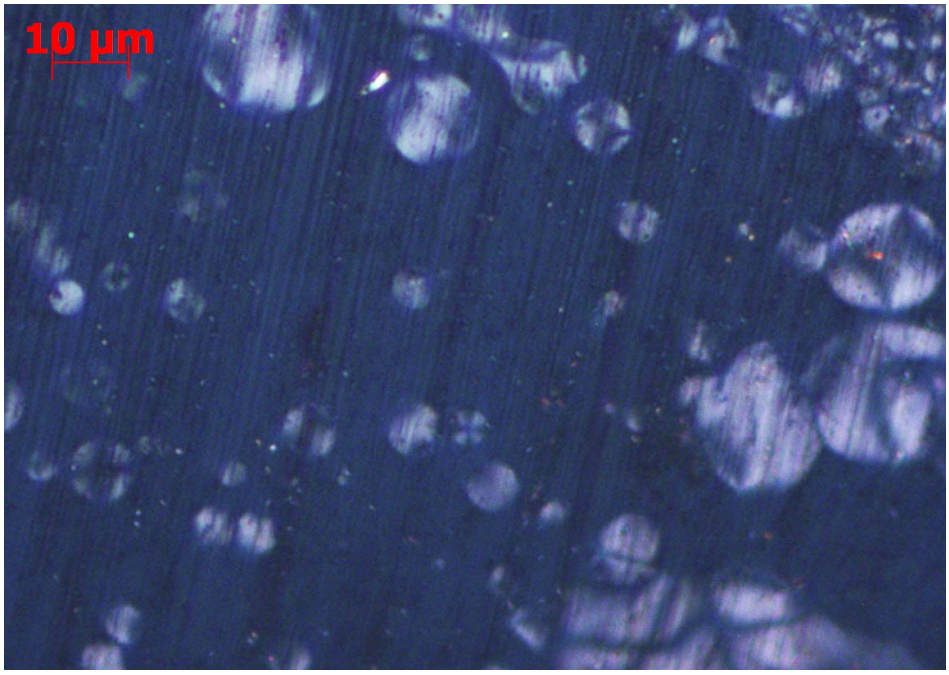

Figure 6-13. Optical micrograph of the cokes from Athabasca vacuum residue heat treated for 65 min under nitrogen at 435°C and 4.1 MPa and stirred at 120 rpm.

significantly and they seem to cover the entire fracture surface. The micron-scale mesophase spheres are easily observed in Figure 6-14, and their surface is covered by many smaller submicron domains which are apparently the building blocks of these larger mesophase spheres. We can assume that because of their ordered structure, the toughness of these small submicron domains should be higher than the surrounding isotropic phase which is amorphous, giving preferential fracturing at the boundary between the mesophase and isotropic phase.

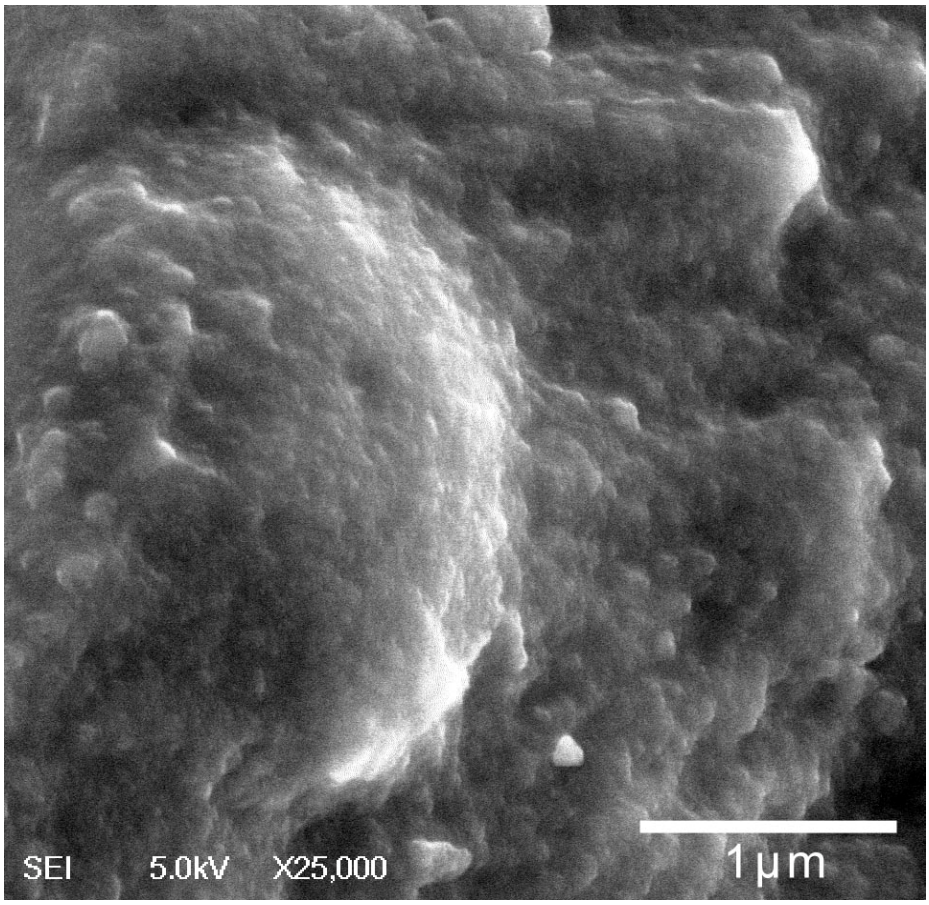

Figure 6-14. Freeze-fractured surface of coke from Athabasca Vacuum residue heat treated for 65 min under SEM (secondary mode). The sample was under nitrogen at 440°C and 4.1 MPa and stirred at 120 rpm. The surface was covered with submicron domains.

6.5. Discussion

6.5.1. Mechanisms of mesophase formation

The physics of scattering of depolarized light scattering can be used to interpret the experimental observations from *in situ* measurements. The components of the liquid pitch would be predominantly disc-like polyaromatic molecules carrying pendant groups and side-chains[46]. The shape anisotropy of such polyaromatic

molecules is large and can result in depolarization of the scattered light[47], In fact the study of Unanue and Bothorel[44] showed that molecular optical anisotropy from benzene to 20–Methylcholanthrene increase 100 times[44]. However, the spatial distribution of molecules can change this anisotropy. For example, solutions of polystyrene or biopolymers can have a negligible depolarization ratio because of an isotropic spatial distribution, such as a spherical conformation[47]. Even the anisotropy of a pair of stacked aromatics is large[48]; however, if the aromatic layers start to form larger clusters, they would gradually lose the shape anisotropy. This hypothesis is consistent with the previous study of Song and Wang[49] who used depolarized Rayleigh scattering to study the aggregation of carbocyanine dye molecules. They measured the intensity of the depolarized Rayleigh scattering as a function of dye. They observed that depolarized Rayleigh scattering intensity steadily decreased with increasing dye concentration which suggests a continuous formation of aggregates as the dye concentration increases. They assumed that dimers, trimers, tetramers, and higher aggregates are then expected to be formed, resulting in a continuous decrease in the optical anisotropy. They suggested that as these aggregates are formed, the optical polarizability anisotropy inside the scattering volume is expected to decrease, because molecular aggregates have less optical anisotropy due to more spherical shape. The initial brightness of the images (Figures 6-7 and 6-8) is consistent with a high depolarization ratio due to the anisotropic shape of the planar aromatic molecules. The gradual decrease of the mean gray values (Figures 6-8 and 6-9) with time of reaction was consistent with increased clustering of the

aromatic rings to reduce the shape anisotropy, giving a gradual decrease in the depolarization ratio of the liquid. Following the mechanism proposed by Mochida et al.[13], the clustering of planar aromatic molecules which leads to the formation of sub-micron spherical domains (in Mochida's work they have been called microdomains, however, we prefer to call them submicron domains in this paper), would account for the scattering data. The transformation of isolated planar aromatic molecules to molecular clusters and finally spherical submicron domains will decrease their shape anisotropy significantly and results in a decrease in the depolarization ratio. These submicron domains are too small to be detected by optical microscope, but can be observed by SEM (Figure 6-14). Oberlin[48] also reported the observation of more or less spherical anisotropic submicron domains as small as 30 nm during the pyrolysis of pitch, which were assumed to be mesophase nuclei. This transition from independent molecules to organized anisotropic domains is illustrated schematically in Figure 6-15.

The data of Figure 6-8 show a linear decrease in the depolarization ratio with time of reaction, based on the reduced intensity of the gray scale. The reduction in the slope of the curve at 33 min likely indicates the point where most of the large aromatics are in spherical submicron domains. The subsequent growth of these domains, so that they become visible by optical microscopy as mesophase (Figure 6-14), would have little impact on the depolarization ratio because their shape would remain spherical. The physical evidence for eventual formation of submicron domains is clear from SEM. The micrograph in Figure 6-11 shows the sample after 20 min of reaction, where approximately 1/3 of the change in the

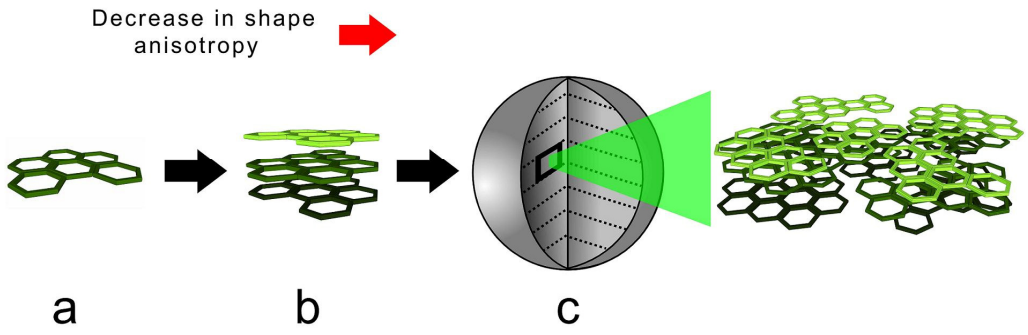

Figure 6-15. Schematic diagram of sequence of mesophase. Aggregation of the planar aromatic molecules forms the clusters and the spherical submicron domains finally. The shape anisotropy of the whole structure decreases gradually which results in a decrease in the depolarized light backscattered by the aggregate. (a) planar aromatic molecules, (b) clusters, (c) spherical submicron domains.

gray scale has take place, but no submicron domains are detected. The observation that the depolarization ratio is lower at this point in the reaction is consistent with clustering of the aromatic molecules at a length scale of a few nanometers, below the resolution of the SEM, as illustrated in Figure 6-15.

Depolarized light scattering in conventional liquid crystals has been studied before[30, 31]. Cameron[30] measured the depolarization ratios as a function of temperature in the nematic and isotropic phase of p-[N-(p-methoxybenzylidene)amino]phenyl acetate (MBPA). The material exhibits a nematic-isotropic transition at 104.9°C. Cameron observed that the perpendicular depolarization ratio at 90° changed from about 0.75 in the isotropic phase to about 1.1 in the nematic phase over a small temperature range between 103.6 to 104°C. Below 103.6 and above 104°C the depolarization ratio was constant. Cameron qualitatively interpreted this behaviour as suggesting that the scattering units were

becoming more anisotropic in the nematic phase relative to the isotropic phase. This sharp change in the perpendicular depolarization ratio, which mainly depends on the lack of spherical symmetry, is the characteristic of a discontinuous or first-order phase transition[50]. Such transitions were not observed in this study because the ongoing reactions were modifying the components in the mixture with time[12]. Hurt et al. assumed that the underlying phase transition for mesophase was similar to stable liquid crystals, and that the unusual temperature behaviour is due to the collateral effects of heating on chemical reaction and vaporization[51]. The results of this study showed that the idea of gradual self assembly is more consistent with the data, and that the phase transitions of the conventional nematic liquid crystals are not observed in these samples. When the sample is cracked at constant temperature, the depolarization ratio starts decreasing immediately with no lag time. The so-called induction time for coke formation is the time needed for the liquid to react and self-assemble the aromatic molecules into mesophase domains which are large enough to be detected by microscopy or be filtered from solutions of toluene. Unlike conventional liquid crystals, the depolarization ratio decreases toward mesophase formation and only increases after the appearance of observable mesophase. These results suggest that the formation of carbonaceous mesophase is not a discontinuous first-order phase transition, rather that is the result of the gradual self-assembly of aromatic molecules above the cracking temperature, as suggested by Marsh[52].

Part of the difficulty in interpreting the data is that the temperatures required to give free-flowing fluid, to allow phase transitions, is also a condition where

ongoing reactions of the vacuum residue components modify the distribution and structure of components in the mixture. Some degree of polymerization likely continues within the mesophase, which stabilizes the domains against dissociation. As a result, the formed mesophase does not disappear by increasing the temperature[52]. Lewis showed that naphthalene pitch can form reversible mesophase for a few cycles of heating and cooling; however, ongoing thermal reactions gradually eliminated the reversible behavior[16]. The alkyl groups in vacuum residue make these components much more likely to undergo addition reactions[53], in comparison to coal-derived naphthalene and anthracene oils. Despite addition reactions, thermal cracking gives net removal of a range of pendant groups[54] which in combination with addition, cyclization and dehydrogenation would be expected to give more large disc-like alkyl aromatics than in the initial mixture. Such a process should definitely increase the shape anisotropy of these molecules and increase the depolarization ratio, however, the actual trend in Figure 6-8 and 6-9 is a progressive decrease until the formation of large bright mesophase domains. This observation suggests that clustering of the reaction products dominates over the increase in the shape anisotropy due to formation of large aromatics. This is consistent with Marsh's hypothesis[16] which suggests that the molecules that form mesophase (mesogens) never have the opportunity to be soluble in the isotropic phase. Once such molecules are created, they immediately self-assemble with each other to form mesophase, so their self-assembly into mesophase totally precludes any possibility of solubility. An alternate explanation is that thermal cracking does not efficiently generate large

aromatics, but rather more complex bridged structures which give less shape anisotropy than simple planar molecules. There may be some molecules in the initial sample which are able to form clusters, but the cracking and polymerization reactions give a progressive increase in clustering, eventually leading to the micron-scale domains of optically anisotropic mesophase (Figure 6-13). Of course, the number of scattering molecules per unit volume of the sample is another important factor which can affect the results. Due to the complexity of the initial sample and the cracking and polymerization reactions, it is not possible to take into account this factor. However, it is unlikely to attribute the decrease in the scattering of the sample to the decrease in the number of scattering molecules in the sample during reaction (if assume that such a thing happens at all). Both the perpendicular and parallel component of the backscattered light should have a linear relationship with this quantity. So if the change in the number of molecules is responsible for a decrease in the intensity of the perpendicular component, then it should have similar effect for the parallel component too. But the results showed that the intensity of the parallel component did not change significantly during the experiment.

The results of depressurization in Figure 6-10 are consistent with our previous study which showed that depressurization before the onset of mesophase formation can induce the formation of observable mesophase earlier than if the reactor has been maintained at pressure[15]. In that study we proposed that the loss of volatiles from the isotropic liquid phase after depressurization reduces the distance between the submicron domains which are already present in the

isotropic liquid but are too small to be detected by optical microscope, promoting coalescence into observable domains[15]. The mean gray values decreased with time continuously before depressurization; however, depressurization caused a sharp change in the brightness of the sample and the mean gray values (Figure 6-10). The volatiles in the sample inhibit mesophase formation by filling the gaps between planar aromatic molecules, and preventing them from collisions to form clusters. As a result, the loss of volatiles suddenly accelerated the aggregation of aromatic molecules and their clusters into spherical submicron domains, giving the sudden change of the mean gray value indicated in Figure 6-10.

The results of this study suggest that mesophase formation is a result of self-assembly of planar aromatic molecules, which happens as a continuous process during the thermal reaction of the liquid phase. The mesophase domains illustrated in Figure 6-14 have the normal physical attributes of a second liquid phase suspended in the reacting liquid, which is the observation of a distinct phase boundary with interfacial tension, giving a spherical shape. The scattering and SEM data indicate, however, that the underlying molecular clustering and assembly processes are too complex to be considered a simple first-order phase transition. Consequently, the concept of two distinct macroscopic phases (isotropic phase and mesophase) when the sample is above the reaction temperature can be discarded as inadequate. In this case, the onset of mesophase formation will be defined by the method of detection, whether by solubility, optical microscopy, SEM, or polarized light scattering.

6.5.2. Prediction of the onset of mesophase formation

Depolarized light scattering has been showed to be a useful method in predicting the onset of mesophase formation. In catalytic hydroconversion, the formation of coke or mesophase is highly undesirable, and an *in situ* method which can predict its onset is of significant importance. In hot-stage microscopy, this point is defined as the time at which the mesophase becomes detectable by the optical microscope; however, this definition depends on the optical resolution of the microscope. Here we suggest a new definition for the practical onset of mesophase formation which seems to be more suitable. We define it as the time at which the scattering curve changes its slope. Mesophase exists in the sample before this onset time, but they are not above a critical size where they begin to deposit as coke on the interior surfaces of process equipment. The mesophase is not yet optically observable at the point the scattering curve changes its slope, so this definition gives a grater margin of safety (in comparison with hot-stage microscopy) to the process at which mesophase formation should be avoided. As a result the depolarized scattering method can be used to develop novel sensors to detect the onset of mesophase formation during conversion of vacuum residue.

6.5.3. The structure of asphaltenes

The results of Figures 6-4 to 6-6 show that the asphaltenes have a lower depolarization ratio than the maltenes at 200-350^{o}C, prior to the onset of any significant chemical reactions. This difference can be either due to differences in molecular structure or due to molecular aggregation. The asphaltenes are the most polar and aromatic fraction of heavy oil. Consequently, the concentration of

polynuclear aromatic groups present in this fraction (which can be the main contributor to light scattering) should be higher than that of maltenes, and the average size of these aromatic groups should be larger. As mentioned before, the aromatics have higher molecular anisotropy than alkanes and this molecular anisotropy increases with increasing the number of carbon ring in the aromatic[44]. So it is logical to assume that the asphaltene fraction should give a higher depolarization ratio. The results of Figure 6-4 to Figure 6-6 showed the opposite, which suggests either that the asphaltenes are in a more aggregated condition at temperatures up to 350^{o}C than the maltenes. This aggregation need not be stable, but must give enough spherical symmetry through at least transient interactions to reduce the shape anisotropy to decrease the shape anisotropy of the asphaltene molecules, giving a lower depolarization ratio (Figure 6-16). Of course, we can not compare the equimolar samples of asphaltenes and maltenes due to the complexity of these fractions. However, the lower depolarization ratio of asphaltenes can not be due to the less number of molecules per volume the sample. If that was the reason, and asphaltene molecules were naturally more anisotropic than that of maltenes (but only with a less molar density), then the addition of asphaltenes to maltenes should increase the net depolarization ratio of the resulting mixture[41]. In addition, the intensities of the parallel component of the backscattered light for asphaltenes and maltenes could be affected by the number of molecules. However, the results showed that the parallel components did not have an observable difference for asphaltenes and maltenes and vacuum residue. The maltenes can play the role of disperser for asphaltenes, but probably can not

dissolve it or dissociate its aggregation state. That's why the addition of asphaltenes to vacuum reside lowers its initial mean gray value and depolarization ratio, and the resulting mean gray value is the weighted average of initial asphaltene and vacuum residue. If maltenes in the vacuum residue could dissociate the asphaltenes aggregate into their constituent molecules which are highly anisotropic, then the depolarization ratio of the mixture should have been increased. As a result the, vacuum residue which has 30.1% asphaltenes has a depolarization ratio between that of the asphaltene and maltenes. As Figure 6-5 shows the asphaltene fraction has a lower depolarization ratio than that of vacuum residue at the same temperature since the intensity of the parallel components of backscattered light is almost the same. But mixing results in a homogenous sample with a mean gray value and depolarization ratio between that of the vacuum residue and asphaltenes themselves. In addition, asphaltenes can keep this aggregated state even at high temperatures as shown in Figure 6-4. The asphaltene fraction can be regarded as a more aggregated fraction phase which needs less time to self assemble itself into mesophase submicron domains. As a result, it turns into mesophase very fast. Asphaltenes aggregates can be dispersed into maltenes and probably act as a nucleation core for mesophase formation. Heating of asphaltenes can dissociate its aggregates somewhat, but even at high temperatures (below the reaction temperature) asphaltene is a more aggregated phase in comparison with maltenes at the same temperature. It is important to note that the aggregation at elevated temperatures below the cracking temperature can not be justified by π-π stacking. Gray et al.[55] has suggested that the π-π stacking

of even very large aromatics is too weak in toluene solutions to account for aggregation of asphaltenes in highly dilute solution or at elevated temperature. They[55] have suggested a supramolecular assembly model for the aggregation of asphaltenes which can explain this behavior. Based on this model the π-π stacking of aromatic rings is a contributing factor rather than the dominant motif and other cooperative binding by Brønsted acid-base interactions, hydrogen bonding, metal coordination complexes, and interactions between cylcoalkyl and alkyl groups to form hydrophobic pockets can contribute to the aggregation of asphaltenes.

6.6. Conclusions

An inverted reflective microscope plus image processing was used to measure the depolarized backscattered light from samples *in situ* during cracking and mesophase formation. The results of this study showed that the intensity of the depolarized backscattered light decreases linearly with time during the cracking of heavy oil fractions. The parallel component of backscattered light did not change with time; therefore, the depolarization ratio was proportional to the intensity of depolarized backscattered light. The scattering curve can be used to define the onset of mesophase formation, and this technique can be used a practical method to detect the onset of mesophase formation.

Depressurization also changes the depolarization ratio instantly, consistent with the sudden removal of the low molecular weight components which accelerates the self assembly of the aromatic molecules. The results suggest that mesophase formation is not the result of a nematic first order phase transition or asphaltene phase separation, and can be described as a homogenous self assembly of planar

aromatic molecules into spherical submicron domains which grow into the optically observable mesophase spheres. The asphaltene fraction shows a lower depolarization ratio in comparison with maltenes even at high temperatures above 300°C.

6.7. References

1. Gray, M. R., Upgrading Petroleum Residues and Heavy Oils. Marcel Dekker Inc.: New York, 1994.
2. Marsh, H.; Latham, C. S., The Chemistry of Mesophase Formation. Am. Chem. Soc., Symp. Ser. 1986, 303, 1-28.
3. Brooks, J. D.; Taylor, G. H., Formation of Graphitizing Carbons from Liquid Phase. Nature 1965, 206, (4985), 697-699.
4. Hu, Y.; Hurt, R. H., Thermodynamics of Carbonaceous Mesophase - II. General Theory for Nonideal Solutions. Carbon 2001, 39, (6), 887-896.
5. Yoon, S. H.; Korai, Y.; Mochida, I., Spinning Characteristics of Mesophase Pitches Derived from Naphthalene and Methylnaphthalene with HF/BF3. Carbon 1993, 31, (6), 849-856.
6. Yamada, Y.; Imamura, T.; Kakiyama, H.; Honda, H.; Oi, S.; Fukuda, K., Characteristics of Meso-Carbon Microbeads Separated from Pitch. Carbon 1974, 12, (3), 307-319.
7. Chang, Y. C.; Sohn, H. J.; Ku, C. H.; Wang, Y. G.; Korai, Y.; Mochida, I., Anodic Performances of Mesocarbon Microbeads (MCMB) Prepared from Synthetic Naphthalene Isotropic Pitch. Carbon 1999, 37, (8), 1285-1297.

8. Rahimi, P.; Gentzis, T.; Dawson, W. H.; Fairbridge, C.; Khulbe, C.; Chung, K.; Nowlan, V.; DelBianco, A., Investigation of Coking Propensity of Narrow Cut Fractions from Athabasca Bitumen Using Hot-Stage Microscopy. Energy Fuels 1998, 12, (5), 1020-1030.
9. Riggs, D. M.; Diefendorf, R. J., A phase diagram for pitches. In Carbon '80, Baden-Baden, 1980; pp 326-329.
10. Mochida, I.; Korai, Y., Chemistry for Preparation of Mesophase Pitches and Design of their Properties Nenryo Kyokaishi 1985, 64, (10), 796-808.
11. Shishido, M.; Inomata, H.; Arai, K.; Saito, S., Application of Liquid Crystal Theory to the Estimation of Mesophase Pitch Phase-Transition Behavior. Carbon 1997, 35, (6), 797-799.
12. Marsh, H.; Menendez, R., Mechanisms of Formation of Isotropic and Anisotropic Carbons. In Introductio to Carbon Science, Marsh, H., Ed. Butterworths: London, 1989; pp 37-73.
13. Mochida, I.; Korai, Y.; Ku, C. H.; Watanabe, F.; Sakai, Y., Chemistry of Synthesis, Structure, Preparation and Application of Aromatic-Derived Mesophase Pitch. Carbon 2000, 38, (2), 305-328.
14. Wiehe, I. A., A Phase-Separation Kinetic-Model for Coke Formation. Ind. Eng. Chem. Res. 1993, 32, (11), 2447-2454.
15. Bagheri, S. R.; Gray, M. R.; McCaffrey, W. C., Influence of Depressurization and Cooling on the Formation and Development of Mesophase. Energy Fuels 2011, 25, (12), 5541-5548.

16. Marsh, H.; Martinez-Escandell, M.; Rodriguez-Reinoso, F., Semicokes from Pitch Pyrolysis: Mechanisms and Kinetics. Carbon 1999, 37, (3), 363-390.

17. Mostowfi, F.; Indo, K.; Mullins, O. C.; McFarlane, R., Asphaltene Nanoaggregates Studied by Centrifugation. Energy Fuels 2009, 23, 1194-1200.

18. Storm, D. A.; Barresi, R. J.; Sheu, E. Y., Flocculation of Asphaltenes in Heavy Oil at Elevated Temperatures. Fuel Sci. Technol. Int. 1996, 14, (1-2), 243-260.

19. Thiyagarajan, P.; Hunt, J. E.; Winans, R. E.; Anderson, K. B.; Miller, J. T., Temperature-Dependent Structural-Changes of Asphaltnes in 1-Methylnaphthalene. Energy Fuels 1995, 9, (5), 829-833.

20. Mishchenko, M. I.; Travis, L. D.; Lacis, A. A., Scattering, Absorption, and Emission of Light by Small Particles. 1st ed.; Cambridge University Press: Cambridge, 2002.

21. Cox, A. J.; DeWeerd, A. J.; Linden, J., An Experiment to Measure Mie and Rayleigh Total Scattering Cross Sections. American Journal of Physics 2002, 70, (6), 620-625.

22. Young, A. T., Rayleigh-Scattering. Phys. Today 1982, 35, (1), 42-48.

23. Bruce J. Berne, B. J.; Pecora, R., Dynamic Light Scattering: With Applications to Chemistry, Biology, and Physics. Wiley: New York, 1976.

24. Starner, S. H.; Bilger, R. W.; Dibble, R. W.; Barlow, R. S., Measurements of Conserved Scalars in Turbulent-Diffusion Flames. Combust. Sci. Technol. 1992, 86, (1-6), 223-236.

25. Schärtl, W., Light Scattering from Polymer Solutions and Nanoparticle Dispersions. Springer: Berlin, 2007.

26. Shimizu, H.; Lee, S. A.; She, C. Y., High Spectral Resolution LIDAR System with Atomic Blocking Filters for Measuring Atmospheric Parameters. Appl. Opt. 1983, 22, (9), 1373-1381.

27. Shimizu, H.; Noguchi, K.; She, C. Y., Atmospheric-Temperature Measurement by a High Spectral Resolution LIDAR. Appl. Opt. 1986, 25, (9), 1460-1466.

28. Sassen, K.; Zhao, H. G.; Yu, B. K., Backscatter Laser Depolarization Studies of Simulated Stratospheric Aerosols - Crystallized Sulfuric-Acid Droplets. Appl. Opt. 1989, 28, (15), 3024-3029.

29. Nastishin, Y. A.; Liu, H.; Shiyanovskii, S. V.; Lavrentovich, O. D.; Kostko, A. F.; Anisimov, M. A., Pretransitional Fluctuations in the Isotropic Phase of a Lyotropic Chromonic Liquid Crystal. Phys. Rev. E 2004, 70, (5), 9.

30. Cameron, L. M., Depolarization of Light Scattered from Liquid Crystals. Mol. Cryst. Liq. Cryst. 1969, 7, 235-252.

31. Kirov, N.; Simova, P.; Sabeva, M., Depolarization of Light Scattered in Nematic Liquid-Crystals. Mol. Cryst. Liq. Cryst. 1976, 33, (3-4), 189-194.

32. Beyerle, G., Detection of Stratospheric Sulfuric Acid Aerosols with Polarization LIDAR: Theory, Simulations, and Observations. Appl. Opt. 2000, 39, (27), 4994-5000.

33. Sassen, K., The Polarization LIDAR Technique for Cloud Research - A Review and Current Assessment. Bull. Am. Meteor. Soc. 1991, 72, (12), 1848-1866.

34. Pal, S. R.; Carswell, A. I., Polarization Properties of LIDAR Backscattering from Clouds. Appl. Opt. 1973, 12, (7), 1530-1535.

35. Nicolet, M.; Stetzer, O.; Luond, F.; Mohler, O.; Lohmann, U., Single Ice Crystal Measurements during Nucleation Experiments with the Depolarization Detector IODE. Atmos. Chem. Phys. 10, (2), 313-325.

36. van de Hulst, H. C., Light Scattering by Small Particles. Wiley: New York, 1957.

37. Mishchenko, M. I.; Hovenier, J. W., Depolarization of Light Backscattered by Randomly Oriented Nonspherical Particles. Opt. Lett. 1995, 20, (12), 1356-1358.

38. Kerker, M., The Scattering of Light and Other Electromagnetic Radiation. Academic Press: New York, 1969.

39. Mishchenko, M. I.; Sassen, K., Depolarization of Lidar Returns by Small Ice Crystals: An Application to Contrails. Geophys. Res. Lett. 1998, 25, (3), 309-312.

40. Rowell, R. L.; Aval, G. M.; Barrett, J. J., Rayleigh-Raman Depolarization of Laser Light Scattered by Gases. J. Chem. Phys. 1971, 54, (5), 1960-1964.

41. Bothorel, P., Determination of Molecular Optical Anisotropy in Solutions and Liquids by Depolarized Light Scattering - Applications to Study of N-Alkanes. J. Colloid Interface Sci. 1968, 27, (3), 529-541.

42. Striegel, A. M., A Method for Studying Optical Anisotropy of Polymers as a Function of Molar Mass. Anal. Chem. 2002, 74, (13), 3013-3018.

43. Schmidt, R. L., Temperature Dependence of Rayleigh Light Scattering nad Depolarization in Pure Liquids. J. Colloid Interface Sci. 1968, 27, (3), 516-528.

44. Unanue, B. A.; Bothorel, P., Etude de la Structure Electronique de Molecules Aromatiques Substituees par Diffusion Rayleigh Depolarisee. Bull. Soc. Chim. Fr. 1964, 573-578.

45. Harris, F. S.; Sherman, G. C.; Morse, F. L., Experimental Comparison of Scattering of Coherent and Incoherent Light. IEEE Trans. Antennas Propag. 1967, AP15, (1), 141-147.

46. Oberlin, A.; Bonnamy, S.; Rouxhet, P. G., Colloidal and Supramolecular Aspects of Carbon. In Chemistry and Physics of Carbon, Vol 26, Marcel Dekker: New York, 1999; Vol. 26, pp 1-148.

47. Olson, E. S.; Diehl, J. W., Anisotropy in Dilute-Solutions of Coal-Derived Materials. Fuel 1991, 70, (3), 349-351.

48. Oberlin, A., High Resolution TEM Studies of Carbonization and Graphitization. In Chemistry and Physics of Carbon, Marcel Dekker: New York, 1989; Vol. 22, pp 1-143.

49. Song, O. K.; Wang, C. H., Dicarbocyanine Dyes in Methanol Solution Probed by Depolarized Rayleigh and Hyper-Rayleigh Light Scattering. J. Chem. Phys. 1996, 104, (21), 8230-8236.

50. Collings, P. J.; Hird, M., Introduction to Liquid Crystals: Chemistry and Physics. . Taylor and Francis: London, 1997.

51. Hurt, R. H.; Chen, Z. Y., Liquid Crystals and Carbon Materials. Phys. Today 2000, 53, (3), 39-44.

52. Marsh, H.; M.A., D., Mesophase of Graphitizable Carbons. In Liquid Crystalline and Mesomorphous Polynzers, Shibaev, V. P.; Lam, L., Eds. Springer: New York, 1993; pp 231-257

53. Alshareef, A. H.; Scherer, A.; Tan, X. L.; Azyat, K.; Stryker, J. M.; Tykwinski, R. R.; Gray, M. R., Formation of Archipelago Structures during Thermal Cracking Implicates a Chemical Mechanism for the Formation of Petroleum Asphaltenes. Energy Fuels 2011, 25, (5), 2130-2136.

54. Karimi, A.; Qian, K. N.; Olmstead, W. N.; Freund, H.; Yung, C.; Gray, M. R., Quantitative Evidence for Bridged Structures in Asphaltenes by Thin Film Pyrolysis. Energy Fuels 2011, 25, (8), 3581-3589.

55. Gray, M. R.; Tykwinski, R. R.; Stryker, J. M.; Tan, X. L., Supramolecular Assembly Model for Aggregation of Petroleum Asphaltenes. Energy Fuels 2011, 25, (7), 3125-3134.

7. Conclusions

7.1. Summary of conclusions

In the previous chapters new insights into the phenomenon of mesophase formation was presented. Based on the results of this thesis we can suggest a mechanism for the mesophase formation in heavy oil.

7.1.1. Mechanism of mesophase formation

1-Mesophase formation is the result of cracking and polymerization reaction which are triggered by heating the sample above cracking temperature. Below the reaction temperature mesophase does not form by heating or depressurization of the sample.

2- By passing the reaction temperature, the aggregation of molecules starts immediately, and this process does not contain any induction period. Phase separation theories suggest that there is an induction time for the formation of mesophase. The literature also suggests that initially the cracking and polymerization reactions form the large planar aromatic molecules (mesogens) which form mesophase and then these mesogens aggregate to form mesophase which also implies an induction time for the formation of mesogens. Such an induction time was not observed by depolarized light scattering, and an immediate continuous decrease in the depolarization ratio was observed after reaching a temperature higher than the reaction temperature.

This study suggests that clustering of the reaction products dominates over the increase in the shape anisotropy due to formation of large aromatics (mesogens).

Once such molecules are created, they immediately self-assemble with each other to form mesophase. An alternate explanation is that thermal cracking does not efficiently generate large aromatics, but rather more complex bridged structures which give less shape anisotropy than simple planar molecules. There may be some molecules in the initial sample which are able to form clusters, but the cracking and polymerization reactions give a progressive increase in clustering, eventually leading to the micron-scale domains of optically anisotropic mesophase.

3-The self-assembly of molecules results in the formation of molecular clusters and then submicron mesophase domains. The existence of these domains can be verified by SEM.

4-Further growth and coalescence of these submicron domains can result in the formation of micron-scale mesophase domains which can be detected by an optical microscope. So the onset time or the induction time that is reported by hot-stage microscopy is the result of the detection limit of the apparatus and not a real induction time for the process of mesophase formation. Consequently, the concept of two distinct macroscopic phases (isotropic phase and mesophase) when the sample is above the reaction temperature can be discarded as inadequate. In this case, the onset of mesophase formation will be defined by the method of detection, whether by solubility, optical microscopy, SEM, or polarized light scattering.

5-The results of chapter 6 suggests that mesophase formation is not the result of a phase separation due to exceeding the solubility limit of the oil medium. Once

mesogens are created, they immediately self-assemble with each other to form mesophase. This self-assembly into mesophase is not consistent with solubility behaviour, and it is not a first-order phase transformation, as observed in nematic liquid crystals. Mesophase formation is clearly the result of the gradual self-assembly of molecules, in parallel with ongoing chemical reactions and elevated temperature.

7.1.2. Growth and coalescence of mesophase

After the formation of submicron mesophase domains, they can grow and coalesce to former larger micron-scale domains. These domains can also coalesce to form very large bulk mesophase domains. The results of chapter 5 show that stirring can significantly improve the process of coalescence, resulting in the formation of a bimodal distribution of mesophase sizes. The results suggest that there is jump in the size from submicron mesophase domains to bulk mesophase which is likely the result of the forced coalescence of these domains.

7.2. Practical implications

7.2.1. Hot-stage reactor

The hot-stage reactor designed in this study proved to be a useful apparatus for investigating mesophase formation in heavy oil. The presence of the stirrer improves the heat transfer and allows the addition of catalyst. The position of the window at the bottom of the reactor removes any gaps between the sample and the window. This feature prevents the condensation of the gases on the inner side of the window and allows the depressurization of the reactor while observing the

sample on the window. The hot-stage reactor also has some limitations. The birefringent and thick and hot sapphire window limits the maximum magnification of the objective lens. Loading the samples (especially liquid samples) is difficult and the reactor has no mechanism for fast cooling of the sample. Further modifications are necessary for this hot-stage reactor.

Some of the results need to be tested for bigger reactors. Unfortunately our knowledge about the fluid mechanics of the reactor is not complete. To calculate the Reynolds number of the reactor the density and viscosity of the sample during the reaction time should be known. We can only rely on the estimations for these quantities, so the actual Reynolds number at the time of reaction remains unknown. As a result, it is difficult to link the quantitative results of this thesis to the expected behaviour in bigger reactors like bubble column reactors used in the industry for slurry hydroconversion.

7.2.2. Sampling the reactors

One important implication of chapter 4 is that sampling reactors in order to define mesophase content requires quenching of samples at the reactor pressure, in order to prevent the loss of volatiles from the isotropic liquid phase and increasing the mesophase content. This effect would be most pronounced when the liquid phase is rich in volatile components, which would depend on the level of conversion and the gas flow rate.

7.2.3. Definition of mesophase

As mentioned in chapter 2, mesophase was first discovered by Brooks and Taylor using polarized microscopy and defined based on its optical anisotropy. Carbonaceous mesophase is now defined as "A liquid-crystalline state of pitch which shows the optical birefringence of disc-like (discotic) nematic liquid crystals. It can be formed as an intermediate phase during thermolysis (pyrolysis) of an isotropic molten pitch or by precipitation from pitch fractions prepared by selective extraction"[7]. In this definition the optical birefringence has been used as a main characteristic of carbonaceous mesophase. As a result, hot-stage microscopy is usually regarded as the most powerful technique for the characterization of mesophase. However, as the results of this study suggest mesophase formation is a continuous process which happens above the reaction temperature. As a result talking about an onset for the formation of mesophase is not logical. Such an onset if exists should be the time at which the sample reaches to the cracking temperature. On the other, once mesophase spheres begin to form, they can coalesce to form larger mesophase domains, which eventually deposits as coke on the interior surfaces of process equipment. Mesophase domains are a problem for the petroleum industry above a certain size, and it is possible to define a practical onset for the formation of mesophase domains (above a certain size) to avoid the problems. We define it as the time at which the scattering curve changes its slope. This definition gives a grater margin of safety to the process at which mesophase formation should be avoided in comparison with hot-stage microscopy, since at this time the mesophase is not yet optically observable. In

this way the depolarized scattering method can be used to develop novel sensors to detect the onset of mesophase formation during conversion of vacuum residue.

7.2.4. Role of catalyst

The whole process of mesophase formation can be thought as the aggregation of molecules and clusters to form submicron domain and the coalescence of these domains with each other or more molecular clusters to form bigger domains resulting in the formation of ultimate bulk mesophase. As a result, any process or material which can prevent the collision of molecules, clusters, submicron domains or even bigger domains can slow down the growth of mesophase. The results of depressurization experiments showed that depressurization before the onset of mesophase formation can induce the formation of observable mesophase earlier than if the reactor has been maintained at pressure. The volatiles from the isotropic phase in the sample inhibit mesophase formation by filling the gaps between planar aromatic molecules, and preventing them from collisions to form clusters. As a result, the loss of volatiles suddenly accelerated the aggregation of aromatic molecules and their clusters into spherical submicron domains.

The results of this study are consistent with the results of Cheng et al.[1] who studied the effect of supercritical water on vacuum residue upgrading. They observed that the addition of supercritical water can improve the cracking behaviour and the yield in light oil. The decrease in coke formation was attributed to the dispersion effect of supercritical water. They suggested that supercritical water can disperse asphaltenes as an emulsion and reduce the asphaltene concentration for coking[1]. In fact the supercritical water can play the role of the

low molecular weight components in dispersions of coke precursors as discussed above.

Catalyst can have both chemical and physical effects on the growth of mesophase. The chemical effect increases the time of onset of mesophase formation and the physical effect decreased the tendency of mesophase spheres to form bulk mesophase. Catalyst can also play the role of a dispersant in this way to stop the growth of mesophase (physical role of catalyst). An ideal nano-sized catalyst should be able to stop the coalescence of submicron mesophase domains. However, the results of this study indicates that agglomeration of catalyst particles, which increases their size and reduces their exterior surface area, makes them less effective at suppressing the coalescence of these submicron mesophase domains. They are still effective at stabilizing larger micron-scale mesophase domains. SEM analysis showed that catalyst particles agglomerated and stuck to the outer surface of mesophase domains and prevented their coalescence. Although the agglomeration of catalyst particles likely decreased their efficiency for suppressing the formation of small mesophase domains of a few microns in diameter, the agglomerated material was still effective in suppressing the formation of bulk mesophase. The results showed that there was a maximum for the onset of mesophase observation as a function of catalyst concentration. As a result, addition of more catalyst does not necessarily increase its efficiency for suppressing mesophase formation due to the extensive large-scale agglomeration of catalyst particles at high catalyst concentrations.

7.3. Recommendations for future work

The size of the hot-stage reactor can be increased to test the results of chapters 5 and 6 for more realistic fluid flow conditions. Increasing the size of the stirrer can increase the Reynolds number of the reactor under similar conditions. The high pressure of hydrogen and related safety issues will be the biggest challenge for a larger reactor; however, most of the components of the current apparatus, like the sapphire window and the magnet stirrer, can be still useful for such a larger reactor. The effect of turbulence on mesophase formation should be studied in larger reactors. The formation of a bimodal distribution, if verified for larger reactors, needs more attention. The effect of catalyst on mesophase formation and finding the optimum concentration of the catalyst seems to be essential. The agglomeration of catalyst is an important issue that needs more attention. Finding new ways for improving the dispersion of catalyst in the reactor can significantly increase the efficiency of catalyst for suppressing formation of the problematic mesophase domains in the micron size range. The light scattering method in chapter 6 has the potential to be used for larger reactors. The method may be implemented by using a portable sensor using optical fibers, with the sensor inserted into the reactor for *in situ* observation of the sample, and sending the information to an external light detector for the depolarized scattering analysis.

7.4. References

1. Cheng, Z. M.; Ding, Y.; Zhao, L. Q.; Yuan, P. Q.; Yuan, W. K., Effects of Supercritical Water in Vacuum Residue Upgrading. Energy Fuels 2009**,** 23, 3178-3183.

Appendix A: XRD analysis of mesophase formation

0.4 g of Athabasca vacuum residue was heated in the hot-stage reactor at 440°C under nitrogen at 4.1 MPa and stirred at 120 rpm. The heater turned off after a certain amount of time. Four experiments were done with reaction times of 18, 30, 65, and 240 min. These times were chosen to study the samples both before and after the microscopic observation mesophase. After each experiment the remaining sample was removed out of the hot-stage reactor, and dried in the oven at 70°C for a few hours. Part of the sample was polished and checked under microscope for mesophase formation and the other part was crushed into a fine powder for XRD analysis. XRD analysis was done using a Rigaku Ultima III X-ray diffractometer with Cu-Ka radiation source l=1.5406 Å). All samples were in the form of a fine powder.

The initial vacuum residue was not a complete solid at room temperature; it did not contain any optical anisotropy. For vacuum residue heat treated for 18 min, the polished surface of this sample showed no optical anisotropy. Vacuum residue heat treated for 30 min was again optically isotropic. Heat treatment of Vacuum residue for 65 min resulted in the formation of observable mesophase (with the *in situ* microscopy) after 42 min. The polished surface of the cooled sample which used for XRD showed mesophase spheres bigger than 10 μm. In the vacuum residue sample heat treated for 240 min mesophase spheres had grown in size and coalesced to form bulk mesophase regions.

Figure A-1 shows the diffraction patterns of all these 4 samples. The diffraction pattern of fresh vacuum residue showed that it was completely amorphous.

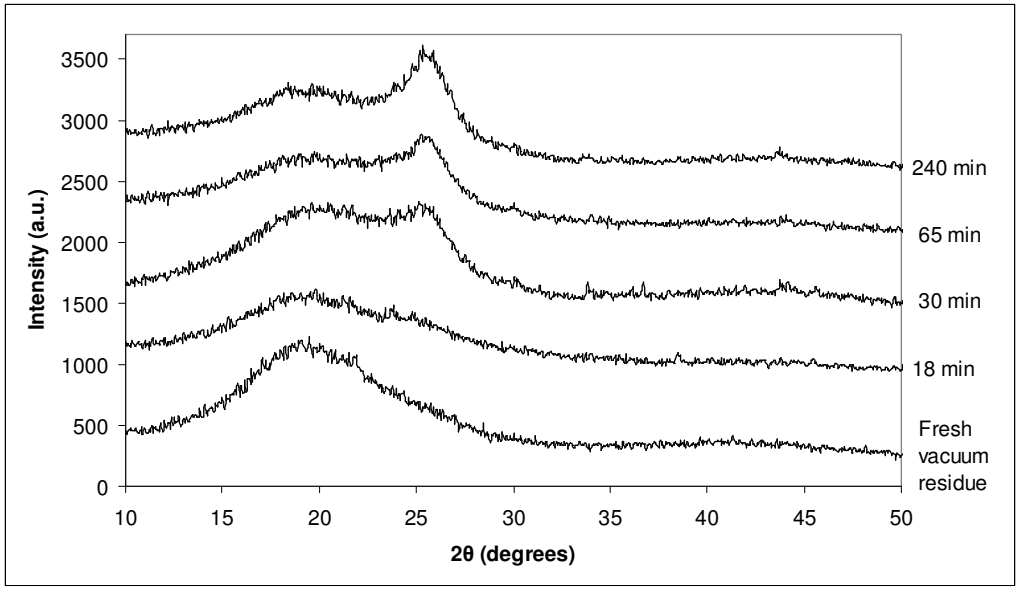

Figure A-1. X-ray diffraction pattern of the coke samples from Athabasca Vacuum heat treated under nitrogen at 440°C and 4.1 MPa and stirred at 120 rpm.

However, after 18 min, the pattern has started to change. After 30 min the (002) peak at 2θ~25° started to develop in the sample which grew with time and became sharper after 65 and 240 min. The development of (002) peak is associated to the ordering of the mesogen molecules which form the mesophase. (002) is in fact the miller index for basal plane of graphite structure, but in pregraphitic samples like semicokes, it indicates the stacking of graphene sheets. These results show that the formation of mesophase is a continuous process. The sample heat treated for 30 min is optically isotropic, but the XRD clearly results show that mesophase as a liquid crystalline phase exists in this sample. This is also consistent with the results of chapter 6 in which SEM proved the existence of mesophase in heat treated samples before they become optically anisotropic. The results also suggest that mesophase formation is a continuous process. XRD analysis of the sample

heat treated after 18 min does not show the 002 peak, however, the diffraction pastern has clearly changed and is different from that of fresh vacuum residue. The sample is undergoing a continuous change toward formation of observable mesophase. This is consistent with depolarized light scattering results.